SCUBE3 loss-of-function causes a recognizable recessive developmental disorder due to defective bone morphogenetic protein signaling

Yuh-Charn Lin,[1,2,33] Marcello Niceta,[3,33] Valentina Muto,[3,33] Barbara Vona,[4,5,33] Alistair T. Pagnamenta,[6] Reza Maroofian,[7] Christian Beetz,[8] Hermine van Duyvenvoorde,[9] Maria Lisa Dentici,[3] Peter Lauffer,[10] Sadeq Vallian,[11] Andrea Ciolfi,[3] Simone Pizzi,[3] Peter Bauer,[8] Nana-Maria Grüning,[8] Emanuele Bellacchio,[3] Andrea Del Fattore,[3] Stefania Petrini,[12] Ranad Shaheen,[13,14] Dov Tiosano,[15,16] Rana Halloun,[15] Ben Pode-Shakked,[17,18] Hatice Mutlu Albayrak,[19] Emregül Işık,[19] Jan M. Wit,[20] Marcus Dittrich,[4,21] Bruna L. Freire,[22] Debora R. Bertola,[23] Alexander A.L. Jorge,[22] Ortal Barel,[24,29] Ataf H. Sabir,[25,26] Amal M.J. Al Tenaiji,[27] Sulaima M. Taji,[27] Nouriya Al-Sannaa,[28] Hind Al-Abdulwahed,[28] Maria Cristina Digilio,[3] Melita Irving,[25] Yair Anikster,[17,18,29] Gandham S.L. Bhavani,[30] Katta M. Girisha,[30] Genomics England Research Consortium, Thomas Haaf,[4] Jenny C. Taylor,[6] Bruno Dallapiccola,[3] Fowzan S. Alkuraya,[13] Ruey-Bing Yang,[2,31,32,*] and Marco Tartaglia[3,*]

Summary

Signal peptide-CUB-EGF domain-containing protein 3 (SCUBE3) is a member of a small family of multifunctional cell surface-anchored glycoproteins functioning as co-receptors for a variety of growth factors. Here we report that bi-allelic inactivating variants in *SCUBE3* have pleiotropic consequences on development and cause a previously unrecognized syndromic disorder. Eighteen affected individuals from nine unrelated families showed a consistent phenotype characterized by reduced growth, skeletal features, distinctive craniofacial appearance, and dental anomalies. *In vitro* functional validation studies demonstrated a variable impact of disease-causing variants on transcript processing, protein secretion and function, and their dysregulating effect on bone morphogenetic protein (BMP) signaling. We show that SCUBE3 acts as a BMP2/BMP4 co-receptor, recruits the BMP receptor complexes into raft microdomains, and positively modulates signaling possibly by augmenting the specific interactions between BMPs and BMP type I receptors. *Scube3*$^{-/-}$ mice showed craniofacial and dental defects, reduced body size, and defective endochondral bone growth due to impaired BMP-mediated chondrogenesis and osteogenesis, recapitulating the human disorder. Our findings identify a human disease caused by defective function of a member of the SCUBE family, and link SCUBE3 to processes controlling growth, morphogenesis, and bone and teeth development through modulation of BMP signaling.

[1]Department of Physiology, School of Medicine, Taipei Medical University, 110301 Taipei, Taiwan; [2]Institute of Biomedical Sciences, Academia Sinica, 115201 Taipei, Taiwan; [3]Genetics and Rare Diseases Research Division, Ospedale Pediatrico Bambino Gesù, IRCCS, 00146 Rome, Italy; [4]Institute of Human Genetics, Julius Maximilians University, 97074 Würzburg, Germany; [5]Department of Otolaryngology - Head and Neck Surgery, Eberhard Karls University, 72076 Tübingen, Germany; [6]NIHR Oxford Biomedical Research Centre, Wellcome Centre for Human Genetics, University of Oxford, OX3 7BN Oxford, UK; [7]Genetics and Molecular Cell Sciences Research Centre, St George's University of London, Cranmer Terrace, SW17 0RE London, UK; [8]Centogene AG, 18055 Rostock, Germany; [9]Department of Clinical Genetics, Leiden University Medical Center, 2300 RC Leiden, the Netherlands; [10]Department of Paediatric Endocrinology, Emma Children's Hospital, Amsterdam University Medical Center, 1105 AZ Amsterdam, the Netherlands; [11]Department of Cell and Molecular Biology & Microbiology, University of Isfahan, 8174673441 Isfahan, Iran; [12]Confocal Microscopy Core Facility, Research Laboratories, IRCCS Ospedale Pediatrico Bambino Gesù, 00146 Rome, Italy; [13]Department of Genetics, King Faisal Specialist Hospital and Research Center, 11211 Riyadh, Saudi Arabia; [14]Qatar Biomedical Research Institute, Hamad Bin Khalifa University, 34110 Doha, Qatar; [15]Pediatric Endocrinology Unit, Ruth Rappaport Children's Hospital, Rambam Healthcare Campus, 352540 Haifa, Israel; [16]Ruth and Bruce Rappaport Faculty of Medicine, Technion, Israel Institute of Technology, 352540 Haifa, Israel; [17]Edmond and Lily Safra Children's Hospital, Sheba Medical Center, 52621 Tel-Hashomer, Israel; [18]The Sackler Faculty of Medicine, Tel-Aviv University, 6997801 Tel-Aviv, Israel; [19]Department of Pediatric Endocrinology, Gaziantep Cengiz Gökcek Maternity & Children's Hospital, 27010 Gaziantep, Turkey; [20]Department of Pediatrics, Leiden University Medical Center, 2333ZA Leiden, the Netherlands; [21]Institute of Bioinformatics, Julius Maximilians University, 97070 Würzburg, Germany; [22]Unidade de Endocrinologia Genética, Hospital das Clínicas da Faculdade de Medicina da Universidade de Sao Paulo, 01246903 Sao Paulo, Brazil; [23]Unidade de Genética do Instituto da Criança, Hospital das Clínicas da Faculdade de Medicina da Universidade de Sao Paulo, 05403000 Sao Paulo, Brazil; [24]Sheba Cancer Research Center, Sheba Medical Center, 52621 Tel-Hashomer, Israel; [25]Department of Clinical Genetics, Guy's and St Thomas' NHS Foundation Trust, SE1 9RT London, UK; [26]Birmingham Women's and Children's NHS Foundation Trust, University of Birmingham, B4 6NH Birmingham, UK; [27]Department of Paediatrics, Sheikh Khalifa Medical City, 51900 Abu Dhabi, United Arab Emirates; [28]Johns Hopkins Aramco Healthcare, 34465 Dhahran, Saudi Arabia; [29]Wohl Institute for Translational Medicine, Sheba Medical Center, 52621 Tel-Hashomer, Israel; [30]Department of Medical Genetics, Kasturba Medical College, Manipal Academy of Higher Education, Manipal 576104, India; [31]Ph.D. Program in Drug Discovery and Development Industry, College of Pharmacy, Taipei Medical University, 110301 Taipei, Taiwan; [32]Institute of Pharmacology, School of Medicine, National Yang-Ming University, 112304, Taipei, Taiwan
[33]These authors contributed equally
*Correspondence: rbyang@ibms.sinica.edu.tw (R.-B.Y.), marco.tartaglia@opbg.net (M.T.)
https://doi.org/10.1016/j.ajhg.2020.11.015.

Introduction

The extracellular microenvironment provides the biochemical signals that control cell behavior and coordinate developmental and physiological processes. In this three-dimensional and dynamic network, a repertoire of secreted and cell surface-anchored modulators is known to contribute to the fine tuning of signal strength by boosting or antagonizing the information transmitted by growth factors, hormones, and cytokines to their cognate receptors.[1] Any imbalance of such delicate regulation can considerably affect development and homeostasis.[2,3] In this framework, bone morphogenetic protein (BMP) signaling is archetypal. BMPs are secreted extracellular matrix (ECM)-associated proteins of the TGF-β superfamily controlling cell growth, apoptosis, and differentiation, and coordinating a variety of developmental processes, playing an important role in body-plan patterning, morphogenesis, and organogenesis.[4,5] Besides the large number of secreted signal molecules and multiple cell-surface receptors, the complexity of BMP signaling regulation is linked to the presence of secreted antagonists that are able to inhibit binding of individual ligands to their cognate receptors, or co-receptors that modulate the activity of the receptor complex.[6] Indeed, pathogenic variants in genes encoding these auxiliary proteins can dramatically affect development and physiology.[7–9]

The signal peptide-complement protein C1r/C1s, Ugef, and Bmp1 (CUB)-epidermal growth factor (EGF)-like domain-containing (SCUBE) protein family comprises three related multi-functional glycoproteins that act as co-receptors augmenting signaling promoted by a variety of growth factors.[10–12] Their conserved structure is characterized by a signal peptide, nine tandemly arranged EGF-like domains, a spacer region, three cysteine-rich motifs, and a single CUB domain located at the C terminus.[11–13] While the N-terminal and C-terminal regions are involved in protein-protein interactions,[12,14] the spacer region and cysteine-rich repeats mediate protein anchoring to the cell surface by at least two different membrane-associating mechanisms involving electrostatic and lectin-glycan interactions.[15] Proteolytic cleavage within the spacer region is believed to control the modulatory function mediated by the CUB domain and secretion of the N-terminal portion of the protein in the extracellular microenvironment.[16] SCUBE proteins modulate signaling elicited by a variety of growth factors, including members of the BMP, hedgehog, vascular endothelial growth factor and fibroblast growth factor families.[17–20] These proteins are prominently expressed in various developing tissues, which implies their potential role during development, but have distinct expression patterns. While *SCUBE1* (MIM: 611746) is mainly expressed in platelets and endothelial cells[10] and *SCUBE2* (MIM: 611747) is more widely expressed,[12] the most recently discovered member of this family, *SCUBE3* (MIM: 614708), is expressed in a more restricted fashion, with highest levels in osteoblasts, craniofacial regions, and limb buds.[11,21]

Here we report that bi-allelic, largely inactivating variants in *SCUBE3* underlie a developmental disorder characterized by reduced growth, skeletal features, dental anomalies, and a distinctive craniofacial appearance. We demonstrate that the disease-causing variants affect protein synthesis, secretion, and/or function, with a subset of them directly perturbing BMP2 signaling. We also show that SCUBE3 functions as a BMP co-receptor and that *Scube3*$^{-/-}$ mice have defective endochondral bone growth due to impaired BMP-mediated chondrogenesis and ossification.

Subjects and methods

Study approval

Affected subjects were analyzed in the context of research projects dedicated to "undiagnosed patients," or referred for diagnostic genetic testing. All clinical investigations were conducted according to Declaration of Helsinki principles. This project was approved by the local Institutional Ethical Committee of the Ospedale Pediatrico Bambino Gesù (1702_OPBG_2018), Rome. Clinical data, photographs, DNA specimens, and other biological material were collected, used for genetic analyses, and stored after signed informed consents from the participating subjects/families were obtained. Permission was obtained to publish the photographs of all subjects shown in Figure 1.

All experimental *in vivo* procedures were performed in accordance with national and institutional guidelines for animal care and experiments. Animal handling protocols and experiments were reviewed and approved by the Institute Animal Care and Utilization Committee of Academia Sinica (Protocol ID: 19-11-1358).

Genomic analyses

Genomic analyses were performed using DNA samples obtained from leukocytes. All families except families 4 and 6 were analyzed by WES. Families 4 and 6 were investigated by WGS, the former as part of the 100KGP, a national genome sequencing effort delivered jointly by the UK's National Health Service and Genomics England. Target enrichment kits, sequencing platforms, and WES/WGS statistics are reported in Table S1. Data processing, sequence alignment to GRCh37/GRCh38, and variant filtering and prioritization by allele frequency, predicted functional impact, and inheritance models were performed as previously reported.[22–28] WES data output is summarized in Table S1. Co-segregation analysis was performed by Sanger sequencing in all but family 7. Primer sequences available on request.

Minigene splicing analysis

The *SCUBE3* genomic portion encompassing exons 18 to 21 was amplified by PCR from the MCF-7 cell line genomic DNA (ATCC) (primers available on request). The amplified fragments were cloned into the pGEM-T easy vector (Promega), and clones were randomly selected, and sequenced. The minigene construct was generated by subcloning the *SCUBE3* genomic region of interest into the pEGFP-C2 vector (Clontech). The minigene plasmids were introduced into human HEK293T and MG-63 cells using Lipofectamine 3000. At 48 h after transfection, total RNA was

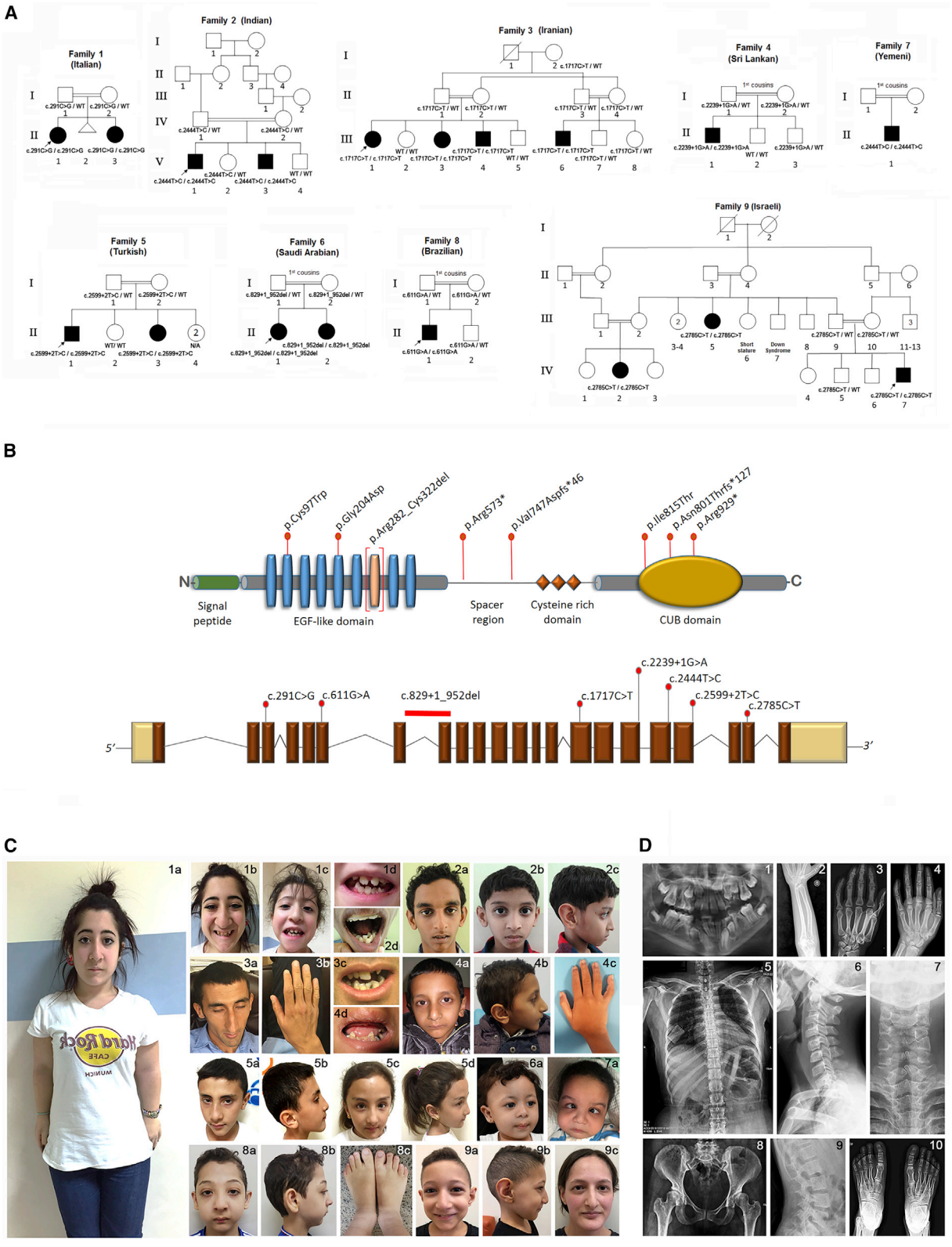

Figure 1. Pedigrees of the families included in the study, domain structure of SCUBE3, and clinical features of subjects with bi-allelic pathogenic *SCUBE3* variants

(A) Pedigrees and segregation data for the nine families included in the study. Affected and unaffected subjects are indicated by filled and open squares/circles, respectively.

(B) Cartoons showing the genomic organization of *SCUBE3* and functional domains of its encoded protein. Location of the disease-causing variants is shown. c.2599+2T>C is predicted to result in multiple aberrantly processed transcripts, with p.Asn801Thrfs*127 representing the prevalent out-of-frame product (see Figure S3).

(legend continued on next page)

extracted by the TRIzol method (Life Technologies), first-strand cDNA was synthesized with SuperScript II reverse transcriptase (Life Technologies), and PCR was performed using a primer pair designed to anneal to exons 18 and 21. The amplified fragments were cloned into the pGEM-T easy vector (Promega). After cloning, at least 10 clones of each transfection were randomly selected, and their sequences were determined by Sanger sequencing.

Plasmids and transfection

SCUBE3 constructs were generated to include a FLAG tag immediately after the signal peptide cleavage site (pFLAG-CMV-1, Sigma) and a Myc tag at the C-terminus (pSecTag2, Invitrogen). HEK293T, HepG2, and SAOS-2 cells were transfected by using Lipofectamine 3000 (Invitrogen) according to the manufacturer's instructions.

Cell cultures

C3H/10T1/2, HEK293T, HepG2, and SAOS-2 cells were from the American Type Culture Collection and cultured according to the supplier's recommendations. Cells were maintained in Eagle's basal medium supplemented with 10% heat-inactivated fetal bovine serum, 2 mM L-glutamine, 100 units/mL penicillin, and 100 μg/mL streptomycin at 37°C, 5% CO_2. Primary chondrocyte culture was performed as previously described,[29] and primary BMSCs were obtained from 4-week-old *Scube3*$^{-/-}$ and control littermates as described.[30]

FACS analysis

Transfected cells were collected and resuspended in FACS buffer (2% FBS PBS). Cell suspensions were incubated with fluorescein-labeled FLAG antibody (Sigma) (4°C, 1 h). After washing with ice-cold PBS three times, cells were resuspended in FACS buffer. FACS analyses were performed using a FACSCalibur (BD Biosciences).

Co-immunoprecipitation assays and western blot analyses

For western blot analyses, transfected cells were lysed on ice in lysis buffer (25 mM HEPES [pH 7.6], 150 mM NaCl, 5 mM EDTA, 10 μg/mL aprotinin, 5 μg/mL leupeptin, 10% glycerol, and 1% Triton X-100). Cell lysates (20 μg) or samples from conditioned medium (20 μL) were separated by SDS-polyacrylamide gel and transferred to PVDF membranes. For immunoprecipitation assays, cell lysates (500 μg) were incubated with 1 μg of the indicated antibody and 20 μL of 50% (v/v) protein A-agarose (GE) (2 h with gentle rocking). The precipitated complexes were then separated by SDS-polyacrylamide gel and transferred to PVDF membranes. After blocking, membranes were incubated with-anti-FLAG (Sigma), anti-HA (Cell Signaling Technology), or anti-Myc antibodies (Cell Signaling Technology) for 1 h. After 3 washes, the blots were incubated with horseradish peroxidase-conjugated goat anti-rabbit IgG (Jackson ImmunoResearch Laboratories) (1 h). The reactive bands were visualized by use of the VisGlow chemiluminescent substrate, HRP system (Visual Protein).

Luciferase reporter assay

HepG2 cells were transfected with the BMP-responsive luciferase reporter, BRE-luc, together with the individual *SCUBE3* constructs (or a mock vector) and a Renilla luciferase reporter as internal control, by using Lipofectamine 3000 (Invitrogen). Cells were cultured for an additional 2 days, harvested, and prepared for reporter assay with the Dual-Luciferase reporter assay system (Promega) according to the manufacturer's instructions.

Alkaline phosphatase activity assay

Cells were washed with PBS and lysed with 0.05% Trixton X-100 solution. Alkaline phosphatase (ALP) activity in lysates was determined by using p-nitrophenol-phosphate as substrate as previously reported.[31]

Confocal laser scanning microscopy

SAOS-2 cells (2×10^4) were seeded in 24-well cluster plates onto 12-mm cover glasses, transfected with the various FLAG-tagged constructs (48 h), and fixed with 4% paraformaldehyde (30 min, 4°C). Cells were stained with mouse monoclonal IgG anti-FLAG M2 (1:500, SIGMA) (2 h, room temperature), rinsed twice with PBS, and incubated with the secondary goat anti-mouse antibody conjugated with Alexa Fluor 594 (1 h, room temperature) (Molecular Probes). After staining, coverslips were rinsed and mounted on slides by using Vectashield mounting medium (Vector Laboratories) containing 1.5 μg/mL DAPI. Alexa Fluor 488 phalloidin dye was used to stain the cortical actin associated with the plasma membrane. Observations were performed on a Leica TCS-SP8X laser-scanning confocal microscope (Leica Microsystems) equipped with a tunable white light laser source and a 405 nm diode laser. Sequential confocal images were acquired by LAS X software (Leica Microsystems) using a HC PLAPO 63x oil-immersion objective (1.40 numerical aperture).

Isolation of lipid rafts

Lipid rafts were prepared as described.[32] In brief, cells were lysed with 1.3 mL ice-cold RIPA buffer. The homogenized lysates were resuspended in a final 40% OptiPrep solution. The mixture was vortexed vigorously and transferred to a 12.5 mL ultracentrifuge tube, and a discontinous OptiPrep gradient (30%, 5%) was formed above the lysate by adding 4 mL 30% OptiPrep and then 4 mL 5% OptiPrep. The gradient was ultracentrifuged (20 h, 39,000 rpm, 4°C). Twelve fractions were collected from top to bottom and designated as fractions 1–12. To verify the separation, a specific caveolin-1 antibody was used.

(C) Clinical features of affected individuals. (1a) Whole body appearance of subject F1S1; (1b, 1c) facies of subjects F1S1 and F1S2; (1d) dental anomalies in F1S2; (2a–2c) facies of subjects F2S1 and F2S2; (2d) dental anomalies in F2S1; (3a) facies of subject F3S3; (3b) finger joint swelling in F3S3; (3c) dental anomalies in F3S3; (4a, 4b) facies of subject F4S1; (4c) 5th finger camptodactyly in F4S1; (4d) dental anomalies in F4S1; (5a–5d) facies of subjects F5S1 and F5S2; (6a) facies of subject F6S1; (7a) facies of subject F7S1; (8a, 8b) facies of subject F8S1; (8c) bilateral shortening of 4th and 5th toes in F8S1; (9a–9c) facies of subjects F9S1 and F9S2.
(D) Radiological findings in affected subjects. (1) dental anomalies in F1S2 shown by panoramic dental X-ray; (2) bowed radius in F2S1; (3) reduced epiphyses including the metacarpal heads, capitate-3rd-metacarpal and trapezoid-2nd-metacarpal coalitions and camptodactyly in F3S1; (4) trapezoid-2nd metacarpal coalition and cuneiform bones-2nd and 3rd metatarsals coalitions in F8S1; (5) absent 12th rib pair in F3S1; (6–7) partial fusion of C5-C6 and failure of the posterior arch fusion in C7-T1 in F8S1; (8) narrow iliac wings in F3S1; (9) squared vertebral bodies in F2S1; (10) tarsal-metatarsal coalition in both feet in F2S1.

Table 1. List of the homozygous pathogenic *SCUBE3* variants identified in the study.

Nucleotide change	dbSNP	MAF	Amino Acid Change	M-CAP	REVEL	CADD	ACMG	Domain	Family, subject
c.291C>G	–	N/A	p.Cys97Trp	0.526729	0.911	26.1	VoUS	EGF-like 2	F1, subjects 1, 2
c.611G>A	–	N/A	p.Gly204Asp	0.576042	0.696	26.2	VoUS	EGF-like 5	F8, subject 1
c.829+1_952del (in-frame exon 8 deletion)	–	N/A	p.Arg282_Cys322del	N/A	N/A	N/A	VoUS	EGF-like 7	F6, subjects 1, 2
c.1717C>T	rs1436996181	0.4E−5	p.Arg573*	N/A	N/A	38	pathogenic	–	F3, subjects 1-4
c.2239+1G>A	–	N/A	p.Val747Aspfs*46	N/A	N/A	34	pathogenic	–	F4, subject 1
c.2444T>C	rs751478115	0.2E−4	p.Ile815Thr	0.078026	0.776	27.9	VoUS	CUB	F2, subjects 1, 2 F7, subject 1
c.2599+2T>C	–	N/A	p.?[a]	N/A	N/A	27.2	pathogenic	–	F5, subjects 1, 2
c.2785C>T	rs1397172310	N/A	p.Arg929*	N/A	N/A	45	pathogenic	–	F9, subjects 1-3

VoUS, variant of uncertain significance. Threshold of pathogenicity of the M-CAP, REVEL and CADD predictive tools: M-CAP > 0.025; REVEL > 0.75; CADD_PHRED > 15.
[a]c.2599+2T>C is predicted to result in multiple aberrantly processed transcripts, with p.Asn801Thrfs*127 representing the prevalent out-of-frame product (see Figure S3).

Mouse phenotyping

Wild-type C57BL/6JNari mice were provided by the National Laboratory Animal Center (NLAC), NARLabs, Taiwan. *Scube3*$^{-/-}$ mice (C57BL/6JNari) were generated as previously described.[21] Adult male mice were used in skeletal phenotype analysis, whereas sex of embryos or neonates was not determined. Radiography, 3-D-reconstructed CT images, and bone mineral density (BMD) analysis were performed as previously described.[33] Alcian blue hematoxylin/orange G staining of paraffin sections was performed as described,[34] with modification. Briefly, deparaffinized sections were placed in acid-alcohol (0.37% hydrochloric acid in 70% ethanol) for 30 s, alcian blue hematoxylin (1% alcian blue in Mayer's acid hematoxylin) for 40 min and washed gently in distilled water to remove excess stain from tissue. Sections were placed in acid-alcohol for 3 s, 0.5% ammonium water for 15 s, 95% EtOH for 1 min, and eosin/orange G solution (0.12% eosin, 0.074% phloxin B, and 0.064% orange G in 90% ethanol [pH 4.8]) for 1 min 30 s. After washing with distilled water, sections were dehydrated and mounted in Entellan new (Merck).

Proliferation assays (BrdU) of skeletal tissue sections

To determine the quantity of newly generated cells, the DNA synthesis marker 5-bromo-2′-deoxyuridine (BrdU) was administered intraperitoneally (50 mg/kg body weight) to mice. A single dose of BrdU was injected into mice at E18. All pups were euthanized, fixed, and processed for BrdU immunohistochemistry on P1.

Micromass culture assay

Micromass cultures of whole E12.5 limb buds were prepared as described.[35]

Quantification and statistical analysis

Data are presented as mean ± SD and were analyzed by Student t test (for 2 groups) or one-way ANOVA (for ≥3 groups) with Tukey multiple comparison analysis by using Prism 7 (GraphPad Software). $p < 0.05$ was considered statistically significant.

Results

Bi-allelic *SCUBE3* variants underlie a disorder affecting development and growth

Nine unrelated consanguineous families with one or more individuals affected by an unrecognized condition severely impairing growth and sharing homozygous putative pathogenic variants in *SCUBE3* (GenBank: NM_152753.4) were identified by GeneMatcher,[36] Decipher,[37] and networking (Table 1, Figures 1A and 1B). All subjects showed a consistent phenotype characterized by peculiar craniofacial features, short stature, and dental and skeletal abnormalities (see below). In all tested individuals, exome/genome sequencing analysis excluded the presence of other functionally relevant variants compatible with known Mendelian diseases based on the expected inheritance model and clinical presentation (Table S1). The identified variants were distributed along the entire *SCUBE3* coding sequence and included nonsense, frameshift, missense, and canonical splice site changes as well as a complex intragenic rearrangement. Genomic DNA was available for relatives from all but family 7, and co-segregation of the trait and homozygosity for the *SCUBE3* variant was confirmed in all families tested (Figures 1A and S1).

Two novel variants were predicted to affect transcript processing (c.2239+1G>A [p.Val747Aspfs*46], family 4; c.2599+2T>C, family 5), and other two were truncating (c.1717C>T [p.Arg573*], rs1436996181, MAF = 0.000004, family 3; c.2785C>T [p.Arg929*], not previously reported, family 9). Total RNA was available for the affected individual of family 4, allowing us to confirm the activation of a cryptic donor site of exon 17, retention of four nucleotides of the flanking intronic region, and premature termination of the coding sequence (p.Val747Aspfs*46) (Figure S2). Biological material from the proband was not available for

functional validation of the c.2599+2T>C variant, which was indirectly attained using a minigene splicing assay, confirming aberrant splicing of the genomic portion of *SCUBE3* encompassing exons 18–21, with occurrence of multiple mRNA variants all predicted to encode prematurely truncated proteins (Figure S3).

Three different missense changes were identified in four families. These variants affected conserved residues among SCUBE3 orthologs and paralogs (Figure S4) and were predicted to be damaging by multiple *in silico* predictors (Table 1). The two affected sibs of family 1 (F1S1 [II-1] and F1S2 [II-3]) were homozygous for a novel substitution (c.291C>G [p.Cys97Trp]) within the second EGF-like module, affecting one of the invariant cysteine residues participating to the disulfide bonding network that stabilizes the structure of the EGF-like domains. Substitution of Cys^{97} implies loss of one of the three conserved disulfide bridges and consequently a structural rearrangement of the motif (Figure S4). Of note, pathogenic variants at equivalent positions in multiple EGF-like modules of the FBN1, FBN2, and LTBP3 proteins have previously been reported (Figure S5),[38–40] further supporting the functional relevance of the variant. Subject F8S1 (family 8, II-1) was homozygous for a previously unreported missense change (c.611G>A [p.Gly204Asp]) affecting a conserved glycine residue within the fifth EGF-like module. The nonconservative substitution was predicted to impair proper module folding locally and impact the interaction with the adjacent EGF-like module (Figure S4). The third missense variant (c.2444T>C [p.Ile815Thr]), identified in families 2 and 7 (F2S1 [V-1], F2S2 [V-3], and F7S1 [II-1]), is a rare substitution (rs751478115, MAF = 0.000024), never reported in the homozygous state, involving a buried apolar residue located in the core of the CUB domain. Its replacement by a polar residue was predicted to considerably destabilize the structure of the hydrophobic cluster involving residues Trp^{832}, Ile^{896}, and Ile^{911} (Figure S4) and, in turn, perturb the overall folding of the domain and its ability to mediate SCUBE3 binding to interactors.

Finally, homozygosity for a complex intragenic rearrangement in *SCUBE3* (deletion plus inverted duplication) was documented in one family (family 6, F6S1 [II-1] and F6S2 [II-2]). The rearrangement was novel and thought to have originated from a two-step fork-switching and template-stalling (FoSTeS) process, causing the complete deletion of exon 8 (c.829_952del [p.Arg282_Cys322del]) with conservation of the coding frame of the *SCUBE3* mRNA, resulting in an EGF-like domain lacking the seventh EGF-like module (Figure S6). Equivalent intragenic structural rearrangements resulting in deletions of single EGF-like modules in FBN1 and FBN2 have previously been reported to dramatically affect protein function.[41,42]

Clinical profiling of subjects with bi-allelic pathogenic *SCUBE3* variants

Detailed clinical information was collected for 15 of the 18 individuals carrying the homozygous *SCUBE3* variants. These subjects shared a consistent condition characterized by short stature, distinctive facial dysmorphia, dental and skeletal anomalies, in the absence of developmental delay or intellectual disability (Figure 1C, Table 2, Supplemental Note: Case Reports). These subjects showed a reduced birth length (<–2 SDS) (8/11), with or without decrease of other birth parameters, and had severely reduced postnatal height and weight (15/15) (Figure S7) and head circumference (9/13). Facial features included a long/triangular face in older individuals with high/broad forehead (14/14), high nasal bridge (13/15), long nose (13/15), which was short and upturned in the two younger subjects (F6S1 and F7S1), thick lips (7/15), and a short or receding chin at young age (14/14), which may become slightly pointed at older ages (11/13) (Figure 1C). Of note, two individuals (F7S1 and F8S1) had the Pierre-Robin sequence, and one (F1S2) had cleft palate and micrognathia. Peculiar dental defects were frequently observed, including enamel dysplasia and hypodontia/oligodontia (7/15). These signs are quite suggestive of disturbance in odontogenesis and might be considered as major key signs of the condition. The remaining eight affected individuals presented with less specific dental findings, such as dental crowding and misalignment, which however strongly indicate that dental involvement is an invariant feature in subjects with bi-allelic inactivating *SCUBE3* variants. Skeletal features occurred in all subjects (15/15), with thin and short long bones (6/11), 11 pairs of ribs (4/13), abnormal vertebrae (6/12), including odontoid hypoplasia and fusions, squared lumbar vertebral bodies (5/13), and scoliosis (6/13) representing recurrent features. Upper and lower limbs presented changes in almost all affected subjects, resulting in short stature with rhizomelia/mesomelia in some instances (Figure 1C). Bowed radius with abnormal radial head occurred in some individuals (F1S1, F1S2, F3S1 [III-1], and F8S1). Shortening of both metacarpal/metatarsal bones and phalanges was documented. Bone age was assessed in four subjects and found delayed in three. Variable joint involvement was also documented (5/8). Other less common features were cardiac anomalies (4/14) and conductive hearing loss (4/12). One subject had ventricular extrasystoles with first degree AV block, while pulmonary hypertension was found in two.

Overall, the consistent phenotype was highly suggestive of a developmental disorder characterized by severe short stature and a distinctive gestalt overlapping, in part, with a recently reported syndromic condition caused by monoallelic loss-of-function variants in *BMP2*.[43] Since the occurrence of a bowed radius and short stature, differential diagnosis may include Lery-weill dyschondrosteosis (MIM: 127300), which however is characterized by the presence of Madelung deformity, whose onset typically occurs mid-to-late childhood and does not present the craniofacial features and enamel dysplasia observed in subjects with bi-allelic inactivating *SCUBE3* variants. The disorder differs from other common conditions with short meso-acromelic involvement, such as geleophysis and

Table 2. Phenotypic features of the 15 individuals with biallelic pathogenic *SCUBE3* variants included in the study.

Individual	F1S1	F1S2	F2S1	F2S2	F3S1	F3S2	F3S3	F4S1	F5S1	F5S2	F6S1	F7S1	F8S1	F9S1	F9S2	
SCUBE3 variant/change	p.Cys97Trp		p.Ile815Thr		p.Arg573*			p.Val747Asp_fs*46	c.2599+2T>C		p.Arg282_Cys322del	p.Ile815Thr	p.Gly204Asp	p.Arg929*		Total (%)
Age	19 y	10 y	22 y	15 y	39 y	29 y	25 y	11.5 y	11.6 y	7.3 y	16 m	26 m	12.8 y	8 y	22.5 y	
Gender	F	F	M	M	F	F	M	M	M	F	F	M	M	M	F	
Prenatal growth retardation (−2 SDS)	+	−	+	+	+	N/A	N/A	+	N/A	N/A	+	+	+	−	−	8/11 (82)
Postnatal growth retardation (−2 SDS)	+	+	+	+	+	+	+	+	+	+	+	+	+	+	+	15/15 (100)
DD/ID	−	−	−	−	−	−	−	−	−	−	−	+	−	−	+	1/15 (7)
Speech delay	−	−	−	−	−	−	−	−	−	−	−	+	−	−	+	3/15 (20)
Hypotonia	−	−	−	−	−	N/A	−	−	−	−	+	+	−	−	−	2/14 (14)
Craniofacial																
Microcephaly (−2 SDS)	−	−	+	+	+	N/A	−	+	+	+	+	N/A	+	−	+	9/13 (69)
Long/triangular face	+	+	+	+	+	+	+	+	+	+	+	N/A	+	+	+	14/14 (100)
High forehead	+	+	+	+	+	+	+	+	+	+	+	+	+	+	+	15/15 (100)
High nasal bridge	+	+	+	+	+	+	+	+	+	+	−	−	+	+	+	13/15 (73)
Long nose	+	+	+	+	+	+	+	+	+	+	−	−	+	+	+	13/15 (87)
Thick lips	+	+	−	+	−	−	−	+	−	−	+	+	+	−	−	7/15 (47)
Short chin	+	+	+	+	+	N/A	+	+	+	+	+	+	+	+	+	14/14 (100)
Pointed chin[a]	+	+	+	+	N/A	N/A	+	+	+	+	−	−	+	+	+	11/13 (85)
Pierre Robin sequence/cleft palate	−	CP	−	−	−	N/A	−	−	−	−	−	PRS	PRS	−	−	3/14 (21)
Dental anomalies	H,DC	H,ED, DC	DC	DC	DC	DC	O, DC	MD,ED,DC,ET	ED	ED	DC,MA	MA	DC	DC	O,DC, MA	15/15 (100)
Skeletal anomalies	+	+	+	+	+	+	+	+	+	+	+	+	+	+	+	15/15 (100)
Short hands/brachydactyly	+	+	+	+	+	+	−	+	+	−	−	+	+	+	+	12/15 (80)
Hip defects	NIW/CV	CV	NIW,CV	NIW, CV	NIW,AD	NIW	N/A	NIW,CV	CV	−	−	−	−	−	−	9/14 (64)
Thin/short long bones	+	+	N/A	N/A	−	N/A	N/A	+	+	+	−	−	+	−	−	6/11 (54)
Squared vertebrae	+	+	−	+	+	N/A	N/A	−	−	−	−	−	+	−	−	5/13 (39)

(*Continued on next page*)

Table 2. *Continued*

Individual	F1S1	F1S2	F2S1	F2S2	F3S1	F3S2	F3S3	F4S1	F5S1	F5S2	F6S1	F7S1	F8S1	F9S1	F9S2	
SCUBE3 variant/change	p.Cys97Trp		p.Ile815Thr		p.Arg573*			p.Val747Asp_fs*46	c.2599+2T>C		p.Arg282_Cys322del	p.Ile815Thr	p.Gly204Asp	p.Arg929*		Total (%)
Abnormal cervical vertebrae	+	+	N/A	N/A	–	N/A	N/A	N/A	–	–	+	–	+	–	–	4/10 (40)
11 pairs of ribs	+	+	–	–	+	N/A	N/A	–	–	–	–	–	+	–	–	4/13 (31)
Scoliosis	+	+	–	+	–	N/A	N/A	–	+	+	–	–	+	–	–	6/13 (46)
Joint abnormalities	+[b]	+[b]	–	–	N/A	N/A	N/A	–	N/A	N/A	+[c]	N/A	+[c]	+[c]	N/A	5/8 (63)
Hearing loss (conductive)	–	–	+	+	–	N/A	+	–	N/A	N/A	–	–	+	–	–	4/12 (33)
Cardiac defects	–	–	–	–	–	N/A	–	–	–	CA	ASD	PFO	–	–	ASD	4/14 (29)
Other defects	–	–	–	–	–	–	–	–	–	–	–	OD,TM, HS, ST	BCC	Ny, SBH	Ny, AST, SBH	

AD, acetabular dysplasia; ASD, atrial septal defect; AST, astigmatism; BCC, bilateral coronal synostosis; CA, cardiac arrhythmia (ventricular extrasystoles, atrioventricular block); CP, cleft palate; CV, coxa valga; DC, dental crowding; ED, enamel dysplasia/multiple caries; ET, ectopic teeth; H, hypodontia; HD, hip dislocation (bilateral); HS, hypospadias; MA, misalignment of incisor; MD, macrodontia; N/A, not assessed; NIW, narrow iliac wing; Ny, nystagmus; O, oligodontia; OD, oropharyngeal dysphagia; PFO, patent foramen ovale; PRS, Pierre Robin sequence; SBH, sparse brittle hair; ST, strabismus; TM, tracheo-bronchomalacia.

[a]This feature becomes more evident at older ages.

[b]Joint hypermobility.

[c]Joint stiffness (F6S1); limited flexion of the proximal interphalangeal joints in both hands (F8S1); limited flexions of fingers, and hand grip difficulties (F9S1).

acromicric dysplasias (MIM: PS231050 and 102370, respectively), by the absence of plump or cone-shaped epiphyses and the distinctive facial features. By reviewing other conditions with short stature and ectodermal defects, the overall phenotype of these subjects may be suggestive of cranioectodermal dysplasia (CED [MIM: PS218330]), a rare ciliopathy characterized by short stature with prevalent rhizomelic shortening, having some facial features reminiscent of the subjects of this series (i.e., frontal bossing, full cheeks, short chin), brachydactyly with mild radiographic changes, and strikingly overlapping dental features. Nonetheless, subjects with bi-allelic *SCUBE3* variants lack macrocrania and other skeletal features distinctive of CED.

SCUBE3 binds to BMP2/4 and BMP receptors, is an enhancer for BMP signaling, and is involved in BMP-dependent osteoblast differentiation

Based on the suggested role of SCUBE3 in BMP/TGF-β signaling,[16] the role of BMP2 in skeletogenesis,[4] and the remarkable phenotypic overlap between the subjects with pathogenic *SCUBE3* variants and those with mutated *BMP2*, we hypothesized a role of SCUBE3 as an auxiliary modulator of BMP2 function. BMPs bind to a subset of type I or type II serine/threonine kinase receptors (BMPR-I and BMPR-II) forming activated heterotetrameric complexes that phosphorylate SMAD proteins, allowing them to translocate to the nucleus and upregulate transcription of ligand-responsive genes.[5] To assess whether SCUBE3 interacts with ligands and receptors of the BMP signaling pathway, co-immunoprecipitation assays were performed using lysates of HEK293T cells transfected to co-overexpress FLAG-tagged SCUBE3 with Myc-tagged BMP2, BMP4, and BMP7, the three major BMP ligands implicated in early limb patterning and skeletogenesis,[44] or TGF-β1, as a negative control. Immunoprecipitation with anti-Myc antibody followed by immunoblotting with anti-FLAG antibody documented co-precipitation of SCUBE3 with BMP2 and BMP4 and a slightly reduced co-immunoprecipitation with BMP7 (Figure 2A). The interaction was specific as no significant co-precipitation was attained with TGF-β1. In addition, domain mapping analysis further revealed that the CUB domain of SCUBE3 could specifically interact with the BMP2 ligand protein (Figure S8). The same experiments were performed co-expressing FLAG-SCUBE3 with HA-BMPR-IA, HA-BMPR-IB, or Myc-BMPR-II in cells stimulated with BMP2 or BMP4 (50 ng/mL, 20 min) or left untreated. The BMPR-I or -II protein was immunoprecipitated with its corresponding anti-epitope antibody and individual immunoprecipitates were analyzed by immunoblotting (Figure 2B). SCUBE3 co-immunoprecipitated with BMPR-IA and BMPR-IB in a ligand-dependent manner, while co-immunoprecipitation with BMPRII was ligand independent. Together, these data suggested a potential BMP ligand-inducible association between SCUBE3 and BMPR-IA or -IB but not BMPR-II.

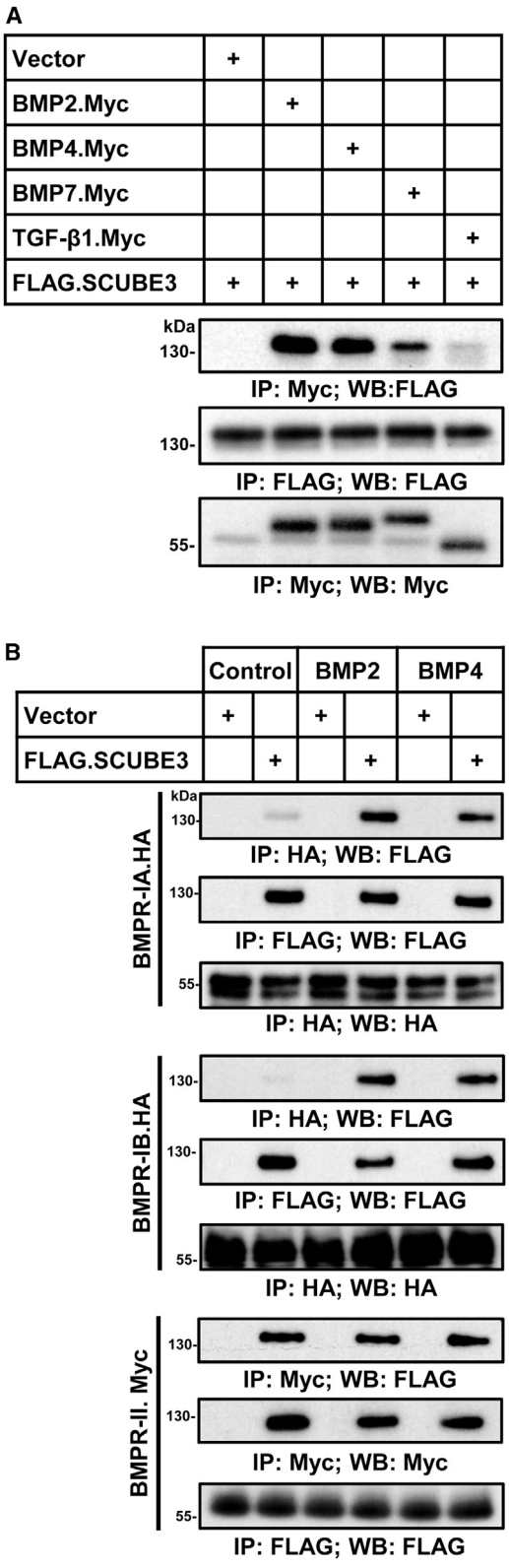

Figure 2. SCUBE3 interacts with ligands and receptors of the BMP signaling pathway

(A) SCUBE3 specifically interacts with BMP proteins but not TGF-β1. The expression plasmids encoding Myc-tagged BMP2, BMP4, BMP7, and TGF-β1 were co-transfected with a FLAG-tagged SCUBE3 construct in HEK293T cells. After 48 h, cell lysates underwent immunoprecipitation (IP), followed by western blot (WB) analysis with indicated antibodies to determine protein-protein interactions. Representative blots from one experiment of three performed are shown.

(B) SCUBE3 interacts with the receptors of the BMP signaling pathway. Plasmids encoding FLAG-tagged SCUBE3 were co-transfected with a HA-tagged BMPRIA, HA-tagged BMPRIB, or Myc-tagged BMPRII construct in HEK293T cells. After 48 h, transfected cells were stimulated with recombinant BMP2 or BMP4 protein for 20 min, and cell lysates were immunoprecipitated. Western blot analysis with the indicated antibodies was performed to determine protein protein interactions. Representative blots from one experiment of three performed are shown.

Based on the clinical phenotype of subjects and the observation that impaired BMP2 and BMP4 signaling is associated with defective bone formation and osteoblast differentiation,[43,45] we further investigated the effect of SCUBE3 on BMP2/4-stimulated osteoblast differentiation by measuring the induced alkaline phosphatase (ALP) activity and the phosphorylation status of Smad1/5/8 in the mouse mesenchymal progenitor cell line C3H10T1/2. Two different *Scube3*-targeting short hairpin RNA lentiviruses (SCUBE3-shRNA #1 and #2) were used to knock down endogenous *Scube3* expression. The specificity and efficiency of shRNA-mediated knockdown of mRNA expression of *Scube3* were validated by RT-PCR analysis (Figure 3A), and a shRNA lentivirus targeting bacterial β-galactosidase (lacZ) was used as negative control. BMP2-, BMP4-, or BMP7-induced ALP activity (Figure 3B) and downstream activation of Smad1/5/8 (Figures 3C and S9A) were significantly and concomitantly suppressed by *Scube3* knockdown. Consistently, ectopic SCUBE3 overexpression in C3H10T1/2 cells resulted in a marked induction of ALP activity (Figures 3D and 3E) as well as in an enhanced BMP2/4-induced phosphorylation of Smad1/5/8 (Figures 3F and S9B). These findings provided evidence of a positive modulatory role of SCUBE3 on BMP2/4 signaling exerting osteogenic function by modulating BMP-stimulated osteoblast differentiation, at least *in vitro*.

Pathogenic *SCUBE3* variants variably affect BMP signaling

The bi-allelic occurrence and wide spectrum of identified variants pointed to a disruptive impact on SCUBE3 function as the pathogenetic mechanism. To validate this hypothesis, the consequences of a representative panel of variants affecting different domains of the protein (p.Cys97Trp, p.Arg573*, and p.Ile815Thr) on SCUBE3 stability, secretion, proper membrane anchoring, and functional behavior were investigated by transient transfection experiments. Western blot analyses using whole cell lysates and conditional media, confocal analysis, and flow cytometry documented that the p.Cys97Trp and p.Ile815Thr variant protein levels were comparable to that of the wild-type SCUBE3 and were properly secreted and tethered on the cell surface; in contrast, while the truncated variant protein levels were comparable to the wild-type counterpart, it was neither expressed on the cell surface nor was secreted in the medium, providing

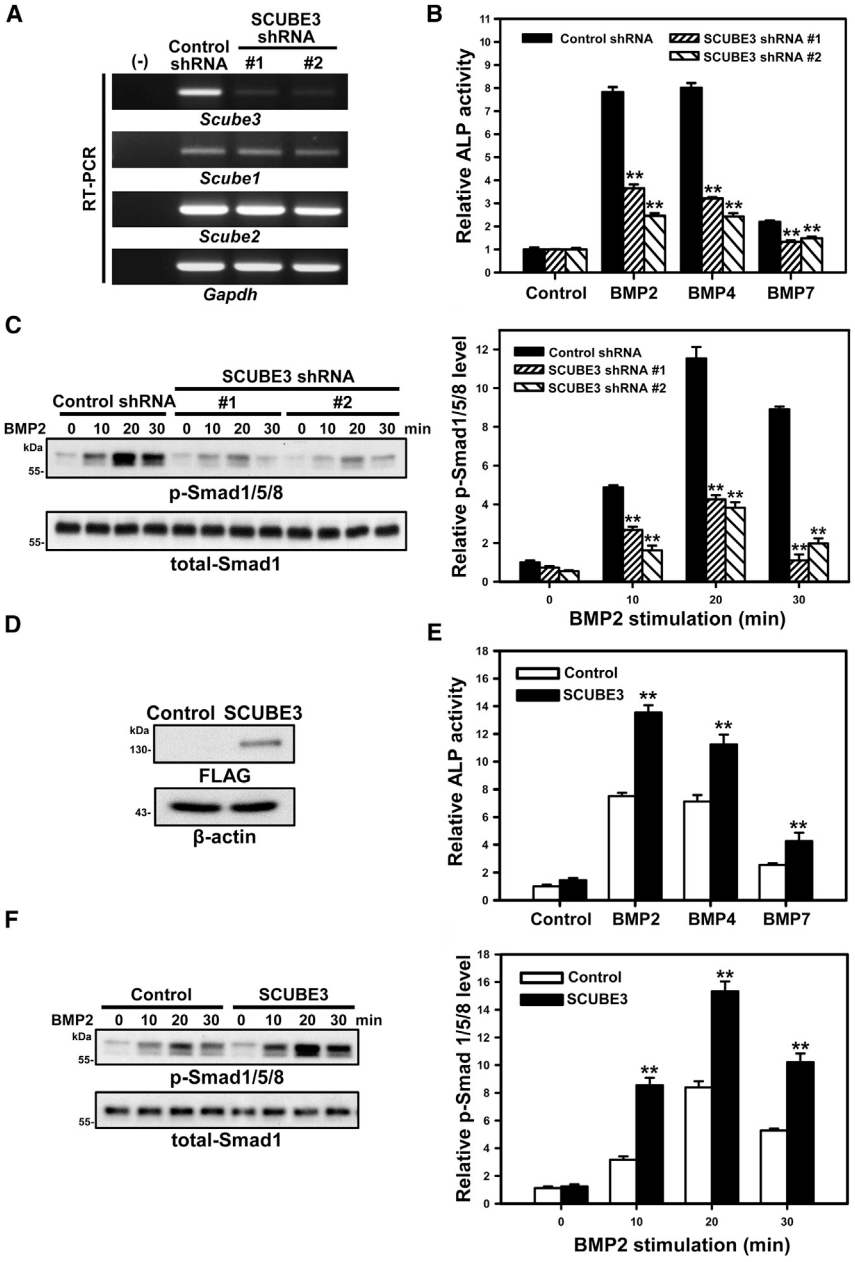

Figure 3. SCUBE3 is an enhancer of BMP signaling and is involved in BMP-induced osteoblast differentiation

(A) Endogenous *SCUBE3* expression was suppressed by two different *SCUBE3*-targeting short hairpin RNA (shRNA) lentiviruses (SCUBE3-shRNA #1 or #2). A luciferase shRNA lentivirus was used as a negative control (Control-shRNA). The efficiency and specificity of Scube3 mRNA knockdown was confirmed by RT-PCR. *Gapdh* mRNA level was used as internal control. Expression levels from one experiment of three performed are shown.

(B) C3H10T1/2 cells expressing control-shRNA or *SCUBE3*-targeting shRNAs were cultured without or with BMP (50 ng/mL) for 7 days. Relative ALP activity normalized with control values is shown. The experiments were performed 3 times in triplicate. Data are mean ± SD. **p < 0.01.

(C) Effect of *SCUBE3* knockdown on the BMP2-stimulated phosphorylation of Smad1/5/8 were assessed by western blot analysis, and total-Smad1 expression was used as an internal control (left panel). Quantification by densitometric analysis of BMP2-induced phosphorylation of Smad1/5/8 in control or *SCUBE3* knockdown C3H10T1/2 cells. Data are mean ± SD from 3 independent experiments. **p < 0.01 (right panel).

(D) Exogenous expression of FLAG-tagged *SCUBE3* in C3H10T1/2 cells by a recombinant lentivirus. Protein overexpression of SCUBE3 was confirmed by western blot analysis. β-actin was used as internal control. Representative blots from one experiment of three performed are shown.

(E) SCUBE3 overexpression enhances BMP2-stimulated osteoblast differentiation in C3H10T1/2 cells. C3H10T1/2 control (empty lentivirus) or *SCUBE3*-overexpressing cells were cultured with or without BMP (50 ng/mL) for 7 days. Relative ALP activity was calculated by normalizing with the respective control value. The experiments were performed 3 times in triplicate. Data are mean ± SD. **p < 0.01.

(F) *SCUBE3* overexpression enhances BMP2 downstream signaling in C3H10T1/2 cells. Western blot analysis (left panel) and quantification (right panel) of BMP2-induced phosphorylation of Smad1/5/8 with control and *SCUBE3* overexpression in C3H10T1/2 cells. Data are mean ± SD from three independent experiments. **p < 0.01.

evidence of protein mistargeting possibly due to a trafficking defect and endoplasmic reticulum retention (Figures 4A and 4B). For this nonsense variant, an impact on mRNA stability due to nonsense-mediated decay as an alternative loss-of-function effect could not be assessed experimentally and cannot be ruled out.

SCUBE proteins are known to both homo- and heterodimerize.[11] To evaluate a possible impact of mutations on dimerization, HEK293T cells were transfected to express FLAG-tagged wild-type SCUBE3 or individual variants with the respective Myc-tagged SCUBE3 proteins. Co-immunoprecipitation assays documented a reduced homodimerization of the p.Cys97Trp variant protein compared to wild-type SCUBE3, and the p.Arg573* and p.Ile815Thr variants (Figure S10A), suggesting a diverse mechanism of functional dysregulation promoted by the variants affecting the EGF-like and CUB domains. Co-transfection experiments using FLAG-tagged SCUBE1, SCUBE2, and SCUBE3 with Myc-tagged wild-type SCUBE3 or the p.Cys97Trp variant documented a less efficient dimerization of the variant with wild-type SCUBE3, while no significant difference was observed in its binding to SCUBE1 and SCUBE2 (Figure S10B).

Based on the positive modulatory role of SCUBE3 on BMP signaling, a BMP2 transactivation assay was finally performed to assess the impact of mutations on proper

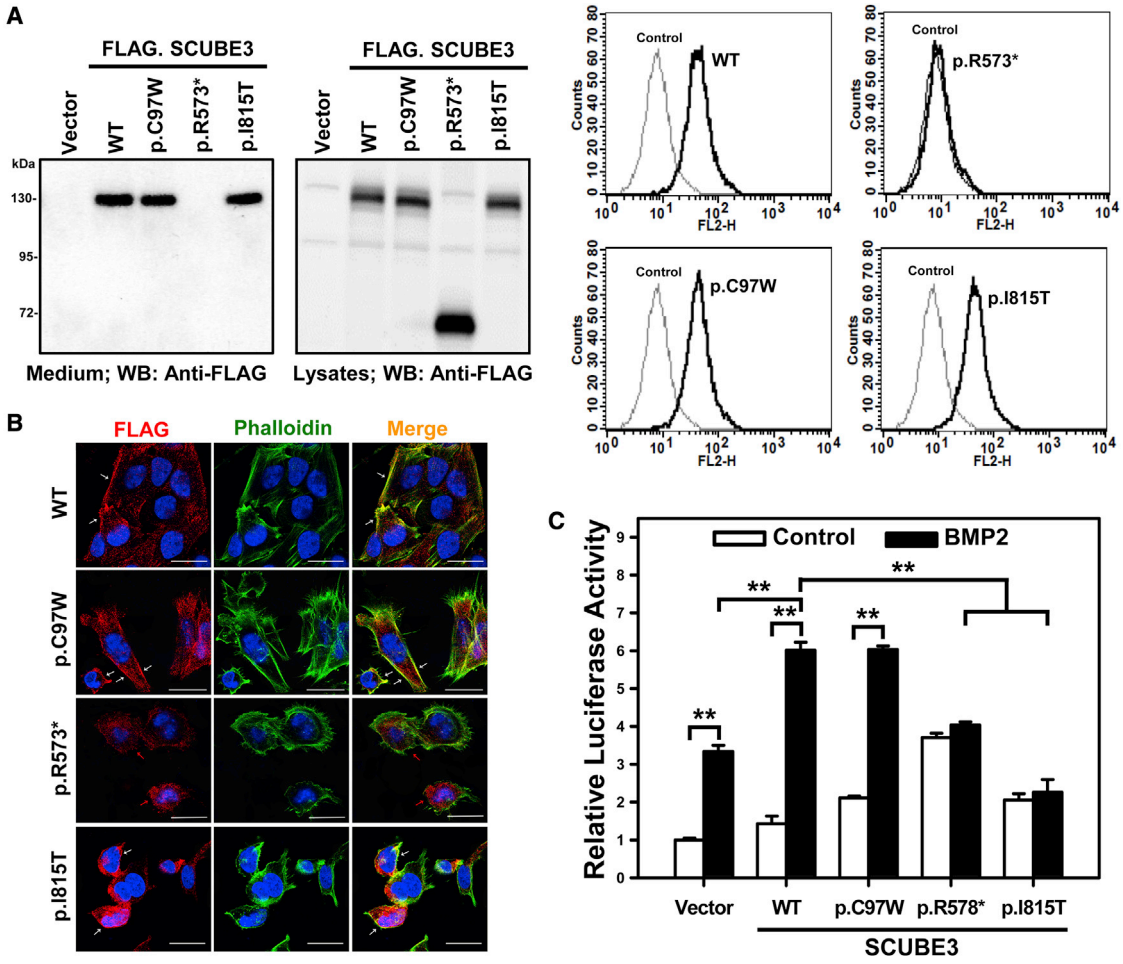

Figure 4. Effect of disease-causing *SCUBE3* variants on cell-surface protein levels and secretion and on BMP2 signaling
(A) SCUBE3 levels were analyzed in HEK293T cells. Samples from conditioned media and total cell lysates were collected and analyzed by western blot analysis using an anti-FLAG antibody (left panel). Empty vector-transfected cells were used as control. Representative blots from single experiments of three performed each are shown. A set of transfected cells was stained with anti-FLAG antibody and underwent flow cytometry (right panel).
(B) SAOS-2 cells were transfected with the expression plasmids encoding wild-type (WT) SCUBE3 and disease-associated variants (p.Cys97Trp, p.Arg573*, and p.Ile815Thr). After 48 h, transfected cells were stained with mouse anti-FLAG antibody, Alexa Fluor 594 goat anti-mouse secondary antibody (red) and were analyzed by confocal microscopy. Alexa Fluor 488 phalloidin dye was used to stain the cortical actin associated with the plasma membrane (green). Nuclei are DAPI stained (blue). Merged images are shown in the right panels. White arrows indicate the distribution of the SCUBE3 proteins on the cellular surface in transfected cells. Red arrows indicate the dispersed localization of the p.Arg573* SCUBE3 variant in transfected cells. Scale bars represent 25 μm.
(C) HepG2 cells were transfected with the BMP-responsive luciferase reporter (BRE-luc) and pRL-TK alone or with the indicated expression plasmids. After 24 h, transfected cells were incubated for another 24 h with and without BMP2 (50 ng/mL), then luciferase activity was measured. Relative luciferase activity represents firefly luciferase values normalized to Renilla activity. The experiments were performed 3 times in triplicate. Data are mean ± SD. **$p < 0.01$.

boosting of BMP signaling. HepG2 cells were transfected with a BMP-responsive luciferase reporter (BRE-Luc) alone or with wild-type SCUBE3 or each variant protein (Figure 4C), and stimulated with BMP2 (50 ng/mL, 24 h) or left unstimulated. While overexpression of the wild-type protein resulted in a 5-fold increase of BMP2 signaling activity, no difference in the transactivation activity of cells expressing the p.Ile815Thr or p.Arg573* SCUBE3 protein was observed after BMP2 stimulation, indicating a disruptive effect of both mutants on BMP signaling *in vitro*. No reduction in the transactivation assay was observed in cells expressing the p.Cys97Trp SCUBE3 protein, supporting further the view of a different perturbing effect of pathogenic variants affecting the EGF-like modules, at least in the used experimental conditions.

Scube3$^{-/-}$ mice have defective skeletogenesis and compromised endochondral bone formation due to defective BMP signaling

We performed a detailed phenotypic and molecular characterization of a previously generated *Scube3* knock-out mouse model.[21] As previously reported, *Scube3*$^{-/-}$ mice were viable and did not show any macroscopically visible abnormality at birth. However, *Scube3*$^{-/-}$ pups

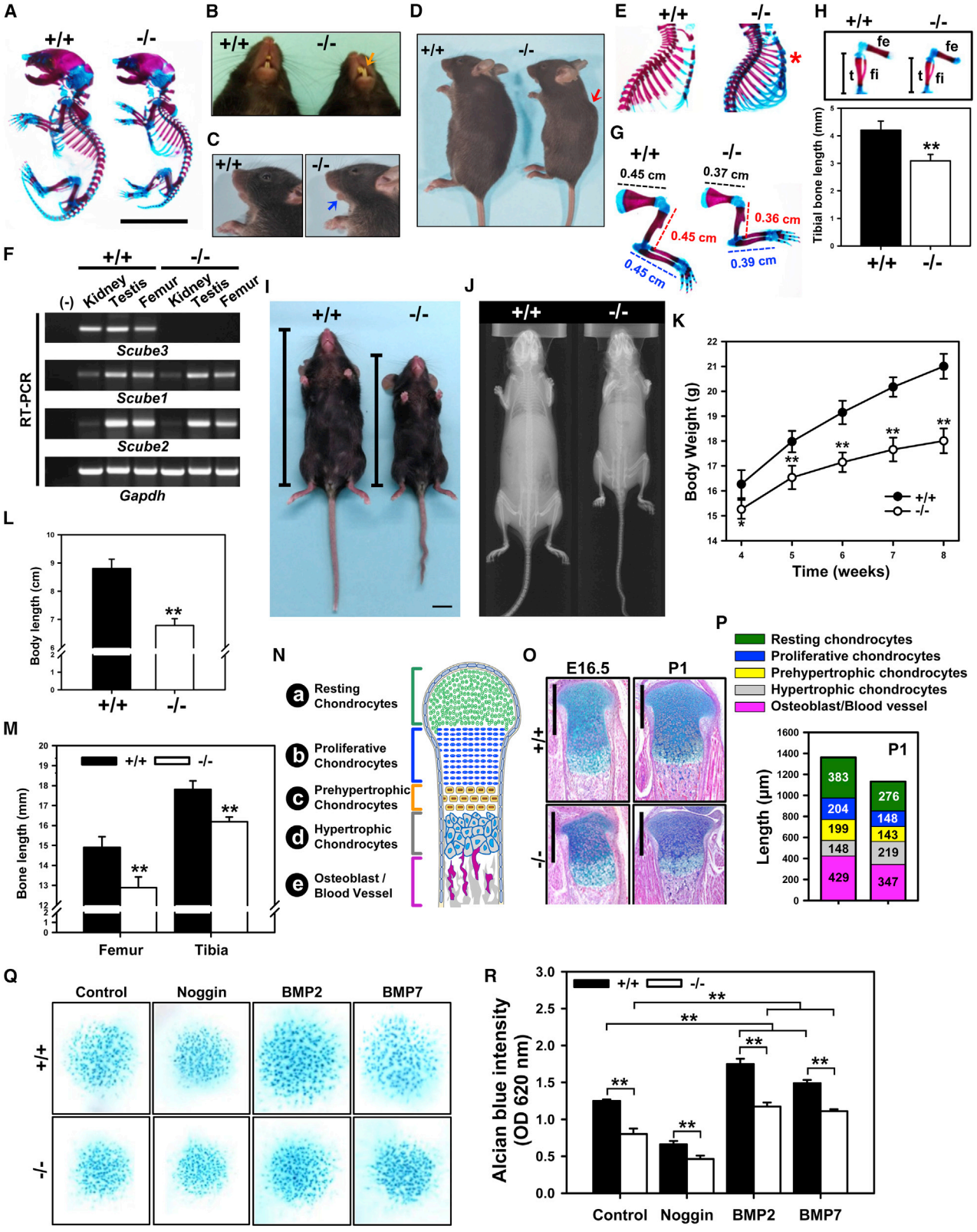

Figure 5. Impaired endochondral bone formation and chondrogenesis in *Scube3*-deficient mice

(A) Skeletons of WT *Scube3* (+/+) and *Scube3* KO (−/−) newborns (P1) stained with Alizarin red (calcified tissue) and Alcian blue (cartilage). Scale bar = 1 cm.

(B) Misaligned incisors observed in −/− 8-week-old mice.

(C) Small lower jaw in −/− 8-week-old mice.

(D) Hunchback spine in −/− 8-week-old mice.

(legend continued on next page)

(P1, postnatal day 1) were shorter than their control littermates (Figure 5A). Consistent with the clinical features of affected individuals, *Scube3*$^{-/-}$ animals also showed misaligned upper/lower incisors (Figure 5B) and altered craniofacial development, including a shorter and narrower face, a smaller forehead, and a shorten frontonasal and mandibular region (Figure 5C). Occasionally, a hunchback spine (Figure 5D) and protruding rib cage (Figure 5E) were also observed.

Based on the reduced growth and skeletal features associated with bi-allelic *SCUBE3* variants, we explored the role of Scube3 on processes linked to skeletal development. RT-PCR and quantitative RT-PCR analyses performed on control newborn pups showed that *Scube3* expression is highly expressed in long bone tissues as compared with *Scube1* and *Scube2* (Figure S11). Of note, loss of *Scube3* expression did not induce compensatory upregulation of *Scube1* and *Scube2* in femoral tissues (Figure 5F). Immunohistochemical staining revealed that *Scube3* is specifically expressed in the periosteum and trabecular endosteum, where osteoprogenitor cells and osteoblasts reside (Figure S12). High expression levels were also observed in proliferative/prehypertrophic chondrocytes of the growth plate, where also BMP2 and BMP4 are highly expressed,[46,47] suggesting a role of the protein in BMP-mediated chondrogenesis and/or osteoblastogenesis.

In line with the skeletal expression of *Scube3*, Alcian blue (chondrocyte matrix) and Alizarin red (mineralized tissue) staining documented proper position and number of the skeletal elements in *Scube3*$^{-/-}$ mice. Yet, skeletogenesis was apparently defective, with all appendicular (forelimbs and hindlimbs) and axial (skull, vertebral column, and rib cage) skeletal elements smaller in *Scube3*$^{-/-}$ mice compared control littermates (Figures 5A, 5E, 5G, and 5H). The defective skeletal growth persisted up to adulthood, as the adult body size was reduced as compared with control littermates and the general skeletal structure (e.g., skull, axial skeleton, ribs, pelvis, and long bones), as revealed by whole-body radiography, appeared grossly normal but smaller than control animals (Figures 5I and 5J). Quantification of physical parameters revealed reduced body weight (−14%), nose-to-anus body length (−23%), femoral bone length (−14%), and tibial bone length (−9%) (Figures 5K–5M). In line with these findings, micro-CT analysis revealed a marked reduction of trabecular volumetric bone mineral density (−22%), trabecular bone volume (−42%), trabecular thickness (−17%), and trabecular number (−37%) (data not shown). Analysis of the growth plate structure of proximal tibia of *Scube3*$^{-/-}$ embryos (E16.5) and pups (P1) documented a consistently reduced length of the plate compared to age-matched littermates (Figures 5N and 5O). Histological analysis also revealed a significant reduction in length of the resting, proliferative, and prehypertrophic chondrocyte zone of growth plates in P1 *Scube3*$^{-/-}$ pups compared to control animals (Figures 5P and S13A). In addition, a significant reduction of the osteoblast/blood vessel invasion zone was observed, indicating reduced endochondral ossification at the growth plates (Figures 5P and S13A). Notably, osteoblasts derived from *Scube3*$^{-/-}$ embryos (E18.5) cultured in osteogenic differentiation media showed reduced ALP activity compared to the corresponding osteoblast cultures from control embryos (Figure S14). Furthermore, high-density micromass cell cultures of embryonic tibiae mesenchymal cells from *Scube3*$^{-/-}$ and control animals documented less efficient chondrogenic differentiation in the former (Figures 5Q and 5R). These cells were less responsive to BMP2- or BMP7-stimulated chondrogenic differentiation, suggesting a costimulatory role of Scube3 in BMP-mediated osteo-/chondrogenesis (Figures 5Q and 5R). We further analyzed chondrocyte proliferation by BrdU labeling and showed that chondrocyte proliferation in tibiae was markedly reduced (−70%) in P1 *Scube3*$^{-/-}$ mice compared to control animals (Figures S13B and S13C). Finally, the expression of a panel of osteogenic markers (i.e., *Runx2*, *Col1a1*, *Alpl*, *Bglap*, *Osx*, and

(E) Thoracic cavity of +/+ and −/− animals (P1) stained with Alizarin red and Alcian blue. The asterisk shows the sternum protrusion in −/− mice.
(F) RT-PCT analysis of Scube1/2/3 expression in kidney, testis and femur from +/+ and −/− adult animals (8 week-old). Expression of Gapdh was used as an internal control. The experiments were performed 3 times.
(G) Forelimb of +/+ and −/− animals (P1) stained with Alizarin red and Alcian blue. The dotted line indicates the corresponding length.
(H) Hindlimbs of +/+ and −/− animals (P1) stained with Alizarin red and Alcian blue. fe, femur; t, tibia; fi, fibula. Tibial lengths are marked (upper panel) and quantified (lower panel). Data are mean ± SD (n = 5 in each group). **p < 0.01.
(I) Photographs of adult (8-week-old) +/+ and −/− mice (nose-to-anus was marked). Scale bar = 1 cm.
(J) Whole-body radiographs. X-ray images of 8-week-old +/+ and −/− male mice.
(K) Body weight from 4- to 8-week-old +/+ (n = 7) and −/− (n = 9) mice. Data are mean ± SD. **p < 0.01.
(L) Body length of 8-week-old +/+ (n = 7) and −/− (n = 9) mice. Data are mean ± SD. **p < 0.01.
(M) Femur and tibia length of 8-week-old +/+ (n = 8) and −/− (n = 7) mice. Data are mean ± SD. **p < 0.01.
(N) Graphic illustration showing the structure of the growth plate, including resting chondrocytes (a), proliferative chondrocytes (b), prehypertrophic chondrocytes (c), hypertrophic chondrocytes (d), and osteoblast/blood vessel (e).
(O) Alcian blue hematoxylin/orange G staining showing a shorter growth plate in E16.5 (n = 5) and P1 (n = 6) −/− mice. Scale bar = 100 μm.
(P) Quantification of different chondrocyte layer lengths in growth plates of P1 +/+ and −/− animals (n = 6).
(Q and R) Chondrocyte micromass cultures of mesenchymal cells from E12.5 +/+ (n = 5) and −/− (n = 5) mouse limbs treated with/without BMP signaling inhibitor (noggin) (50 ng/mL), BMP2 or BMP7 for 9 d (Q). Alcian blue staining was quantified by solubilizing the sample in 6 M guanidine hydrochloride, followed by OD_{620} measurement by spectrophotometry (R). Data are mean ± SD (n = 5). **p < 0.01.

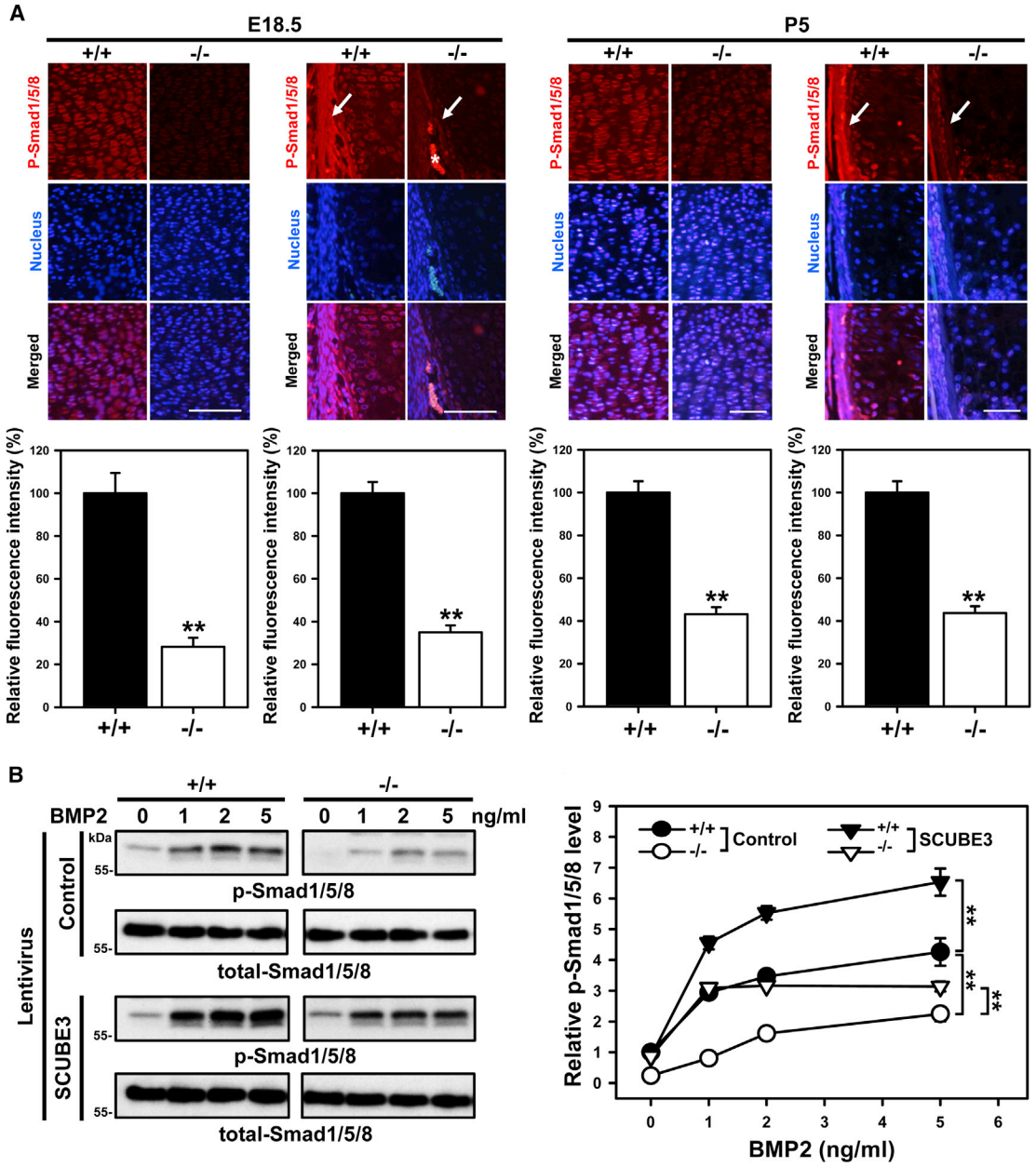

Figure 6. Reduction of Smad1/5/8 phosphorylation in Scube3-deficient proliferative chondrocytes and periosteal osteoprogenitor cells

(A) Immunohistochemical analysis of p-Smad1/5/8 in proliferative chondrocytes (left panel) and periosteal osteoprogenitor cells (right panel) of E18.5 or P5 *Scube3* wild-type (+/+) or knock-out (−/−) mouse bone tissues. Sections of tibiae were stained with a rabbit polyclonal antibody for p-Smad1/5/8. Arrows marked p-Smad1/5/8 signal within periosteal osteoprogenitor cells. The asterisk indicates red blood cell autofluorescence. Scale bar = 100 μm. Fluorescence intensity of p-Smad1/5/8 signals was quantified by ImageJ. Data are mean ± SD (n = 5 in each group). **$p < 0.01$.

(B) SCUBE3 modulates BMP2 signaling in primary cultured chondrocytes. Chondrocytes were isolated from +/+ and −/− mice (P2). Exogenous *SCUBE3* expression was produced by *SCUBE3* lentiviruses. Chondrocytes were serum-starved overnight, then stimulated with indicated doses of BMP2 for 20 min. Western blot analysis (left panel) and quantification (right panel) of BMP2-induced phosphorylation of Smad1/5/8 in chondrocytes. Data are mean ± SD from 3 independent experiments. **$p < 0.01$.

Bsp) was markedly reduced in *Scube3*$^{-/-}$ cultured chondrocytes and isolated long bones (Figure S15).

To further confirm the positive co-receptor role of Scube3 in promoting BMP signaling, the phosphorylation status of Smad1/5/8 was examined in proliferative chondrocytes and periosteal osteoprogenitor cells in long-bone sections of embryonic (E18.5) and postnatal stages (P5) *Scube3*$^{-/-}$ animals by immunofluorescence staining, and in freshly isolated chondrocytes treated with recombinant BMP2 by western blot analysis. In both *ex vivo* and *in vitro* conditions, Smad1/5/8 phosphorylation was significantly decreased in *Scube3*$^{-/-}$ mice-derived tissues/cells (Figures 6A and 6B).

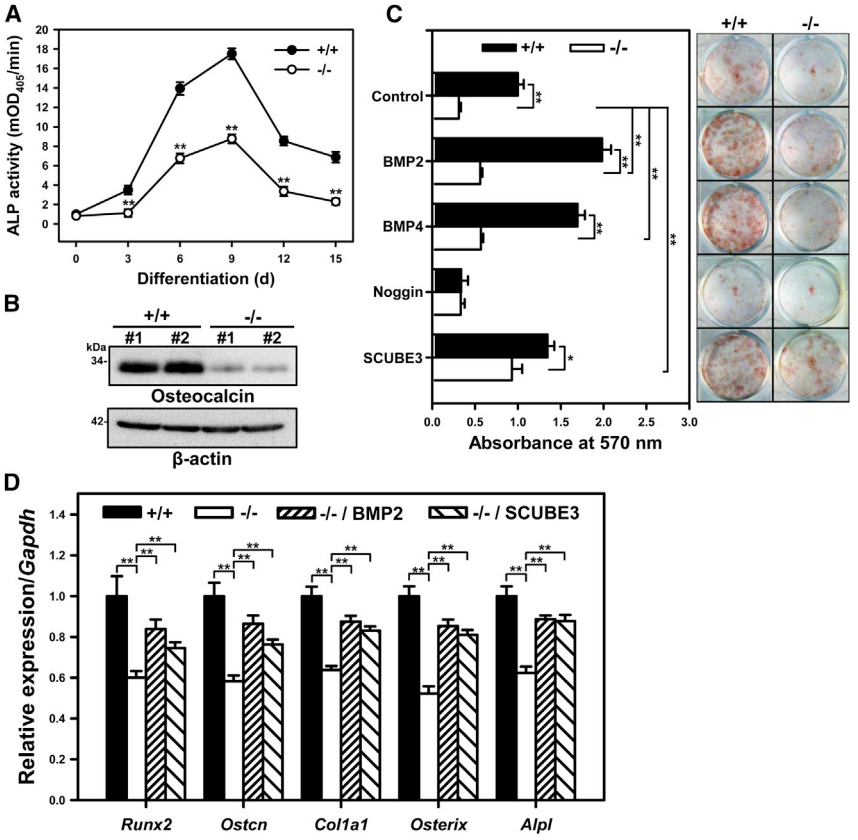

Figure 7. *Ex vivo* osteogenic differentiation of *Scube3*$^{+/+}$ and *Scube3*$^{-/-}$ bone-marrow stromal cell (BMSCs) assessed by ALP activity, osteocalcin expression, and Alizarin red staining

(A) ALP activity of *Scube3* wild-type (+/+) and knock-out (−/−) BMSCs under osteoblast differentiation conditions at days 3, 6, 9, 12, and 15. The experiments were performed 3 times in triplicate. Data are mean ± SD mOD405, milli-absorbance units at 405 nm. **p < 0.01.

(B) The protein expression of osteocalcin in +/+ and −/− BMSCs under osteoblast differentiation conditions at day 9. Two independent BMSC cultures (#1 and #2) were used for western blot analysis, and each experiment was performed 3 times.

(C) Bone nodule formation in BMSC cultures under osteoblast differentiation conditions (right panel). Quantification of Alizarin red staining (left panel). The experiments were performed 3 times in triplicate. Data are mean ± SD. *p < 0.05; **p < 0.01.

(D) The mRNA expression of direct targets of BMP signal activity and osteoblast marker genes in +/+ and −/− BMSCs under osteoblast differentiation conditions at day 9. The experiments were performed 3 times in triplicate. Data are mean ± SD. **p < 0.01.

Consistently, BMP2 treatment increased Smad1/5/8 phosphorylation in a dose-dependent manner in control chondrocytes, while a significantly less efficient induction was observed in *Scube3*$^{-/-}$ cultures (Figure 6B). Notably, lentivirus-mediated ectopic expression of *Scube3* rescued the defective BMP2 signaling in *Scube3*$^{-/-}$ chondrocytes and further enhanced BMP2 signaling in control chondrocytes (Figure 6B), confirming the role of the protein in regulating BMP-induced Smad signaling in proliferative chondrocytes and periosteal osteoprogenitor cells.

To test the hypothesis that *Scube3*$^{-/-}$ mice have defective osteoblast differentiation, bone-marrow stromal cells (BMSCs) derived from *Scube3*$^{-/-}$ and control mice were cultured in osteogenic differentiation media, and the degree of *ex vivo* osteogenic differentiation was evaluated by measuring ALP activity, osteocalcin expression, and Alizarin red staining for matrix mineralization. ALP activity increased over time and peaked at day 9 in BMSC cultures for both genotypes, with marked reduced level in *Scube3*$^{-/-}$ cell cultures (by 30% to 50%) (Figure 7A). Likewise, protein levels of osteocalcin were significantly lower in *Scube3*$^{-/-}$ cell cultures (>90%) (Figure 7B), and matrix mineralization was significantly reduced both basally and following stimulation with BMP2 or BMP4 (Figure 7C). Of note, restoration of SCUBE3 levels by lentiviral ectopic expression rescued, in part, matrix mineralization (Figure 7C). Consistent with these findings, *Scube3*$^{-/-}$ BMSC osteogenic cultures showed a reduced expression of diverse osteogenic marker genes (e.g., *Runx2*, *Ostcn*, *Col1a1*, *Osterix*, and *Alpl*); such defects could be rescued by the exogenous addition of BMP2 or ectopic expression of SCUBE3 (Figure 7D), further demonstrating that BMP2/4 signaling is involved in *Scube3*-mediated osteoblast differentiation and bone matrix production.

Overall, the collected data indicate that *Scube3*$^{-/-}$ mice have craniofacial and dental defects, reduced body size, and defective endochondral bone growth, recapitulating the human disorder, and that defective skeletogenesis and compromised endochondral bone formation results from defective BMP signaling.

Scube3 is required for BMP receptor complex recruitment in lipid rafts

Because BMP receptor association with membrane microdomains (i.e., lipid rafts) is a critical event for BMP signaling[48] and overexpressed SCUBE3 is a raft-associated protein (Figures S16A and S16B), we examined whether raft recruitment of BMP receptors is altered in *Scube3*$^{-/-}$ chondrocytes. Quantitative PCR and western blot analyses showed a comparable level of osteogenic BMP ligands and their receptor subunits in *Scube3*$^{-/-}$ and control chondrocytes (Figure S17). Chondrocytes were homogenized and fractionated by Opti-Prep density gradient centrifugation. Among the 12 isolated fractions, fraction 5 was identified as the lipid raft fraction, as shown by the distribution of the raft marker protein, caveolin-1.[49] BMP receptors (IA, IB, and II) do not localize in the raft fraction under

unstimulated conditions (data not shown), but translocated into the lipid raft fraction following BMP stimulation (Figure S16C). Strikingly, this BMP-induced raft association of BMP receptors was completely abolished in *Scube3*$^{-/-}$ chondrocytes (Figure S16C), indicating a requirement of SCUBE3 for this stimulus-dependent redistribution of receptors. Overall, these data suggest a model in which SCUBE3 facilitates BMP2-induced BMP receptor association with lipid raft microdomains.

Discussion

The three members of the *SCUBE* gene family encode cell surface-anchored glycoproteins functioning as auxiliary receptors to modulate signaling elicited by a variety of growth factors. Despite their versatile role in signaling, these proteins had not previously been implicated in Mendelian diseases. Here we establish that bi-allelic, mostly inactivating variants in *SCUBE3* underlie a recognizable developmental disorder and mechanistically link the defective growth characterizing this novel condition to a compromised endochondral bone formation due to defective BMP signaling.

SCUBE3 has been reported to be highly expressed in primary osteoblasts and long bones, as well as in cartilaginous condensation regions of the axial skeleton, including ribs and vertebrae.[11,50] In mice, the protein has been detected in ectodermal, mesodermal, and endodermal derivatives.[21] SCUBE3 has been proposed to modulate FGF, hedgehog, and TGF-β signaling,[16,20,32,51] even though the precise molecular mechanisms implicated in signal modulation have not been characterized in detail. Conflicting data have apparently been collected regarding its role during development.[21,52] Our findings indicate that, despite being dispensable for embryogenesis, Scube3 is required for appropriate skeletal development and growth. Specifically, we show that Scube3 contributes to fine-tuning BMP-dependent endochondral bone formation by regulating both chondrogenic differentiation and chondrocyte proliferation and also osteogenic differentiation. Of note, this osteogenic function is reminiscent of biglycan, which directly binds BMP2 and its receptors to accelerate osteoblast differentiation by positively modulating BMP2/4 activity.[53]

We show that cell surface-bound SCUBE3 is expressed in osteoblasts and chondrocytes and likely functions as a BMP2/4 co-receptor in a cell-autonomous manner. Mechanistically, our data reveal that SCUBE3 facilitates BMP2/4 ligand binding with BMP type I receptors and promotes BMP-induced BMP receptor complex association with lipid rafts, which are cholesterol- and caveolin-enriched domains serving as signaling platforms.[54] These findings suggest a model in which SCUBE3 might form a complex with heterodimerized BMP receptors to facilitate and stabilize the BMP receptor complex in the lipid rafts. The precise nature and kinetics of SCUBE3-assisted recruitment of BMP receptor complexes in lipid rafts remains to be further investigated.

Detailed clinical phenotyping of 15 affected individuals allows us to profile the disorder resulting from impaired SCUBE3 function as a relatively homogeneous recessive trait characterized by short stature, perturbed skeletal and tooth development, and a distinctive facies. Notably, the condition overlaps, in part, with the disorder caused by heterozygous loss-of-function *BMP2* mutations, whose cardinal features include short stature, skeletal malformations, dental crowding and enamel defects, palatal anomalies, and congenital heart defects.[43] The observation that flawed tooth development and altered bone metabolism are recurrently associated with inactivating mutations in *BMP4*[45] further highlights the clinical relatedness and functional link of SCUBE3 with the two BMP ligands. In the context of bone metabolism, subjects harboring *BMP4* mutations manifested early-onset osteopenia or osteoporosis. Although we could not perform bone densitometry in any subject of the present cohort, a marked reduction of trabecular volumetric bone mineral density (−22%) in *Scube3*$^{-/-}$ mice was observed compared to control animals. Remarkably, a similar phenotype had previously been reported in *BMP2*$^{-/-}$ mice.[55] It should be noted that, differently from other human disorders linked to dysfunctional BMP signaling, these clinically related conditions do not show evidence of bone dysplasia.[4]

Consistent with the clinical features shared by the reported subjects with bi-allelic inactivating *SCUBE3* variants, *Scube3*$^{-/-}$ mice displayed reduced growth associated with smaller forelimbs and hindlimbs. In addition, *Scube3*$^{-/-}$ mice frequently showed misaligned upper and lower incisors and craniofacial defects, including a shorter and narrower face, smaller forehead, and reduced frontonasal and mandibular regions. Occasionally, a protruding rib cage or hunchback spine was also observed. While no overt phenotype had previously been reported in *Scube3*$^{-/-}$ mice, features consistent with those we presently observed were reported in homozygous mice carrying a missense change within the seventh EGF-like domain of the protein (p.Asn294Lys), including skeletal defects (reduced upper and lower limbs, vertebral and thoracic malformations), altered bone metabolism, and conductive hearing loss.[52] Additional investigations are required to further clarify this issue.

While our functional studies support the idea that disease-causing *SCUBE3* variants differentially impact protein synthesis, processing (i.e., secretion), and function (dimerization versus enhancement of BMP2 signaling), the molecular impact of the variants affecting the EGF-like domain on intracellular signaling remains to be characterized. Consistent with our findings, pathogenic variants at equivalent positions within EGF-like domains have been identified in other proteins (e.g., FBN1, FBN2, and LTBP3) and proven to impair TGF-β signaling,[38–40] and a bi-allelic missense variant (p.Asn294Lys) within the seventh EGF-like module in the mouse Scube3 ortholog has

been shown to cause morphological abnormalities of the skeleton and alteration of bone metabolism.[52] We speculate that this group of mutations may hamper specific processes linked to the extracellular microenvironment, including protein-matrix assembly and protein shedding from the membrane,[51,56] which, in turn, control or modulate SCUBE3 function.[57]

In summary, we identify a developmental disorder caused by defective function of SCUBE3, link this secreted glycoprotein to processes controlling growth, morphogenesis, and teeth development, and provide evidence of its relevant role in BMP signaling-mediated skeletogenesis.

Data and Code Availability

All mutations identified in this work have been submitted to ClinVar (Genbank: NM_152753.4: c.291C>G, SCV001438405; NM_152753.4: c.611G>A, SCV001438406; NM_152753.4: c.829+1_952del, SCV001438407; NM_152753.4: c.1717C>T, SCV001438408; NM_152753.4: c.2239+1G>A, SCV001438409; NM_152753.4: c.2444T>C, SCV001438410; NM_152753.4: c.2599+2T>C, SCV001438411; NM_152753.4: c.2785C>T, SCV001438412). WES datasets have not been deposited in a public repository due to privacy and ethical restrictions but are available from the corresponding authors on request.

Supplemental Data

Supplemental Data can be found online at https://doi.org/10.1016/j.ajhg.2020.11.015.

Acknowledgments

The authors wish to thank the participating families and Drs. R.A.J. Nievelstein (University Medical Center Utrecht) and D. Barbuti (Ospedale Pediatrico Bambino Gesù) for radiological advice. The authors would also thank Prof. Kassim Javaid and other members of musculoskeletal GeCIP (Genomics England). This research used data and findings generated by the 100,000 Genomes Project. This work was supported by grants from: Fondazione Bambino Gesù (*Vite Coraggiose* to M.T.) and Italian Ministry of Health (CCR-2017-23669081 to M.T., Ricerca Corrente 2019 to M.N., and Ricerca Corrente 2019 and 2020 to M.L.D.), Academia Sinica and Ministry of Science and Technology of Taiwan (109-3111-Y-001-001, 109-2320-B-001-012-MY3, 107-3111-Y-001-048, 107-0210-01-19-01, 107-2320-B-001-015-MY3, 106-2320-B-001-017-MY3, 106-0210-01-15-02 to R.-B.Y. and 107-2321-B-001-036-MY3 to Y.-C.L.), São Paulo Research Foundation (FAPESP 2013/03236-5 to A.A.L.J. and 2018/10893-6 to B.L.F.), University of Tübingen Intramural Funding (fortüne 2545-1-0 to B.V.), Ministry of Science, Research and Art Baden-Württemberg (to B.V.), and Department of Science and Technology, Government of India (SB/SO/HS/005/2014 to K.M.G.). The 100,000 Genomes Project is funded by the National Institute for Health Research and NHS England. The 100,000 Genomes Project is managed by Genomics England Limited and uses data provided by patients and collected by the National Health Service as part of their care and support. See supplemental information for consortium details. Additional support was from the Wellcome Trust (203141/Z/16/Z) and the NIHR Biomedical Research Centre Oxford (to A.T.P. and J.C.T.).

Declaration of interests

C.B., P.B., and N.-M.G. declare no additional conflicts of interest beyond their employment affiliation. All the other authors declare no competing interests.

Received: September 23, 2020
Accepted: November 20, 2020
Published: December 11, 2020

WEB resources

ClinVar, https://www.ncbi.nlm.nih.gov/clinvar/
dbSNP, https://www.ncbi.nlm.nih.gov/projects/SNP/
gnomAD Browser, https://gnomad.broadinstitute.org/
InterVar, http://wintervar.wglab.org
OMIM, https://www.omim.org/

References

1. Hynes, R.O. (2009). The extracellular matrix: not just pretty fibrils. Science *326*, 1216–1219.
2. Walma, D.A.C., and Yamada, K.M. (2020). The extracellular matrix in development. Development *147*, dev175596.
3. Bonnans, C., Chou, J., and Werb, Z. (2014). Remodelling the extracellular matrix in development and disease. Nat. Rev. Mol. Cell Biol. *15*, 786–801.
4. Wu, M., Chen, G., and Li, Y.P. (2016). TGF-β and BMP signaling in osteoblast, skeletal development, and bone formation, homeostasis and disease. Bone Res. *4*, 16009.
5. Salazar, V.S., Gamer, L.W., and Rosen, V. (2016). BMP signalling in skeletal development, disease and repair. Nat. Rev. Endocrinol. *12*, 203–221.
6. Brazil, D.P., Church, R.H., Surae, S., Godson, C., and Martin, F. (2015). BMP signalling: agony and antagony in the family. Trends Cell Biol. *25*, 249–264.
7. Gong, Y., Krakow, D., Marcelino, J., Wilkin, D., Chitayat, D., Babul-Hirji, R., Hudgins, L., Cremers, C.W., Cremers, F.P., Brunner, H.G., et al. (1999). Heterozygous mutations in the gene encoding noggin affect human joint morphogenesis. Nat. Genet. *21*, 302–304.
8. Michos, O., Panman, L., Vintersten, K., Beier, K., Zeller, R., and Zuniga, A. (2004). Gremlin-mediated BMP antagonism induces the epithelial-mesenchymal feedback signaling controlling metanephric kidney and limb organogenesis. Development *131*, 3401–3410.
9. Bachiller, D., Klingensmith, J., Shneyder, N., Tran, U., Anderson, R., Rossant, J., and De Robertis, E.M. (2003). The role of chordin/Bmp signals in mammalian pharyngeal development and DiGeorge syndrome. Development *130*, 3567–3578.
10. Yang, R.B., Ng, C.K., Wasserman, S.M., Colman, S.D., Shenoy, S., Mehraban, F., Komuves, L.G., Tomlinson, J.E., and Topper, J.N. (2002). Identification of a novel family of cell-surface proteins expressed in human vascular endothelium. J. Biol. Chem. *277*, 46364–46373.
11. Wu, B.T., Su, Y.H., Tsai, M.T., Wasserman, S.M., Topper, J.N., and Yang, R.B. (2004). A novel secreted, cell-surface

glycoprotein containing multiple epidermal growth factor-like repeats and one CUB domain is highly expressed in primary osteoblasts and bones. J. Biol. Chem. *279*, 37485–37490.
12. Lin, Y.C., Chen, C.C., Cheng, C.J., and Yang, R.B. (2011). Domain and functional analysis of a novel breast tumor suppressor protein, SCUBE2. J. Biol. Chem. *286*, 27039–27047.
13. Grimmond, S., Larder, R., Van Hateren, N., Siggers, P., Hulsebos, T.J., Arkell, R., and Greenfield, A. (2000). Cloning, mapping, and expression analysis of a gene encoding a novel mammalian EGF-related protein (SCUBE1). Genomics *70*, 74–81.
14. Tu, C.F., Su, Y.H., Huang, Y.N., Tsai, M.T., Li, L.T., Chen, Y.L., Cheng, C.J., Dai, D.F., and Yang, R.B. (2006). Localization and characterization of a novel secreted protein SCUBE1 in human platelets. Cardiovasc. Res. *71*, 486–495.
15. Tsai, M.T., Cheng, C.J., Lin, Y.C., Chen, C.C., Wu, A.R., Wu, M.T., Hsu, C.C., and Yang, R.B. (2009). Isolation and characterization of a secreted, cell-surface glycoprotein SCUBE2 from humans. Biochem. J. *422*, 119–128.
16. Wu, Y.Y., Peck, K., Chang, Y.L., Pan, S.H., Cheng, Y.F., Lin, J.C., Yang, R.B., Hong, T.M., and Yang, P.C. (2011). SCUBE3 is an endogenous TGF-β receptor ligand and regulates the epithelial-mesenchymal transition in lung cancer. Oncogene *30*, 3682–3693.
17. Tu, C.F., Yan, Y.T., Wu, S.Y., Djoko, B., Tsai, M.T., Cheng, C.J., and Yang, R.B. (2008). Domain and functional analysis of a novel platelet-endothelial cell surface protein, SCUBE1. J. Biol. Chem. *283*, 12478–12488.
18. Tukachinsky, H., Kuzmickas, R.P., Jao, C.Y., Liu, J., and Salic, A. (2012). Dispatched and scube mediate the efficient secretion of the cholesterol-modified hedgehog ligand. Cell Rep. *2*, 308–320.
19. Lin, Y.C., Chao, T.Y., Yeh, C.T., Roffler, S.R., Kannagi, R., and Yang, R.B. (2017). Endothelial SCUBE2 Interacts With VEGFR2 and Regulates VEGF-Induced Angiogenesis. Arterioscler. Thromb. Vasc. Biol. *37*, 144–155.
20. Tu, C.F., Tsao, K.C., Lee, S.J., and Yang, R.B. (2014). SCUBE3 (signal peptide-CUB-EGF domain-containing protein 3) modulates fibroblast growth factor signaling during fast muscle development. J. Biol. Chem. *289*, 18928–18942.
21. Xavier, G.M., Panousopoulos, L., and Cobourne, M.T. (2013). Scube3 is expressed in multiple tissues during development but is dispensable for embryonic survival in the mouse. PLoS ONE *8*, e55274.
22. Flex, E., Niceta, M., Cecchetti, S., Thiffault, I., Au, M.G., Capuano, A., Piermarini, E., Ivanova, A.A., Francis, J.W., Chillemi, G., et al. (2016). Biallelic Mutations in TBCD, Encoding the Tubulin Folding Cofactor D, Perturb Microtubule Dynamics and Cause Early-Onset Encephalopathy. Am. J. Hum. Genet. *99*, 962–973.
23. Lam, M.T., Coppola, S., Krumbach, O.H.F., Prencipe, G., Insalaco, A., Cifaldi, C., Brigida, I., Zara, E., Scala, S., Di Cesare, S., et al. (2019). A novel disorder involving dyshematopoiesis, inflammation, and HLH due to aberrant CDC42 function. J. Exp. Med. *216*, 2778–2799.
24. Turro, E., Astle, W.J., Megy, K., Gräf, S., Greene, D., Shamardina, O., Allen, H.L., Sanchis-Juan, A., Frontini, M., Thys, C., et al.; NIHR BioResource for the 100,000 Genomes Project (2020). Whole-genome sequencing of patients with rare diseases in a national health system. Nature *583*, 96–102.
25. Homma, T.K., Freire, B.L., Honjo Kawahira, R.S., Dauber, A., Funari, M.F.A., Lerario, A.M., Nishi, M.Y., Albuquerque, E.V., Vasques, G.A., Collett-Solberg, P.F., et al. (2019). Genetic Disorders in Prenatal Onset Syndromic Short Stature Identified by Exome Sequencing. J. Pediatr. *215*, 192–198.
26. Vona, B., Mazaheri, N., Lin, S.J., Dunbar, L.A., Maroofian, R., Azaiez, H., Booth, K.T., Vitry, S., Rad, A., Varshney, P., et al. (2020). Biallelic mutation of CLRN2 causes non-syndromic hearing loss in humans. bioRxiv. https://doi.org/10.1101/2020.07.29.222828.
27. Monies, D., Abouelhoda, M., Assoum, M., Moghrabi, N., Rafiullah, R., Almontashiri, N., Alowain, M., Alzaidan, H., Alsayed, M., Subhani, S., et al. (2019). Lessons Learned from Large-Scale, First-Tier Clinical Exome Sequencing in a Highly Consanguineous Population. Am. J. Hum. Genet. *104*, 1182–1201.
28. Bauer, P., Kandaswamy, K.K., Weiss, M.E.R., Paknia, O., Werber, M., Bertoli-Avella, A.M., Yüksel, Z., Bochinska, M., Oprea, G.E., Kishore, S., et al. (2019). Development of an evidence-based algorithm that optimizes sensitivity and specificity in ES-based diagnostics of a clinically heterogeneous patient population. Genet. Med. *21*, 53–61.
29. Mak, K.K., Kronenberg, H.M., Chuang, P.T., Mackem, S., and Yang, Y. (2008). Indian hedgehog signals independently of PTHrP to promote chondrocyte hypertrophy. Development *135*, 1947–1956.
30. Maniatopoulos, C., Sodek, J., and Melcher, A.H. (1988). Bone formation in vitro by stromal cells obtained from bone marrow of young adult rats. Cell Tissue Res. *254*, 317–330.
31. Nishimura, R., Hata, K., Harris, S.E., Ikeda, F., and Yoneda, T. (2002). Core-binding factor alpha 1 (Cbfa1) induces osteoblastic differentiation of C2C12 cells without interactions with Smad1 and Smad5. Bone *31*, 303–312.
32. Zhu, D., Xiong, W.C., and Mei, L. (2006). Lipid rafts serve as a signaling platform for nicotinic acetylcholine receptor clustering. J. Neurosci. *26*, 4841–4851.
33. Lin, Y.C., Roffler, S.R., Yan, Y.T., and Yang, R.B. (2015). Disruption of Scube2 Impairs Endochondral Bone Formation. J. Bone Miner. Res. *30*, 1255–1267.
34. Zhang, M., Ho, H.C., Sheu, T.J., Breyer, M.D., Flick, L.M., Jonason, J.H., Awad, H.A., Schwarz, E.M., and O'Keefe, R.-J. (2011). EP1(-/-) mice have enhanced osteoblast differentiation and accelerated fracture repair. J. Bone Miner. Res. *26*, 792–802.
35. Hoffman, L.M., Garcha, K., Karamboulas, K., Cowan, M.F., Drysdale, L.M., Horton, W.A., and Underhill, T.M. (2006). BMP action in skeletogenesis involves attenuation of retinoid signaling. J. Cell Biol. *174*, 101–113.
36. Sobreira, N., Schiettecatte, F., Valle, D., and Hamosh, A. (2015). GeneMatcher: a matching tool for connecting investigators with an interest in the same gene. Hum. Mutat. *36*, 928–930.
37. Firth, H.V., Richards, S.M., Bevan, A.P., Clayton, S., Corpas, M., Rajan, D., Van Vooren, S., Moreau, Y., Pettett, R.M., and Carter, N.P. (2009). DECIPHER: Database of Chromosomal Imbalance and Phenotype in Humans Using Ensembl Resources. Am. J. Hum. Genet. *84*, 524–533.
38. Collod-Béroud, G., Béroud, C., Ades, L., Black, C., Boxer, M., Brock, D.J., Holman, K.J., de Paepe, A., Francke, U., Grau, U., et al. (1998). Marfan Database (third edition): new mutations and new routines for the software. Nucleic Acids Res. *26*, 229, 3.
39. Belleh, S., Zhou, G., Wang, M., Der Kaloustian, V.M., Pagon, R.A., and Godfrey, M. (2000). Two novel fibrillin-2 mutations

in congenital contractural arachnodactyly. Am. J. Med. Genet. *92*, 7–12.
40. Intarak, N., Theerapanon, T., Thaweesapphithak, S., Suphapeetiporn, K., Porntaveetus, T., and Shotelersuk, V. (2019). Genotype-phenotype correlation and expansion of orodental anomalies in LTBP3-related disorders. Mol. Genet. Genomics *294*, 773–787.
41. Liu, W., Qian, C., Comeau, K., Brenn, T., Furthmayr, H., and Francke, U. (1996). Mutant fibrillin-1 monomers lacking EGF-like domains disrupt microfibril assembly and cause severe marfan syndrome. Hum. Mol. Genet. *5*, 1581–1587.
42. Xu, P., Li, R., Huang, S., Sun, M., Liu, J., Niu, Y., Zou, Y., Li, J., Gao, M., Li, X., et al. (2020). A Novel Splicing Mutation in the *FBN2* Gene in a Family With Congenital Contractural Arachnodactyly. Front. Genet. *11*, 143.
43. Tan, T.Y., Gonzaga-Jauregui, C., Bhoj, E.J., Strauss, K.A., Brigatti, K., Puffenberger, E., Li, D., Xie, L., Das, N., Skubas, I., et al. (2017). Monoallelic BMP2 Variants Predicted to Result in Haploinsufficiency Cause Craniofacial, Skeletal, and Cardiac Features Overlapping Those of 20p12 Deletions. Am. J. Hum. Genet. *101*, 985–994.
44. Bandyopadhyay, A., Tsuji, K., Cox, K., Harfe, B.D., Rosen, V., and Tabin, C.J. (2006). Genetic analysis of the roles of BMP2, BMP4, and BMP7 in limb patterning and skeletogenesis. PLoS Genet. *2*, e216.
45. Yu, M., Wang, H., Fan, Z., Xie, C., Liu, H., Liu, Y., Han, D., Wong, S.W., and Feng, H. (2019). BMP4 mutations in tooth agenesis and low bone mass. Arch. Oral Biol. *103*, 40–46.
46. Feng, J.Q., Xing, L., Zhang, J.H., Zhao, M., Horn, D., Chan, J., Boyce, B.F., Harris, S.E., Mundy, G.R., and Chen, D. (2003). NF-kappaB specifically activates BMP-2 gene expression in growth plate chondrocytes in vivo and in a chondrocyte cell line in vitro. J. Biol. Chem. *278*, 29130–29135.
47. Nilsson, O., Parker, E.A., Hegde, A., Chau, M., Barnes, K.M., and Baron, J. (2007). Gradients in bone morphogenetic protein-related gene expression across the growth plate. J. Endocrinol. *193*, 75–84.
48. Hartung, A., Bitton-Worms, K., Rechtman, M.M., Wenzel, V., Boergermann, J.H., Hassel, S., Henis, Y.I., and Knaus, P. (2006). Different routes of bone morphogenic protein (BMP) receptor endocytosis influence BMP signaling. Mol. Cell. Biol. *26*, 7791–7805.
49. Magee, T., Pirinen, N., Adler, J., Pagakis, S.N., and Parmryd, I. (2002). Lipid rafts: cell surface platforms for T cell signaling. Biol. Res. *35*, 127–131.
50. Haworth, K., Smith, F., Zoupa, M., Seppala, M., Sharpe, P.T., and Cobourne, M.T. (2007). Expression of the Scube3 epidermal growth factor-related gene during early embryonic development in the mouse. Gene Expr. Patterns *7*, 630–634.
51. Yang, M., Guo, M., Hu, Y., and Jiang, Y. (2013). Scube regulates synovial angiogenesis-related signaling. Med. Hypotheses *81*, 948–953.
52. Fuchs, H., Sabrautzki, S., Przemeck, G.K., Leuchtenberger, S., Lorenz-Depiereux, B., Becker, L., Rathkolb, B., Horsch, M., Garrett, L., Östereicher, M.A., et al. (2016). The First Scube3 Mutant Mouse Line with Pleiotropic Phenotypic Alterations. G3 (Bethesda) *6*, 4035–4046.
53. Jongwattanapisan, P., Terajima, M., Miguez, P.A., Querido, W., Nagaoka, H., Sumida, N., Gurysh, E.G., Ainslie, K.M., Pleshko, N., Perera, L., and Yamauchi, M. (2018). Identification of the effector domain of biglycan that facilitates BMP-2 osteogenic function. Sci. Rep. *8*, 7022.
54. Lajoie, P., Goetz, J.G., Dennis, J.W., and Nabi, I.R. (2009). Lattices, rafts, and scaffolds: domain regulation of receptor signaling at the plasma membrane. J. Cell Biol. *185*, 381–385.
55. Kamiya, N., and Mishina, Y. (2011). New insights on the roles of BMP signaling in bone-A review of recent mouse genetic studies. Biofactors *37*, 75–82.
56. Jakobs, P., Schulz, P., Schürmann, S., Niland, S., Exner, S., Rebollido-Rios, R., Manikowski, D., Hoffmann, D., Seidler, D.G., and Grobe, K. (2017). Ca^{2+} coordination controls sonic hedgehog structure and its Scube2-regulated release. J. Cell Sci. *130*, 3261–3271.
57. Wouters, M.A., Rigoutsos, I., Chu, C.K., Feng, L.L., Sparrow, D.B., and Dunwoodie, S.L. (2005). Evolution of distinct EGF domains with specific functions. Protein Sci. *14*, 1091–1103.

The American Journal of Human Genetics, Volume *108*

Supplemental Data

SCUBE3 loss-of-function causes a recognizable recessive developmental disorder due to defective bone morphogenetic protein signaling

Yuh-Charn Lin, Marcello Niceta, Valentina Muto, Barbara Vona, Alistair T. Pagnamenta, Reza Maroofian, Christian Beetz, Hermine van Duyvenvoorde, Maria Lisa Dentici, Peter Lauffer, Sadeq Vallian, Andrea Ciolfi, Simone Pizzi, Peter Bauer, Nana-Maria Grüning, Emanuele Bellacchio, Andrea Del Fattore, Stefania Petrini, Ranad Shaheen, Dov Tiosano, Rana Halloun, Ben Pode-Shakked, Hatice Mutlu Albayrak, Emregül Işık, Jan M. Wit, Marcus Dittrich, Bruna L. Freire, Debora R. Bertola, Alexander A.L. Jorge, Ortal Barel, Ataf H. Sabir, Amal M.J. Al Tenaiji, Sulaima M. Taji, Nouriya Al-Sannaa, Hind Al-Abdulwahed, Maria Cristina Digilio, Melita Irving, Yair Anikster, Gandham S.L. Bhavani, Katta M. Girisha, Genomics England Research Consortium, Thomas Haaf, Jenny C. Taylor, Bruno Dallapiccola, Fowzan S. Alkuraya, Ruey-Bing Yang, and Marco Tartaglia

Supplemental Note: Case Reports

Family 1 (Italy)

Sib 1 **(F1S1)** is a female of 19 years old. She is the first child from consanguineous parents without a history of relevant disorders. Cesarean delivery occurred at 40th week of gestation after an unremarkable pregnancy. Birth weight was 3,020 g (-0.9 SDS), length 46 cm (-2.2 SDS) and occipitofrontal circumference (OFC) 33 cm (-1.1 SDS). Apgar score was 8 and 9 at 1 and 5 minutes, respectively. At birth, short stature and craniofacial dysmorphisms were observed while ultrasound investigations excluded other internal organ defects. Psychomotor development was normal. X-ray analyses at 14 years disclosed growth delay, abnormality of cervical bones (hypoplastic odontoid process), increased distance of the dorsal intervertebral space, and irregularly shaped lumbar vertebral bodies. Oligodontia, abnormality of shape of the residual teeth, dental crowding and malocclusion were also documented. At the last evaluation (19 years), bone age was at least 2 years less than chronologic age, according to Greulich-Pyle; height was 135.4 cm (-4.7 SDS), OFC 54 cm (-0.5 SDS), weight 43.1 kg (-2.3 SDS) and BMI 23.5 (0.6 SDS). She had craniofacial dysmorphisms including a long oval face with high forehead, hypotelorism, blepharoptosis, and a high nasal bridge, piriform nose with bulbous tip, enlarged naris, pointed chin and thick vermilion, and micrognathia. Joint laxity was also observed. Further X-ray analyses confirmed epistrophy hypoplasia, scoliosis with left-convex deviation, and squared lumbar vertebral bodies. Skull bones were normally shaped. Notably, all epiphyses including the metacarpal heads were reduced in length. Further findings included camptodactyly and narrow iliac wings. Dental abnormalities, including agenesis of all molar teeth except mesial molar and dental crowding, were unchanged. Cardiological, abdominal and routine laboratory investigations, also including testing for metabolic disorders, were unremarkable.

Sib 2 **(F1S2)** is a 10-year-old female, second child of the same consanguineous parents. Cesarean delivery occurred at 35 weeks of gestation after an uncomplicated pregnancy. A previous spontaneous miscarriage was recorded. Birth weight was 2,390 g (0.1 SDS), length 43 cm (-1.2 SDS) and OFC 33 cm (0.8 SDS). Apgar score was 9 and 10 at 1 and 5 minutes, respectively. Similar to her older sister, short stature and craniofacial dysmorphisms were observed at birth. Cranial and abdominal US scan were normal; dysmorphisms included triangular face with high forehead, hypotelorism, blepharoptosis, high nasal bridge, piriform nose, pointed chin, thick vermilion and micrognathia. A subcutaneous cleft palate was also seen, and surgically corrected at 5 months. There was no developmental delay nor intellectual disability. At 7 years, X-ray analyses showed vertebral defects (squared lumbar vertebral bodies), limbs defects (reduced thickness of the distal epiphysis of the radius and proximal epiphysis of the tibia), and hip dysplasia (coxa valga with cervico-diaphyseal angle 150°, asymmetry of femoral heads with flattened medial part). At the last evaluation at 10 years, height was 102.6 cm (-5.8 SDS), OFC 53 cm (-1.0 SDS), weight 14.8 kg (-6.0 SDS), and BMI 13.9 (-1.8 SDS). Previously identified defects of vertebral, iliac and limbs bones were confirmed. Dental abnormalities including multiple agenesis of permanent teeth, dental crowding, and multiple caries were also documented. Cardiological, abdominal, laboratory and metabolic investigation were unremarkable.

For both sibs, chromosome and high-resolution CGH-array (180K) analyses excluded the presence of clinically relevant CNVs. Based on their complex phenotype, both sibs were enrolled in the Undiagnosed Patients Program at the Ospedale Pediatrico Bambino Gesù for further molecular

investigations. Collection, use and storage of clinical data, pictures, and biological material of the patients and their parents were attained after written informed consent was secured.

Family 2 (India)

Sib1 **(F2S1)**, a 22-year-old male born to first cousin parents, presented with short stature. He had a history of seizures from 1 to 5 years of age. Hearing loss due to eardrum problems was documented, though records were not available for review. He had myopia of the right eye from 15 years of age. On examination (22 years), his height and weight were 151.5 cm (-3.6 SDS) and 60.5 kg (-1.3 SDS), respectively. He had a long triangular face, high forehead, hypotelorism, blepharoptosis, high nasal bridge, bulbous nose, enlarged nares, prominent ear pinna, deep set eyes, high arched palate, crowded teeth and pointed chin. Cafe-au-lait spots, hypopigmented macules on the abdomen and transverse striae on the back were also observed.

His younger 15-year-old brother **(F2S2)** also presented with short stature. His height and weight were 147 cm (-2.5 SDS) and 39.4 kg (-2.0 SDS), respectively. He reported a single episode of seizures at 1 year of age. Hearing impairment was also documented, which was corrected by adenoid surgery. On examination, he had similar dysmorphic features as his elder brother.

Both probands had cutaneous syndactyly and hallux valgus. Intellectual development was normal for both of them. On radiological survey, thin phalanges, mild scoliosis and squared lumbar vertebral bodies, narrow iliac wings, and coxa valga were observed in both siblings.

Family 3 (Iran)

The proband **(F3S1)** is a female who is presently 39 years old. She is one of five children born to consanguineous parents. Her parents and unaffected sister have a history of miscarriage. Apart from a male cousin who reports the same syndrome, there are no other disorders that have been reported in their distant family. She was born in the 38th gestational week with a birth weight of 1,400 g (-5.8 SDS) and length of 33 cm (-9.2 SDS). Due to lack of prenatal care, there were no concerns about these aspects mentioned in her medical history. She is currently 132 cm (-3.5 SDS) with an OFC of 52 cm (-2.2 SDS). She has a long triangular face, high forehead, hypotelorism, a piriform nose with high nasal bridge and a deviated septum. Mild large ears and dental crowding have been documented. Sonography of the kidney, uterus, and ovaries was unremarkable. X-ray analysis documented narrow iliac wings and acetabular dysplasia. She has elementary education and is not reported to have intellectual disability.

Her 29-year-old sister **(F3S2)** was born in the 38^{th} gestational week after an unremarkable pregnancy and delivery. She is currently 130 cm (-3.8 SDS). She showed craniofacial dysmorphisms including a long triangular face with high forehead, high nasal bridge, and piriform nose.

The third sib **(F3S3)** is a 25-year-old male. He was born in the 38^{th} gestational week after an unremarkable pregnancy and delivery. He currently has a height of 144 cm (-3.5 SDS), a sitting height of 121 cm, waist height of 87 cm, and arm span of 145 cm. He has a BMI of 19.8 (-1.3 SDS). He has several craniofacial dysmorphic features including a long triangular face, high forehead, hypotelorism, high nasal bridge with a deviated septum and a down-pointed nose. Dental abnormalities that include

oligodontia and severe dental crowding were documented. He has narrow iliac wings. X-ray studies are not available. He has a mild hearing loss. No other abnormalities are noted.

Family 4 (Sri Lanka)

The proband **(F4S1)** is an 11.5-year-old male, the first child of normal statured first cousin Sri Lankan parents without a family history of relevant disorders. An antenatal scan at 20 weeks showed reduced growth although the pregnancy was otherwise unremarkable. He was born in good condition at 37 weeks via normal vaginal delivery, weighing 1,590 g (-4.6 SDS), with a length of 41cm (-4.6 SDS) and an OFC of 35 cm (0.1 SDS). He was admitted to the special care unit for 3-4 weeks to establish feeding and required nasogastric tube feeding due to poor sucking. He presented to the genetics team just before 2 years of age due to severe short stature and microcephaly. He crawled at 8 months, walked at 13 months but only spoke 4-5 words aged 2 years. His speech and language were markedly delayed relative to his other milestones. Social interaction was limited, with rigid behaviors and difficulty making friends. Subsequent skeletal survey suggested narrow iliac wings, coxa valga, bowing of long bones, mesomelia (upper limbs more pronounced than lower limbs) and bilateral congenital radial head dislocations (felt to be congenital). Consultation of a gastroenterologist for failure to thrive and restricted intake did not identify any medical cause. Endoscopy (aged 8 years) revealed microscopic mild esophageal eosinophilia. Constipation was recorded in childhood but improved with age. Dental anomalies included large lateral incisors, ectopic permanent teeth, bilateral taurodontism in first permanent molars, multiple dental caries (poor oral hygiene), enamel hypoplasia, and dental overcrowding.

At last evaluation (10.5 years), height was 107.3 cm (-3.4 SDS), OFC 48 cm (-4.4 SDS) and weight 13.7 kg (-5.2 SDS). On examination reduced elbow extension, supination and pronation were noted. He had a triangular facies, very small maxilla and mandible, a beaked nose and a high-pitched voice. His hands, feet and ears impressed as large in childhood. Joint laxity and mild fifth finger clinodactyly were documented. (Table 1, Figure 1 and Table S1). He had two younger brothers, neither of whom had similar clinical features. He was recruited to the 100,000 genome project along with his parents and younger brother. Collection, use and storage of clinical data, photographs, biological materials of the patient and parents were obtained after informed verbal consent was secured.

Family 5 (Turkey)

Sib 1 **(F5S1)** is a male referred for short stature at the age of 11.6 years. He was born as the first out of five children from consanguineous healthy but short parents. After an uneventful pregnancy and delivery at 40 weeks of gestation he was born small for gestational age (birth weight 2,500 g, -2.4 SDS). Birth length and head circumference (OFC) were not measured. Besides severe growth failure, the patient had a history of frequent viral infections of the upper respiratory tract. Early motor development was normal (walking at 1.5 years), but school performance has been poor. At physical examination (11.6 years), height was 123 cm (-3.3 SDS), sitting height/height ratio 0.512 (-0.2 SDS), OFC 47.5 cm (-4.6 SDS), weight 21 kg (-4.1 SDS), and BMI 13.9 (-2.3 SDS). He showed craniofacial dysmorphisms including a long triangular face with high forehead, high nasal bridge, piriform nose with bulbous tip, pointed chin and full lips. There was also severe caries and gingival recession. X-ray analyses at 12.5 years disclosed increased lumbar lordosis, scoliosis, and coxa valga. Skeletal age was

10.5 years at a chronological age of 11.6 years. Cardiological and routine laboratory investigations were unremarkable. Serum IGF-I and IGFBP-3 were within the reference range and the GH peak after clonidine provocation was also normal (17 ng/ml).

Sib 2 **(F5S2)** is a female referred for short stature at 7.3 years of age. She is the third out of five children of these consanguineous parents. The three other siblings are healthy and of normal stature. After an uneventful pregnancy she was born after 36 weeks of gestation with a weight of 2,500 g (-0.2 SDS). Birth length and OFC were not measured. Besides severe growth failure, the patient had a history of frequent viral infections of the upper respiratory tract. Psychomotor development was normal. At physical examination (7.3 years), height was 102 cm (-4.2 SDS), sitting height/height ratio 0.553 (1.3 SDS), OFC 48 cm (-3.9 SDS), weight 14.0 kg (-4.0 SDS) and BMI 13.5 (-1.6 SDS). She showed craniofacial dysmorphisms as observed in her brother, including a long triangular face with high forehead, high nasal bridge, piriform nose with bulbous tip, pointed chin and full lips. There was also severe caries and gingival recession. Cubitus valgus was noticed as well. Skeletal age was 7.1 years at a chronological age of 8.1 years. At 8.1 years, X-ray analyses showed scoliosis. A cardiac rhythm disorder (ventricular extrasystoles accompanying first degree AV block) was observed. Routine laboratory investigations were unremarkable. Serum IGF-I and IGFBP-3 were within the reference range and the GH peak after clonidine provocation was also normal (9.4 ng/ml).

For both sibs, the presence of clinically relevant CNVs was excluded by chromosome analysis [SNP array analysis (CytoScan HD array, Affymetrix) in case 1, karyotyping in case 2]. Based on their complex phenotype, both sibs were enrolled in the Genetics in Growth research program at the Leiden University Medical Center for further molecular investigations. Collection, use and storage of clinical data, pictures, biological material of the patients and their parents were obtained after written informed consent was secured.

Family 6 (Saudi Arabia)

The proband is a 16 month-old baby girl **(F6S1)** who was born at term to a healthy second cousin Saudi Arab couple by a normal vaginal delivery. Pregnancy was complicated by an abnormal prenatal ultrasound at 5 months detecting short extremities with intrauterine fetal growth retardation. At birth, weight was 2,500 kg (-2.3 SDS), length 45.5 cm (-2.4 SDS) and OFC 31.5 cm (-2.5 SDS). Apgar scores were 3 and 6 at 1and 5 minutes, respectively. She required chest compression with intubation and ventilatory support and weaned off to CPAP and then to a nasal cannula. She was noticed to have short limbs, hypotonia and distinct facial features (frontal bossing, depressed nasal bridge, anteverted broad nostrils, flat face, midfacial hypoplasia, posteriorly angulated auricles) and joints stiffness. She had feeding difficulties requiring parenteral nutrition followed by nasogastric tube feeding. The initial echocardiogram showed an atrial septal defect (ASD) with pulmonary hypertension. At follow up (16 months), an intact septum was observed. Skeletal X-rays at 14 months showed abnormal cervical vertebra without other bone abnormalities. At 16 months of age, the child had achieved a normal social and motor development for age. Growth parameters showed a height of 65 cm (-4.9 SDS), OFC 42 cm (-2.8 SDS) and weight of 7 kg (-2.9 SDS). The head showed frontal bossing, bilateral epicanthal folds, depressed nasal bridge, broad nostrils, flat face round face, posteriorly angulated auricles with prominent antihelix, dental abnormalities (malalignment of the lower incisors), and small chin. Extremities showed flat feet with eversion. Array CGH showed excessive homozygosity with a normal

copy number. Metabolic investigations (serum ammonia, lactic acids, plasma acylcarnitines and long chain fatty acids) were normal.

Family 7 (United Arab Emirates)

A 25-month old male infant of Yemeni origin **(F7S1)** was first born to healthy first cousin parents. Mother had regular antenatal follow up with no issues apart from an antenatal scan that showed a mild fluid collection around one of the testicles of the fetus. He was delivered by vacuum-assisted vaginal delivery at term. He was flat at birth with meconium-containing liquor and Apgar scores of 1 and 3 at 1 and 5 minutes, respectively. He required immediate respiratory support but had a difficult intubation due to severe micro-retrognathia, glossoptosis and an anteriorly placed airway, resembling Pierre Robin Sequence. His birth weight was 2,900 g (-1.5 SDS), and OFC at birth was 35.5cm (-0.5 SDS). The earliest measured length was 48 cm at 7 weeks (-2.9 SDS). He subsequently underwent a tracheostomy at 2 months of age. He displayed multiple facial dysmorphic features including frontal bossing, hypertelorism, bilateral strabismus, flat nasal bridge, enlarged nares, cleft palate, low set ears, down slanting palpebral fissures and claw shaped right hand with syndactyly. He had a patent foramen ovale that subsequently had closed at follow up echocardiograms. He exhibited oropharyngeal dysphagia and severe gastroesophageal reflux disease that necessitated gastrostomy tube feeding. Additionally, he had tracheobronchomalacia, hypospadias and cryptorchidism and has had repair of lateral ventral hernia. He had severe growth failure, generalized hypotonia and global developmental delay.

He currently requires nocturnal oxygen support. Because the multiple congenital malformations, he was highly suspected to have a genetic syndrome. Chromosomal microarray did not reveal any pathogenic copy number variants.

Family 8 (Brazil)

The proband **(F8S1)** is a 12.8-year-old boy, the second child of consanguineous, first-degree relatives. His older brother does not present congenital anomalies. During pregnancy, intrauterine growth restriction and oligohydramnios were noted. He was born at 37 weeks, by cesarean section, with a birth weight of 2,315 g (-2.8 SDS), length of 41cm (-4.6 SDS), OFC of 34 cm (-0.8 SDS) and Apgar scores 8/8 at 1/5 minutes. He presented with respiratory distress, requiring mechanical ventilation. Pierre-Robin sequence and bilateral premature closure of the coronal suture were diagnosed at that time. Surgical correction of the craniosynostosis was performed at 3 months of age, followed by mandibular distraction osteogenesis. He required gastrostomy for feeding difficulties from 3 to 15 months of age. Complementary exams disclosed patent foramen ovale and pulmonary hypertension on echocardiogram and normal abdominal ultrasound, audiologic evaluation and G-banded karyotype. He was released from hospital after 6 months. Surgical correction of the palatal anomaly was performed at the age of 4 years. He had normal motor development, but presented difficulty in speech. He presented with recurrent otitis. Audiologic evaluation disclosed conductive hearing loss, requiring hearing aids.

He was first evaluated in our institution at the age of 25 months, showing a weight of 8.2 kg (-3.5 SDS), length of 71cm (-4.3 SDS), OFC of 46.7cm (-1.6 SDS); dysmorphic facial features with brachycephaly, high forehead, arched eyebrows, hypoplastic supraorbital ridges, hypertelorism,

bulbous tip of the nose, small mouth, bifid uvula, microretrognathia, prominent ears, and limited elbow extension.

He attends regular school, with no history of learning problems. Because of short stature, endocrinologic assessment was carried out at the age of 5 years disclosing normal plasma levels of IGF1 and a normal GH response to a GH-stimulation test. Complementary exams showed a normal cranial and temporal CT-scan, ophthalmologic evaluation, echocardiogram and chromosomal breakage study with diepoxybutane. Brainstem evoked response audiometry with mild conductive hearing loss and skeletal survey showed mild hypoplasia of the proximal radius; posterior arch defect in cervico-thoracic region; trapezium-1st metacarpal and cuneiform/cuboid-metatarsal coalitions, with broad phalanges.

Patient initiated treatment with recombinant human growth hormone (rhGH 50 μg/kg/d) at the age of 10.6 years due to severe short stature: height of 116.3 cm (-3.9 SDS), sitting height of 63.9 cm {sitting height/total height SDS of 2.6), weight 19.9 kg (-4.0 SDS), BMI of 14.7 kg/m^2 (-1.4 SDS) and OFC 50.5 cm (-2.1 SDS). Physical examination at the last visit at the age of 13.2 years showed a height of 131.0 cm (-3.4 SDS), sitting height of 71.6 cm (SH/H SDS of 3.5), OFC 51 cm (-2.6 SDS), weight 30.0kg (-3.2 SDS), BMI of 17.5 kg/m^2 (-0.5 SDS) and patient is still on treatment with rhGH. Skeletal survey of the patient at 12.8 years documented spine defects (mild lumbar scoliosis, partial fusion of C5-C6 and failure of the posterior arch fusion in C7-T1), and several long bones abnormalities including generalized flattened epiphysis, bowed radius with abnormal radial head at the elbow joint, hypoplastic styloid processes of the ulna and radius and the tibia and fibula. Hands and feet bone defects included trapezoid-2nd metacarpal coalition in both hands and cuneiform bones-2nd and 3rd metatarsals coalitions, as well as cuboid-4th metatarsal coalition in the feet.

Family 9 (Israel)

Patient **F9S1** is an 8 year-old male, the fourth child born to consanguineous reportedly healthy parents of Arab-Muslim descent. Prenatal follow-up was notable for ultrasound findings of left hydronephrosis and short long bones. Amniocentesis was not performed. He was born via vaginal delivery at 42 weeks of gestation, birth weight was 4,050 g (+1.1 SDS) and OFC 36.5 cm (+1.7 SDS). He was hospitalized for the first 51 days of life due to respiratory problems and failure to gain weight. Renal ultrasound at 4 weeks (and again at 6 weeks of age) showed mild hydronephrosis of the left kidney and minimal pyelectasis of the right kidney. Brain ultrasounds, as well as a total-body radiograph (at 3 weeks) were considered normal, even though large cardiothymic silhouette and bilateral hyperinflation were noticed at chest radiographs. Echocardiogram was normal. At ophthalmic investigation, he was reported to have unexplained nystagmus. MRI of the brain and orbits (at 5.5 years) was considered normal. His development and cognitive status were reportedly normal. Due to short stature, he underwent growth hormone stimulation test that was normal. Total body radiological investigation documented shortened proximal limbs, relatively short 1st metacarpal, fusion of the proximal and middle phalanges of the fifth toe in both feet. The bones of the hand also had a coarse appearance. Inborn errors of metabolism (urine organic acids and acylcarnitine) were ruled out. Chromosomal microarray analysis was considered normal, and showed multiple areas of homozygosity. Physical examination (at 8 years and 1 month) was notable for a peculiar facial appearance, with a long, sparse hair, oval face, a pyriform, pear-shaped nose with bulbous tip and large ears. He also had dental crowding and his front teeth had a saw-like appearance. He showed

pectus excavatum and limited flexion of his fingers and hand grip difficulties. In his last visit, at the age of 8 years and 10 months, his weight was 21.3 kg (-2.0 SDS), height was 116.2 cm (-2.8 SDS), and OFC was 51 cm (-1.15 SDS).

Patient **F9S2** is a 22.5 year-old female, the maternal cousin of Patient F9S1. She is the second of three daughters, born to consanguineous reportedly healthy parents of Arab-Muslim descent. The pregnancy was uneventful, and amniocentesis was not performed. She was born via vaginal delivery at 39 weeks of gestation, birth weight was 3,080 g (-0.8 SDS). At infancy she was breastfed but had showed failure to thrive, for which she was hospitalized and evaluated. Echocardiogram showed ostium secundum ASD, which later resolved itself. As her cousin (F9S1), horizontal nystagmus in both eyes was noticed from as early as the first months of life, for which she underwent Kestenbaum procedure. Visual evoked potential (VEP) and electroretinography (ERG) were considered normal. During the first year of life, she had respiratory illnesses and was diagnosed with unilateral congenital lobar emphysema (of the left upper lobe). Brain CT, EEG and metabolic screening were considered normal. Craniofacial dysmorphisms at 5 years included short, brittle and sparse hair whisker hair and sparse both eyebrows and eyelashes maxillary hypoplasia, pointed chin, hypodontia with agenesis of several lower incisors, dental crowding, and short stature. Radiograph of the left hand at 11.5 years was consistent with a bone age of 10 years, and karyotype was 46,XX. Despite her development and cognitive status were reported to be normal, she was considered to show some behavioral issues in early childhood, and underwent assessments for ADHD, learning difficulties and speech delay. However, she attended at school regularly. At 12.5 years, she showed a long face, bright curly hair, high forehead attached earlobes with a protruding antitragus, downslanting palpebral fissures, anteverted nares and a columella below ala nasi, long pointed and triangular chin, irregular teeth with agenesis of several lower teeth, several cutaneous telangiectasias, hallux valgus of both feet with short first and fifth toes. Her weight was 30.4 kg (-1.9 SDS), height was 137.2 cm (-2.1 SDS), and OFC was 51.5 cm (-2.3 SDS). Upon last evaluation (at 22.5 years) her weight is 44 kg (3rd centile) and her height is 146 cm (-3.1 SDS).

Patient **F9S3** is the maternal aunt of F9S1 and F9S2. She is currently 54 years old, and reported to have short stature (145 cm) and clinical features resembling those observed in her nephew and niece, such as an inability to properly form a fist. She is reported to be cognitively normal. Unfortunately, she was unavailable for in-depth phenotyping.

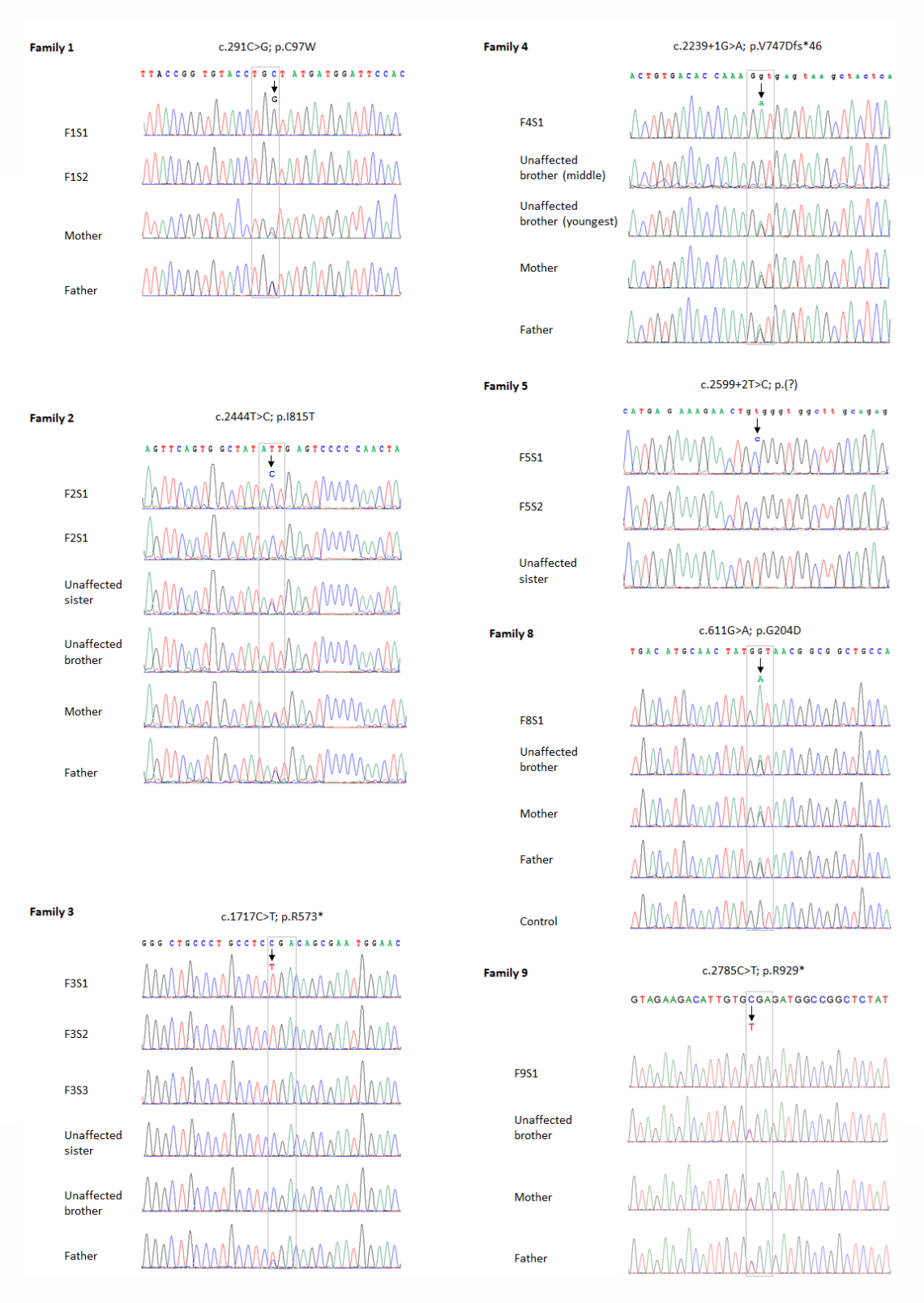

Figure S1. Sanger validation and segregation analyses.
Sequence chromatograms showing homozygosity for the pathogenic *SCUBE3* variants identified in affected members of families 1, 2, 3, 4, 5, 8 and 9.

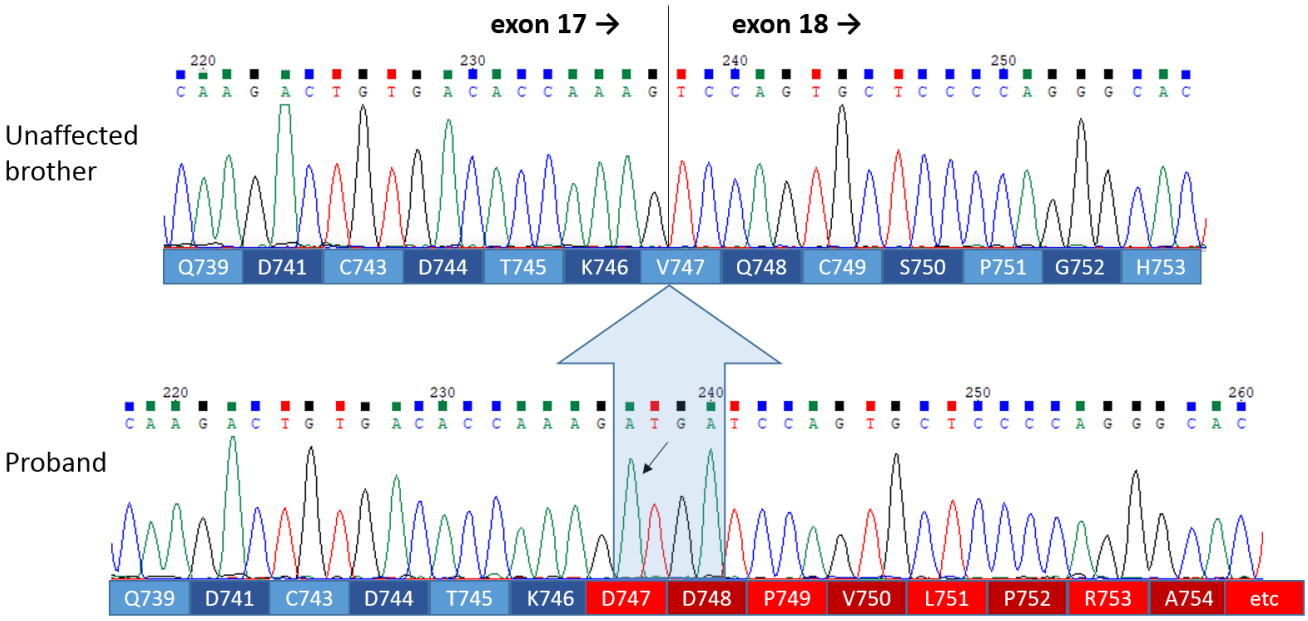

Figure S2. Functional impact of the c.2239+1G>A splice site change (family 4).
Total RNA was used to amplify the relevant cDNA region (exons 17 and 18). Sanger sequencing demonstrates that the c.2239+1G>A variant (black arrow) in *SCUBE3* (NM_152753.2) results in retention of 4 bp of the flanking intronic sequence (blue arrow), predicting an out-of-frame stretch of 45 residues followed by a stop codon (p.Val747Aspfs*46).

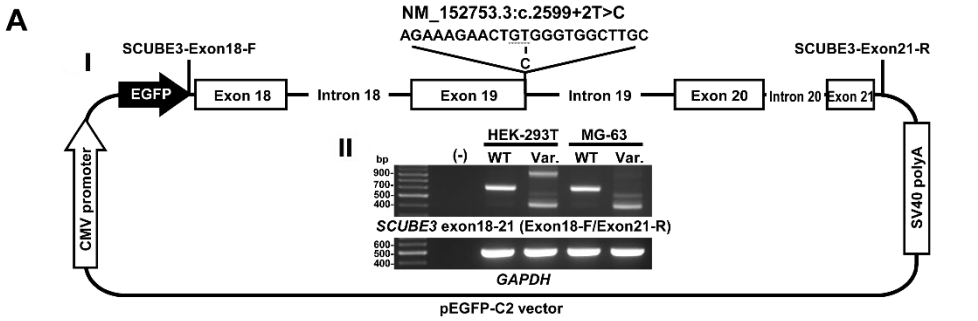

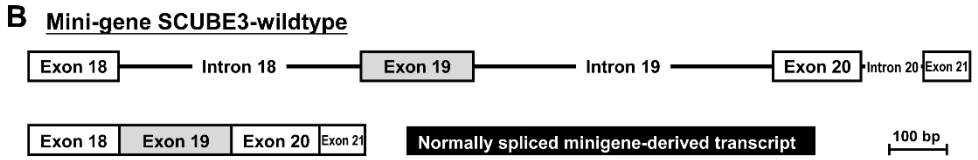

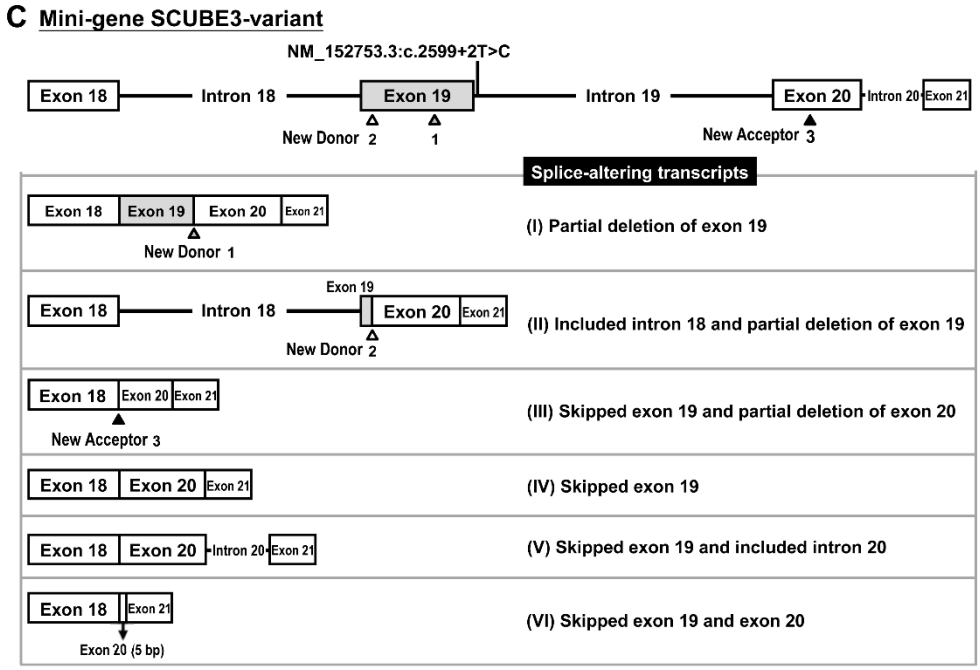

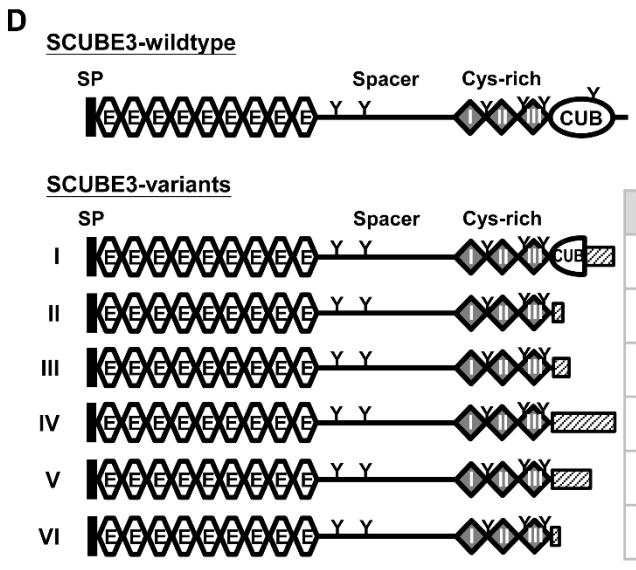

Amino Acid Change	%
p.(Val846Hisfs*57)	4
p.(Asn801Serfs*20)	17
p.(Asn801Argfs*32)	25
p.(Asn801Thrfs*127)	33
p.(Asn801Thrfs*78)	17
p.(Asn801Metfs*8)	4

Figure S3. Mini-gene splicing analysis of the *SCUBE3* c.2599+2T>C variant.

(A) Construction of the splicing vector pEGFP-C2 containing the wild-type (WT) or mutant *SCUBE3* mini-gene. The location of c.2599+2T>C variant (Var.) in the assay is indicated. (I) Straight lines indicate the forward and reverse primers used for RT-PCR. (II) Agarose gel electrophoresis for RT-PCR products. *SCUBE3* Exon18-F and *SCUBE3*-Exon21-R primers were used for RT-PCR amplification of cDNA sequences generated by HEK-293T or MG-63 (an osteosarcoma cell line) cells transfected with each mini-gene. RT-PCR analysis revealed aberrant transcripts produced by the *SCUBE3* mini-gene containing the c.2599+2T>C variant compared to the wild-type *SCUBE3* minigene. *GAPDH* was used as positive RT-PCR control.

(B) The wild-type *SCUBE3* mini-gene contains four exons (open boxes) and 3 functional introns (lines) (upper panel). Normally spliced transcript that excludes intron sequence is depicted (lower panel).

(C) The *SCUBE3* mini-gene contains four exons (open boxes) and 3 introns (lines) (upper panel) and has the disease-associated variant, c.2599+2T>C, which is located in the donor splice site of intron 19. Six splice-altering transcripts were identified in transfected HEK-293T (I to V) or MG-63 cells (II to VI) characterized by: (I) partial deletion of exon 19 (new donor site, gray triangle); (II) inclusion of intron 18 and partial deletion of exon 19 (new donor site, open triangle); (III) skipping of exon 19 and partial deletion of exon 20 (new acceptor site, black triangle); (IV) skipping exon 19; (V) skipping exon 19 and inclusion of intron 20; (VI) skipping of exon 19 and exon 20.

(D) The wild-type *SCUBE3* transcript encodes a polypeptide of 993 amino acids, whereas these splice-altering transcripts result in different out-of-frame products having premature stop codons. Clone frequency (%) for each transcript is shown (n=20). SP, signal peptide; E, EGF-like repeats; Cys-rich, cysteine-rich motifs; CUB, the CUB domain. Y marks potential N-linked glycosylatabled sites.

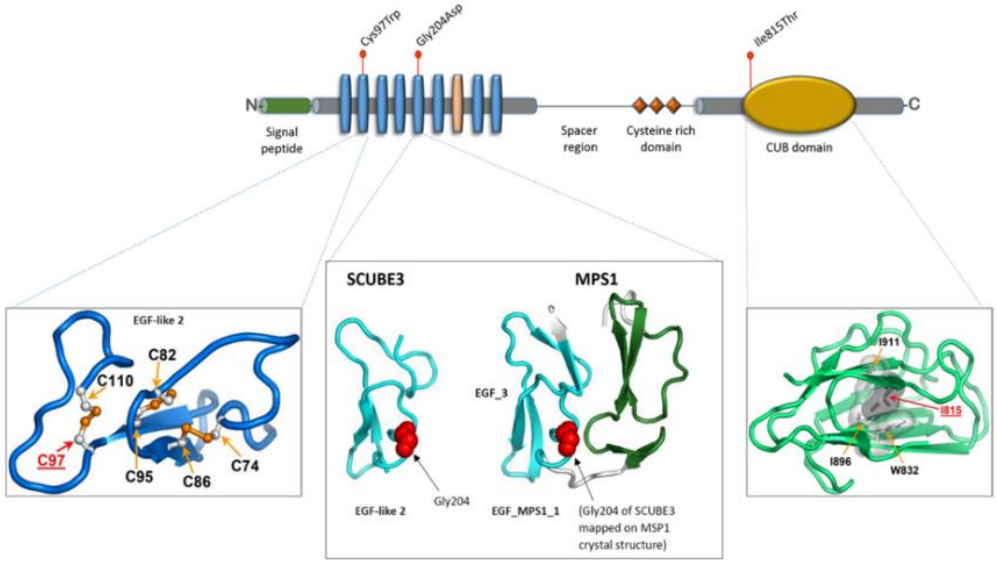

EGF-like2

SCUBE3	*H.sapiens*	DVDECERE-DNAGCVHDCVNIPGNYRCTCYDGFHLAHDGHNCL
Scube3	*P.troglodytes*	DVDECERE-DNAGCVHDCVNIPGNYRCTCYDGFHLAHDGHNCL
Scube3	*C.lupus*	DVDECERE-DNAGCVHDCVNIPGNYRCTCYDGFHLAHDGHNCL
Scube3	*B.taurus*	DVDECERE-DNAGCVHDCVNIPGNYRCTCYDGFHLAHDGHNCL
Scube3	*M.musculus*	DVDECERE-DNAGCVHDCVNIPGNYRCTCYDGFHLAHDGHNCL
Scube3	*R.norvegicus*	DVDECERE-DNAGCVHDCVNIPGNYRCTCYDGFHLAHDGHNCL
Scube3	*G.gallus*	DVDECERE-DNAGCVHECVNIPGNYRCTCYDGFRLAHDGHNCL
Scube3	*D.rerio*	DIDECASE-YNGGCVHECINIPGNYRCTCYDGFHLAHDGHNCL
SCUBE1	*H.sapiens*	DIDECENDYYNGGCVHECINIPGNYRCTCFDGFMLAHDGHNCL
SCUBE2	*H.sapiens*	DIDECGNE-LNGGCVHDCLNIPGNYRCTCFDGFMLAHDGHNCL
LTBP3	*H.sapiens*	DVDECEAG-DVCD-NGICSNTPGSFQCQCLSGYHLSRDRSHCE
FBN2	*H.sapiens*	DVDECEIGAHNCDMHASCLNIPGSFKCSCREGW--IGNGIKCI
FBN1	*H.sapiens*	DINECEIGAHNCGKHAVCTNTAGSFKCSCSPGW--IGDGIKCT

EGF-like5

SCUBE3	*H.sapiens*	--LTCNYGNGGCQHTCDDTEQGPRCGCHIKFVLHTDGKTCI
Scube3	*P.troglodytes*	----------CL
Scube3	*C.lupus*	--LTCNYGNGGCQHTCDDTEQGPRCGCHVKFVLHTDGKTCI
Scube3	*B.taurus*	--LTCNYGNGGCQHTCDDTEQGPRCGCHVKFVLHTDGKTCI
Scube3	*M.musculus*	--LTCNYGNGGCQHTCDDTEQGPRCGCHVKFVLHTDGKTCI
Scube3	*R.norvegicus*	--LTCNYGNGGCQHTCDDTEQGPRCGCHVKFVLHTDGKTCI
Scube3	*G.gallus*	--LTCNYGNGGCQHTCDDTDQGPKCGCHVKFLLHSDGVTCI
Scube3	*D.rerio*	--LTCNYGNGGCQHICEETDHGPKCSCHMKFALHSDGKTCV
SCUBE1	*H.sapiens*	----CNYGNGGCQHSCEDTDTGPTCGCHQKYALHSDGRTC-
SCUBE2	*H.sapiens*	----CNHGNGGCQHSCDDTADGPECSCHPQYKMHTDGRSC-
LTBP3	*H.sapiens*	DVDECEIGAHNCDMHASCLNIPGSFKCSCREGWIGNGIKCI
FBN2	*H.sapiens*	DVDECEIGAHNCDMHASCLNIPGSFKCSCREGWIGNGIKCI
FBN1	*H.sapiens*	DINECEIGAHNCGKHAVCTNTAGSFKCSCSPGWIGDGIKCT

CUB

SCUBE3	*H.sapiens*	CGGELGEFTGYIESPNYPGNYPAGVECIWNIN
Scube3	*P.troglodytes*	CGGELGEFTGYIESPNYPGNYPAGVECIWNIN
Scube3	*C.lupus*	CGGELGEFTGYIESPNYPGNYPAGVECVWNIN
Scube3	*B.taurus*	CGGELGEFTGYIESPNYPGNYPAGVECVWNIN
Scube3	*M.musculus*	CGGELGEFTGYIESPNYPGNYPAGVECVWNIN
Scube3	*R.norvegicus*	CGGELGEFTGYIESPNYPGNYPAGVECIWNIN
Scube3	*G.gallus*	CGGELGEYTGYIESPNYPGNYPANVECTWNIN
Scube3	*D.rerio*	CGGEIGEFIGYIESPNYPGNYPANVECVWTIN
SCUBE1	*H.sapiens*	CGGELGDYTGYIESPNYPGDYPANAECVWHIA
SCUBE2	*H.sapiens*	CGGELGDFTGYIESPNYPGNYPANTECTWTIN
KREMEN1	*H.sapiens*	CGGELGEFTGYIESPNYPGNYPAGVECIWNIN
BMP1	*H.sapiens*	CGGDVKKDYGHIQSPNYPDDYRPSKVCIWRIQ

Figure S4. Structural analyses.

The homology model shows the 2nd EGF-like domain with the invariant Cys^{97} and the other disulfide-forming cysteines. Substitution of Cys^{97} implies loss of one of the three conserved disulfide bridges of the motif (left). Homology model of the 5th EGF-like domain with the conserved Gly^{204}. The nonconservative substitution is predicted to impair proper module folding, and impact the interaction with the adjacent EGF-like module (middle). Homology model of the CUB domain is shown with location of Ile^{815} and surrounding residues (Trp^{832}, Ile^{896}, and Ile^{911}) forming a cluster of buried hydrophobic amino acids in the core of the domain. The introduction of a polar residue is predicted to considerably destabilize the structure of the entire domain (right). Conservation of affected residues in orthologs, paralogs and structurally related proteins is also shown.

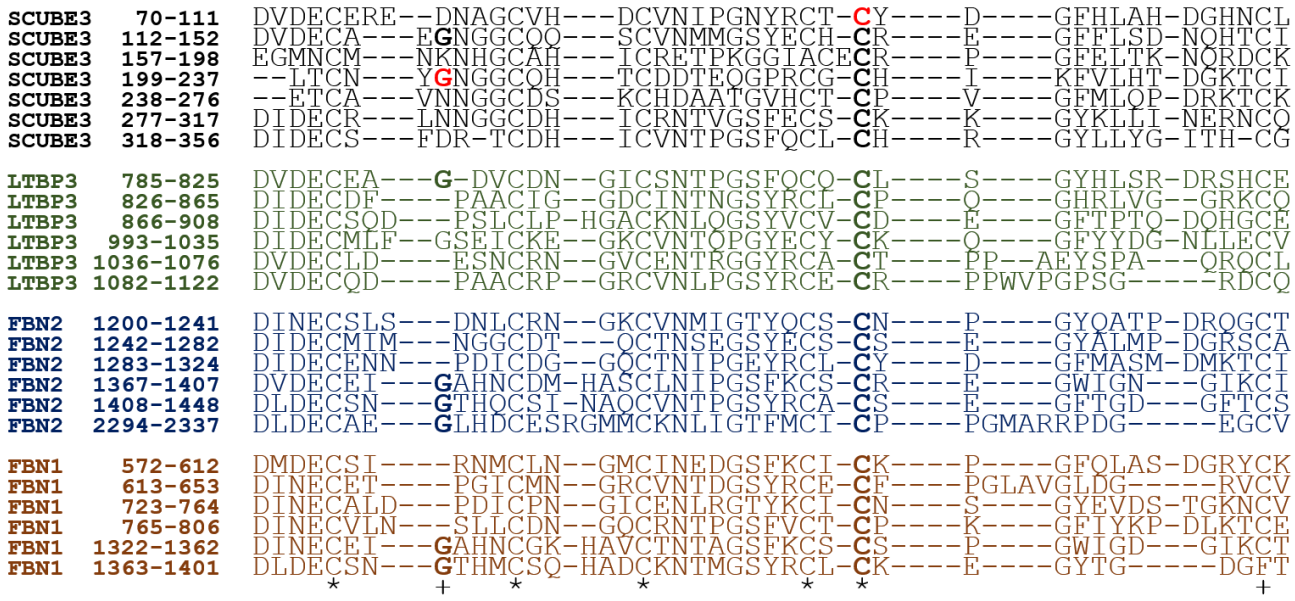

Figure S5. Alignments of the SCUBE3 EGF-like modules with equivalent modules of the LTBP3, FBN2 and FBN1 proteins.

Multiple sequence alignment of EGF-like meta-domains around the sites of the Cys^{97} and Gly^{204} (2^{nd} and 5^{th} EGF-like module of SCUBE3, respectively). (*) identical residues; (+) conserved residues.

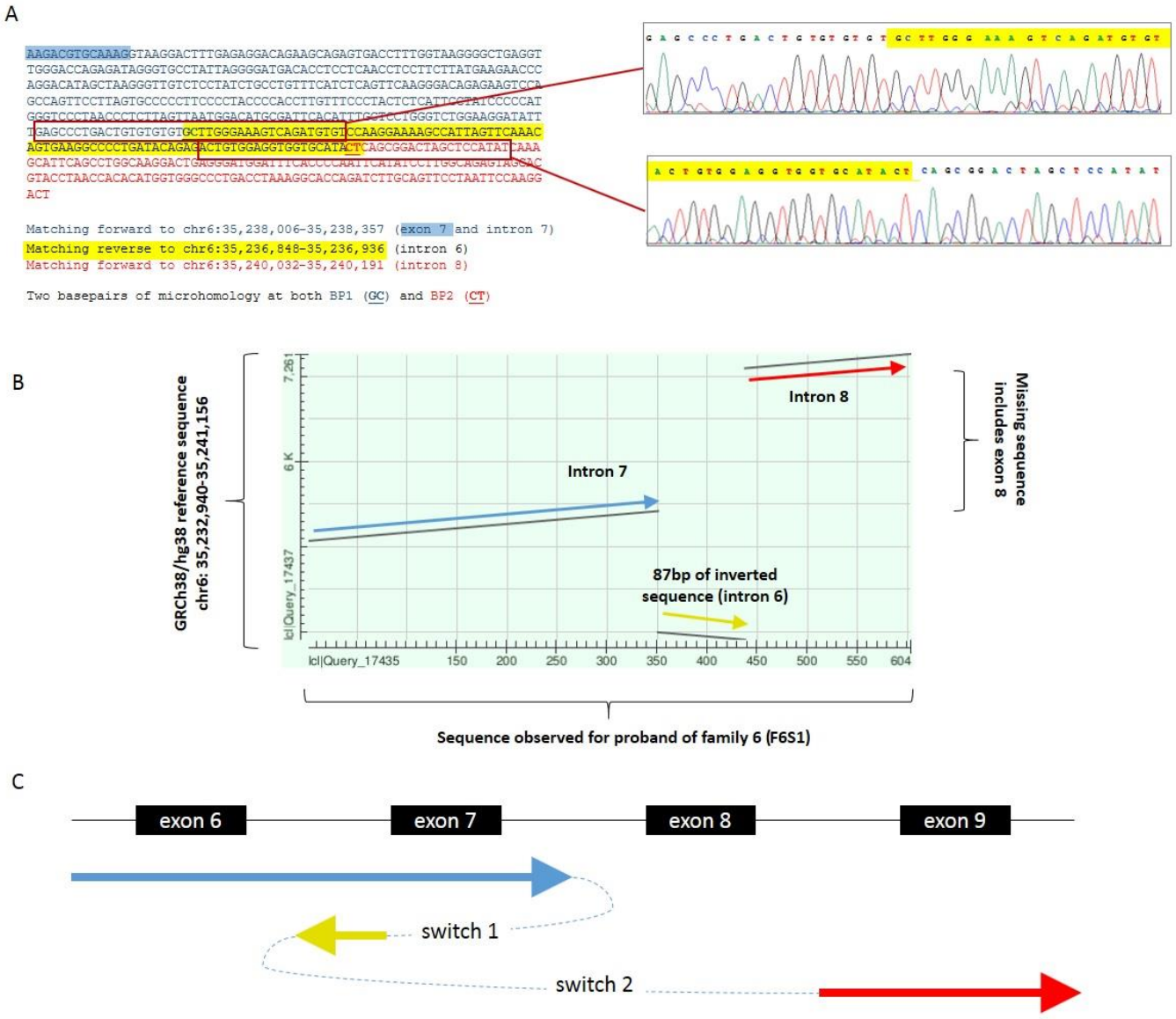

Figure S6. Breakpoints and characterization of the intragenic *SCUBE3* rearrangement involving exon 8 (family 6).

(A) Breakpoints of the rearrangement were confirmed by Sanger sequencing.

(B) Dotplot comparing rearrangement to reference sequence, generated using BLASTN tool (https://blast.ncbi.nlm.nih.gov/).

(C) Schematic diagram of the *SCUBE3* rearrangement. This complex rearrangement (deletion plus inverted duplication) likely originated from a two-step fork-switching and template-stalling (FoSTeS) process (also designated microhomology-mediated break-induced repair, MMBIR).

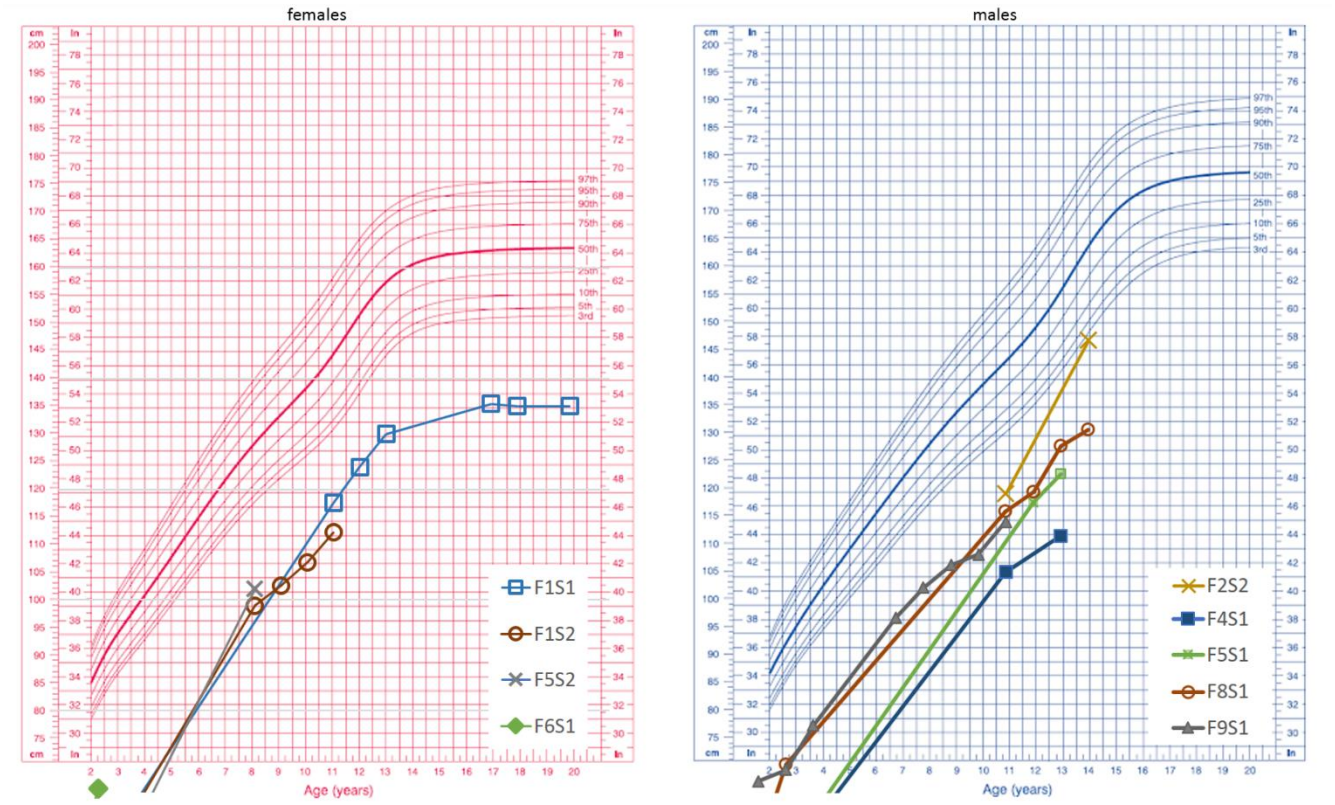

Figure S7. Growth pattern in subjects with biallelic inactivating *SCUBE3* variants. Height data are plotted on the 2000 CDC growth charts (Kuczmarski et al. 2002).

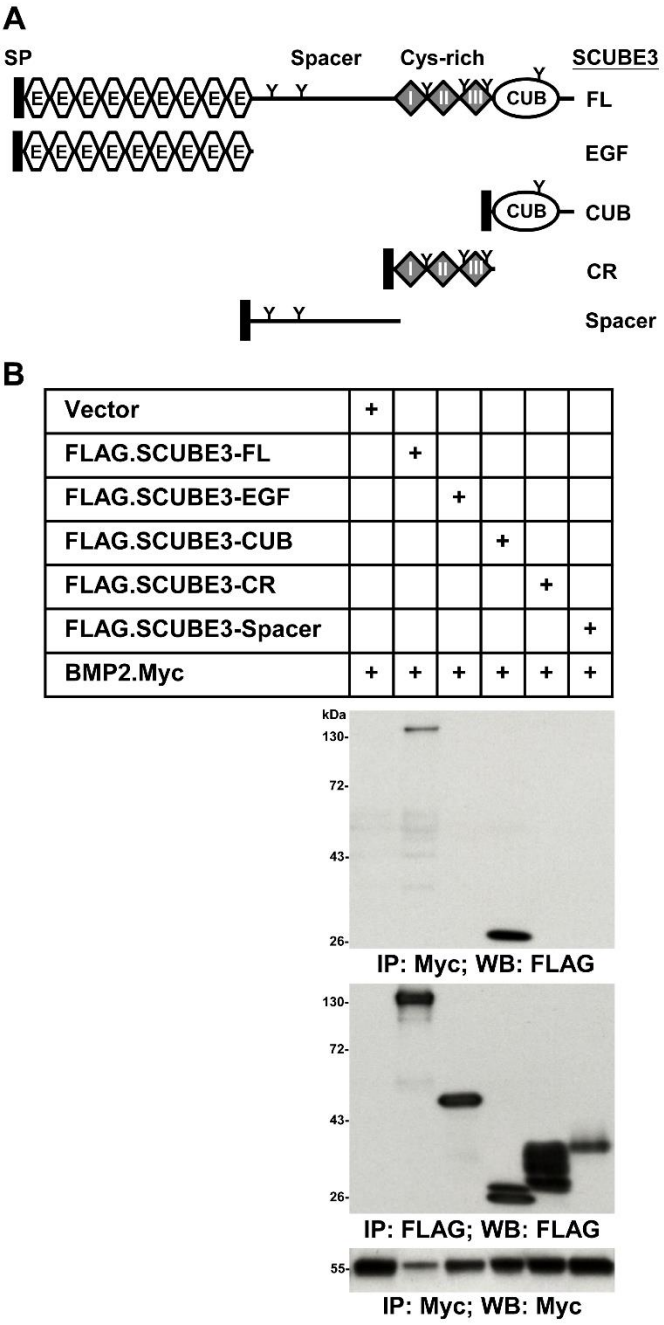

Figure S8. Molecular mapping of the interacting domains between SCUBE3 and BMP2.

(A) Domain organization of the SCUBE3 expression constructs used to map the interacting domains. A FLAG epitope was added immediately after the signal peptide sequence at the NH_2 terminus of each construct. SP, signal peptide; CR, cysteine-rich.

(B) The CUB domain of SCUBE3 interacts with BMP2. The expression plasmids encoding Myc-tagged BMP2 were transfected alone or with a series of FLAG-tagged SCUBE3 constructs in HEK-293T cells. After 48 h, cell lysates underwent immunoprecipitation, followed by western blot analysis with indicated antibodies to determine protein–protein interactions. IP, immunoprecipitation; WB, western blotting. Representative blots from one experiment of three performed are shown.

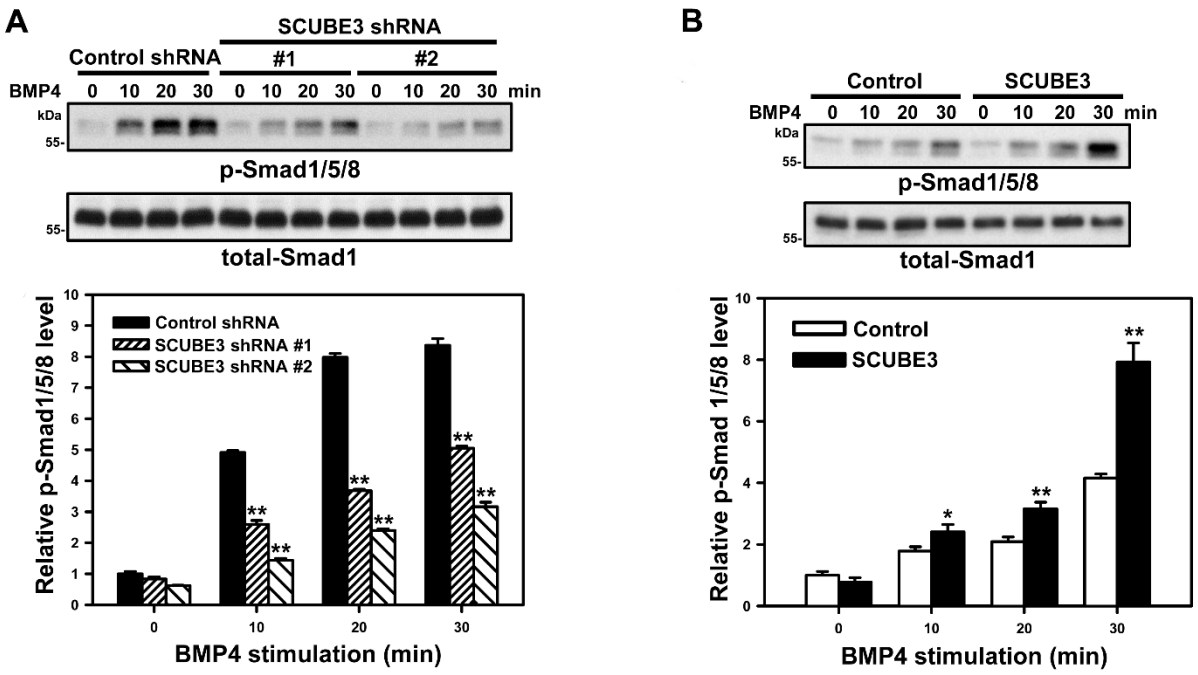

Figure S9. SCUBE3 enhances BMP4-stimulated osteoblast differentiation in C3H10T1/2 cells.
(A) *SCUBE3* knockdown impairs BMP4 signaling in C3H10T1/2 cells. Endogenous *SCUBE3* expression was inhibited by two different *SCUBE3*-targeting short hairpin RNA (shRNA) lentiviruses (SCUBE3-shRNA #1 or #2) in C3H10T1/2 cells. A luciferase shRNA lentivirus was used as a negative control (control-shRNA). Efficiency of *SCUBE3* knockdown and its effect on the phosphorylation of Smad1/5/8 were assessed by western blot analysis with total-Smad1 expression used as an internal control (above). Quantification of BMP4-induced phosphorylation of Smad1/5/8 in control or *SCUBE3* knockdown C3H10T1/2 cells. Data are mean ± SD from three independent experiments. **, P <0.01 compared to control (below).
(B) *SCUBE3* overexpression enhances BMP4 downstream signaling in C3H10T1/2 cells. Exogenous *SCUBE3* expressed in C3H10T1/2 cells transduced with an empty lentivirus or recombinant lentivirus encoding an FLAG-tagged SCUBE3. Western blot analysis (above) and quantification (below) of BMP4-induced phosphorylation of Smad1/5/8 with control and SCUBE3 overexpression in C3H10T1/2 cells. Data are mean ± SD from three independent experiments. *P <0.05; **, P < 0.01 compared with control.

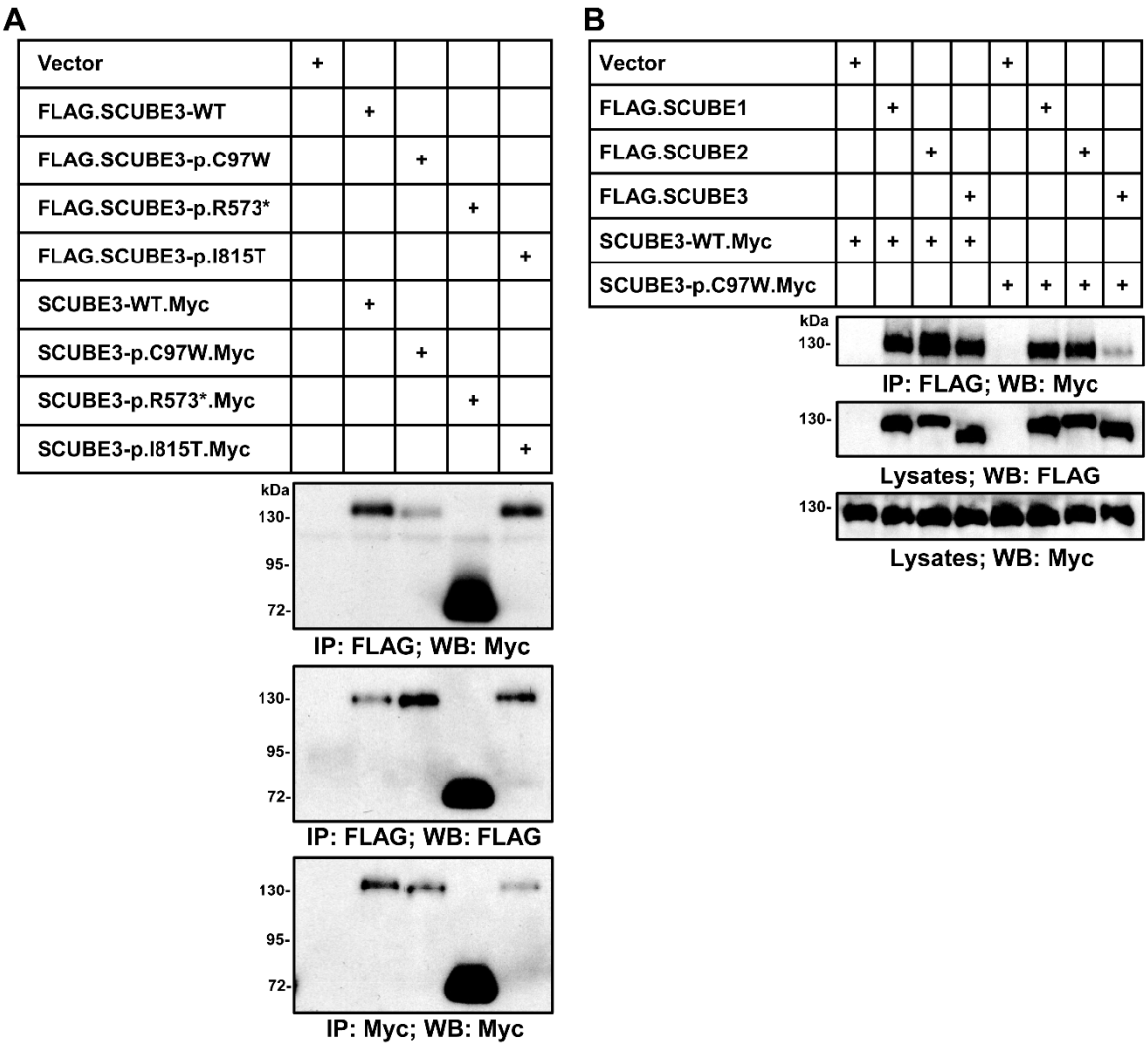

Figure S10. Effect of *SCUBE3* mutations on WT-mutant or mutant-mutant oligomerizations.

(A) Homodimerization assays. HEK-293T cells were transfected with expression plasmids encoding FLAG-tagged wild-type *SCUBE3* or individual mutants pCys97Trp (p.C97W), p.Arg573* (p.R573*) or p.Ile815Thr (p.I815T) together with their corresponding Myc-tagged constructs. Representative blots from one experiment of three performed are shown.

(B) Heterodimerization assays. HEK-293T cells were transfected with the expression plasmids encoding FLAG-tagged SCUBE1, SCUBE2 or SCUBE3 together with Myc-tagged wild-type SCUBE3 or the p.Cys97Trp (p.C97W) SCUBE3 mutants.

Lysates of transfected cells were immunoprecipitated (IP) with an anti-FLAG antibody, and associated protein levels were determined by western blot (WB) analysis with an anti-Myc antibody (top panels). The expression of FLAG or Myc-SCUBE3-WT, C97W, R573* or I815T proteins was verified by anti-FLAG or anti-Myc western blot analysis, respectively (second and third panels). Representative blots from one experiment of three performed are shown.

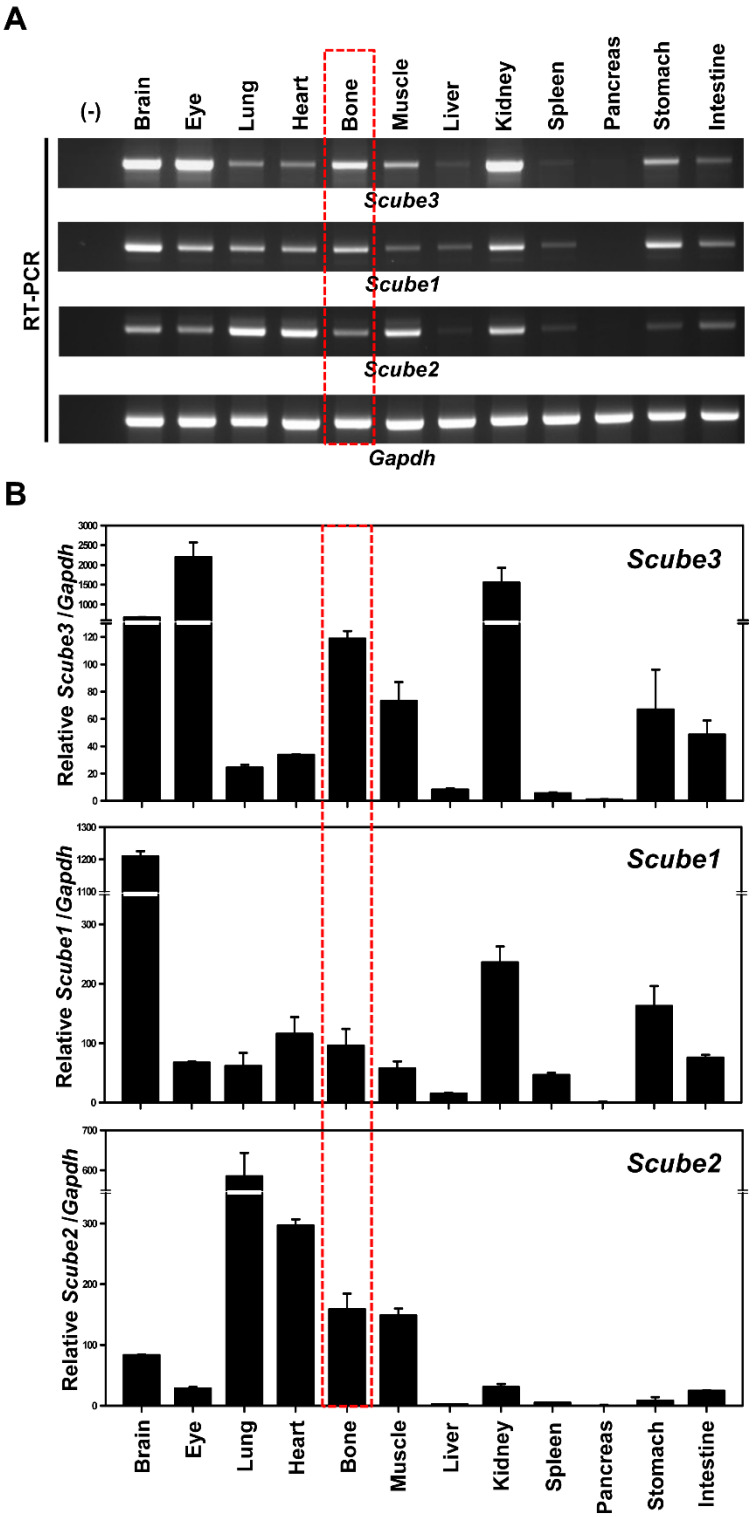

Figure S11. Expression of *Scube* genes in major organs in wild-type newborn mice.
RT-PCR **(A)** and quantitative RT-PCR **(B)** analyses of the expression of *Scube* genes in P1 newborn mice. First-strand cDNAs from brain, eye, lung, heart, bone, muscles, liver, kidney, spleen, pancreas, stomach, and intestine were used for RT-PCR and quantitative RT-PCR with primers specific for each *Scube* gene. Expression of *Gapdh* was used an internal control. Data are mean ± SD from three independent experiments.

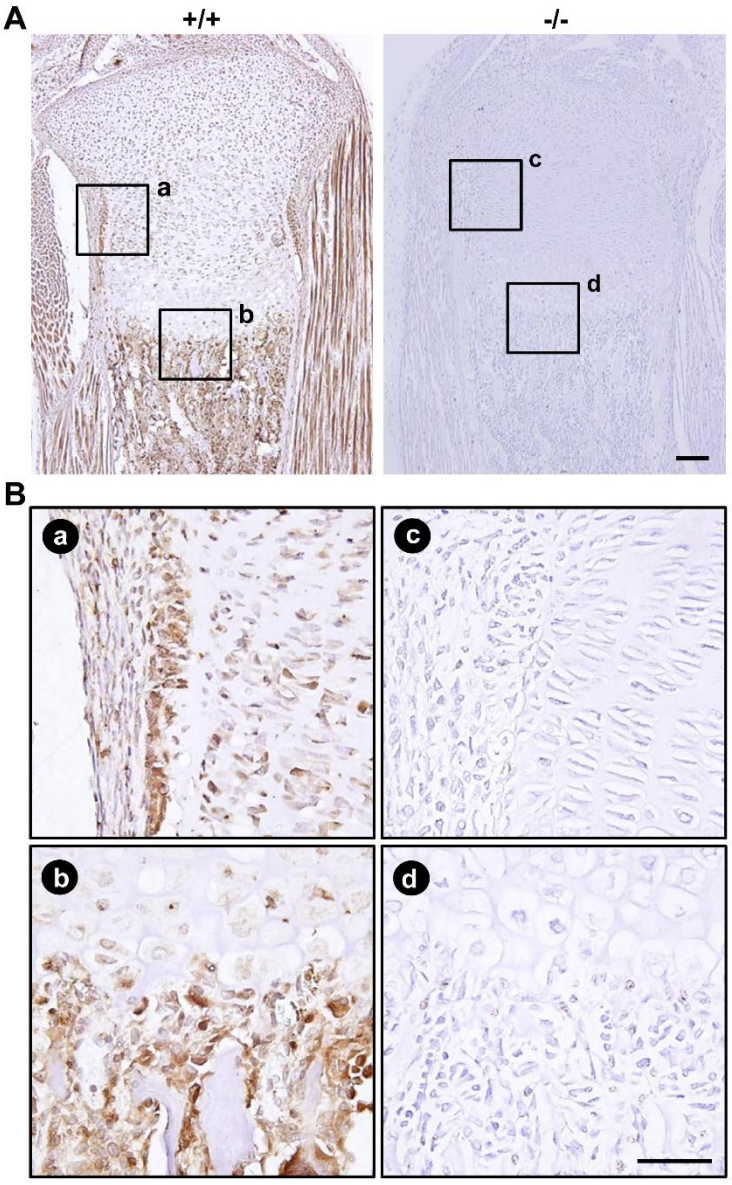

Figure S12. Immunohistochemical localization of SCUBE3 in neonatal mouse bone tissues.
(A) Sections of neonatal (P1) wild-type (+/+) or mutant (-/-) mouse tibiae were stained with a rabbit polyclonal antibody for SCUBE3.
(B) High-power images showing anti-SCUBE3 immunostaining localized in the periosteum (panel a), proliferative/prehypertrophic chondrocytes, and trabecular region (panel b) of +/+ mice, with immunoreactivity completely absent in -/- bones (panels c and d). Scale bars = 100 µm.

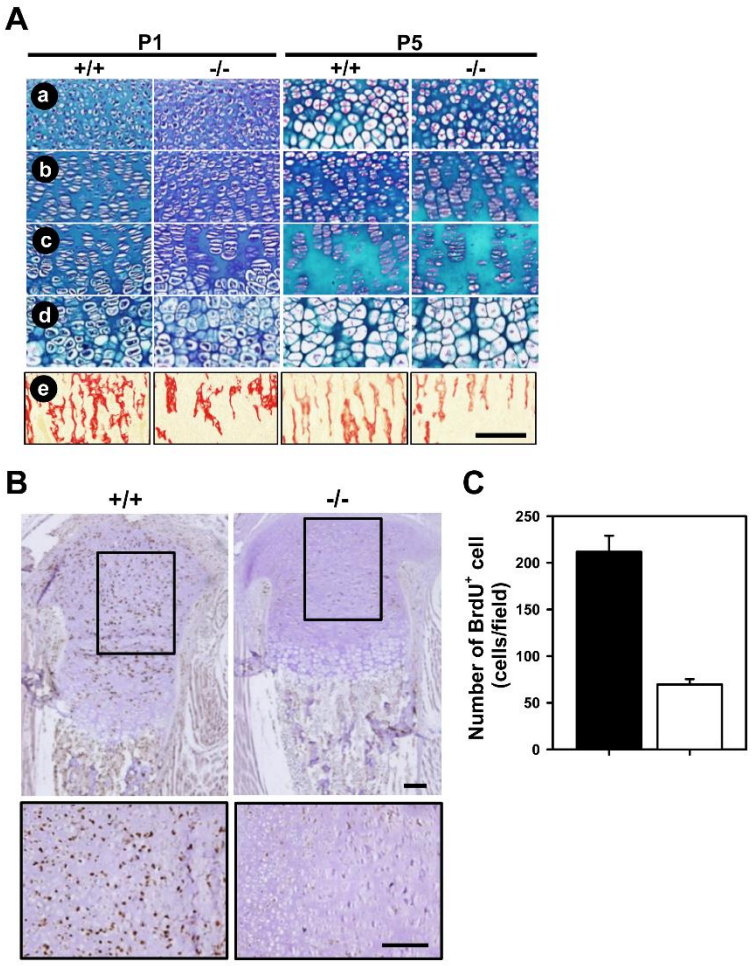

Figure S13. Effect of Scube3 knockout on the structure of growth plates and chondrocyte proliferation.

(A) Alcian blue hematoxylin/orange G of proximal tibia with resting chondrocytes (a), proliferative chondrocytes (b), prehypertrophic chondrocytes (c), and hypertrophic chondrocytes (d) of growth-plate chondrocytes. Cartilage: blue/purple (glycosaminoglycan /proteoglycan); bone: orange; erythrocytes or soft tissues: pink to red (a-d). Total collagen staining of proximal tibia with osteoblast/blood vessels of growth-plate chondrocytes (e). Scale bar =100 μm.

(B and C) Immunohistochemistry of tibiae from BrdU-labeled +/+ and -/- neonatal pups (P1) by using anti-BrdU antibody. Magnified views of the boxed periarticular regions are shown in the same columns (B). BrdU-positive cell number was counted and expressed as BrdU-positive cells/field in the periarticular regions of each section (C). **, $P < 0.01$ (n=5 animals in each genotype group). Scale bar = 100 μm.

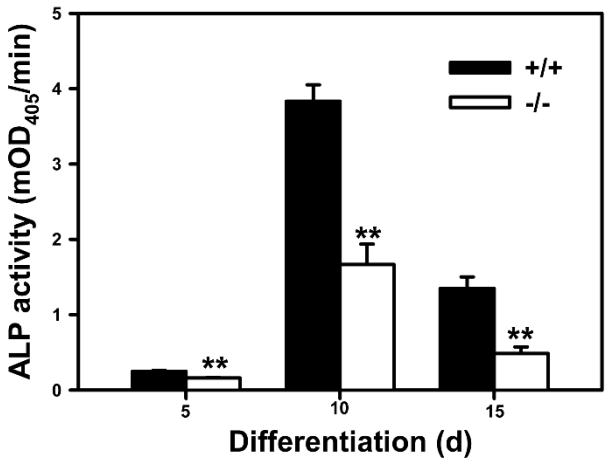

Figure S14. *Ex vivo* osteogenic differentiation of +/+ or -/- embryonic (E18.5) osteoblastic cells assessed by ALP activity.

ALP activity of +/+ and -/- embryonic osteoblastic cells under osteoblast differentiation conditions at days 5, 10, and 15. The experiments were performed 3 times in triplicate with similar results. Data are mean ± SD. mOD_{405}, milli-absorbance units at 405 nm. **, $P < 0.01$.

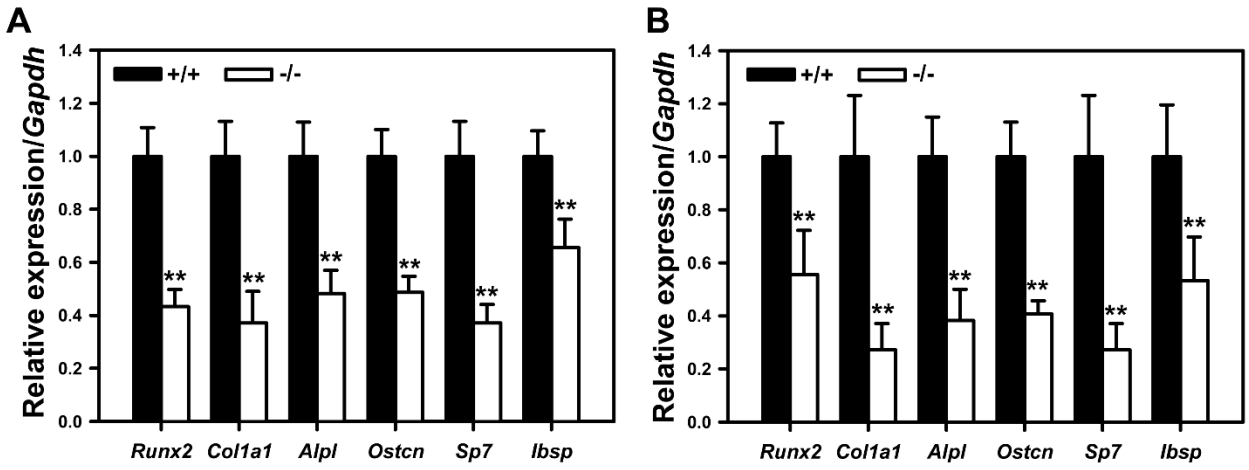

Figure S15. *SCUBE3* knockout reduces the expression of osteogenic marker genes in primary cultured chondrocytes and isolated long bones from +/+ or -/- animals.

Quantitative real-time RT-PCR of osteogenic phenotype markers in primary cultured chondrocytes **(A)** and long bones of hindlimbs **(B)** from +/+ or -/- animals (P2). Expression of osteoblast marker genes, Runt-related transcription factor 2 (*Runx2*, a transcriptional activator of osteoblast differentiation), type I collagen α1 chain (*Col1a1*), alkaline phosphatase (*Alpl*), osteocalcin (*Ostcn*), osterix (also named *Sp7*, a bone specific transcription factor essential for osteoblast differentiation and bone formation), and bone sialoprotein (*Bsp*, also known as integrin-binding sialoprotein *Ibsp*; a major structural protein of the bone matrix), are normalized to *Gapdh* mRNA level. Data are mean ± SD (n=5 in each group). **, $P < 0.01$.

Supplemental Figure 15

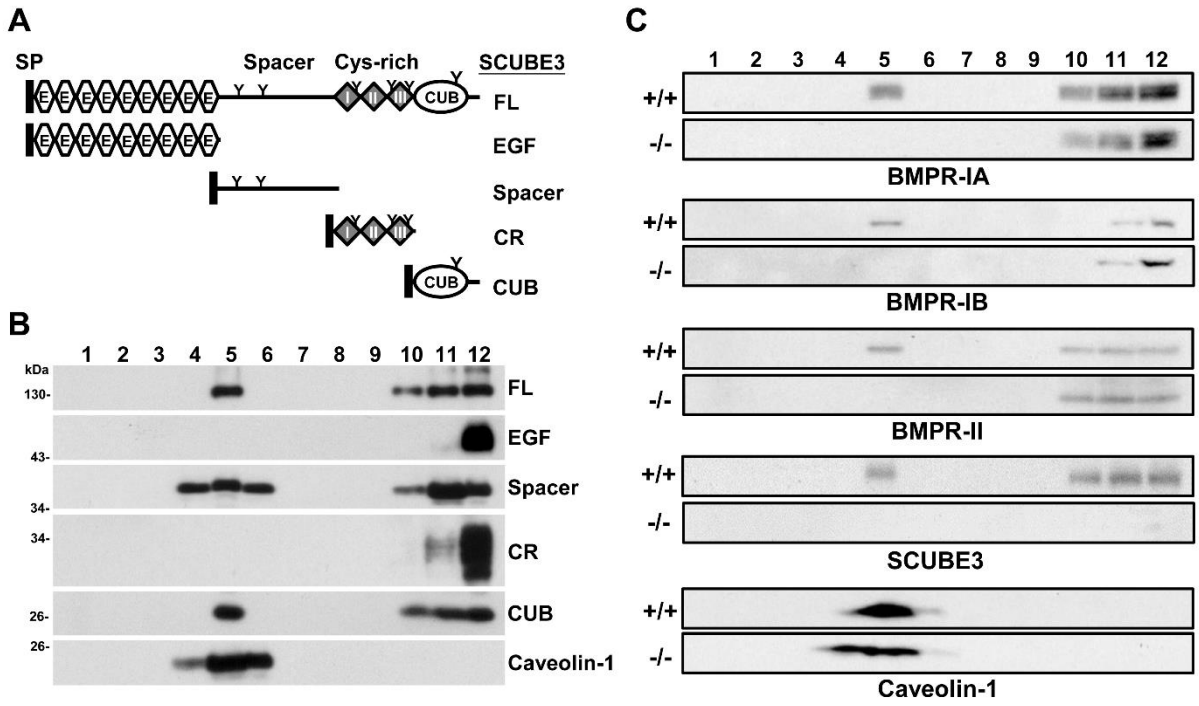

Figure S16. Requirement of SCUBE3 for stimulus-dependent BMP receptor association with lipid rafts.

(A and **B)** The spacer and CUB domain of SCUBE3 is crucial for lipid raft association. Domain organization of the SCUBE3 expression constructs used to map lipid raft-associated domains. The FLAG epitope was added immediately after the signal peptide sequence at the NH2-terminus of SCUBE3 constructs. SP, signal peptide; CR, cysteine-rich (a). SCUBE3-FL, Spacer, and CUB domain detected in lipid raft fraction. The expression plasmids encoding a series of FLAG-tagged SCUBE3 constructs were transfected in HEK-293T cells for 2 days; cell lysates underwent ultracentrifugation analysis and were collected as 12 fractions. Each fraction was examined by western blot analysis with anti-FLAG antibody. Fraction 5, which is enriched in caveolin-1, a marker of lipid raft, represents the lipid raft fraction (b). Representative blots from one experiment of three performed are shown.

(C) Abolished lipid raft association of BMP receptors (IA, IB, and II) in -/- chondrocytes in response to BMP2. Primary cultured chondrocytes were treated with 100 ng/ml BMP2 for 60 min. Cell lysates underwent ultracentrifuge analysis and were collected as 12 fractions. Each fraction was examined by western blot analysis with the indicated antibodies. Representative blots from one experiment of three performed are shown.

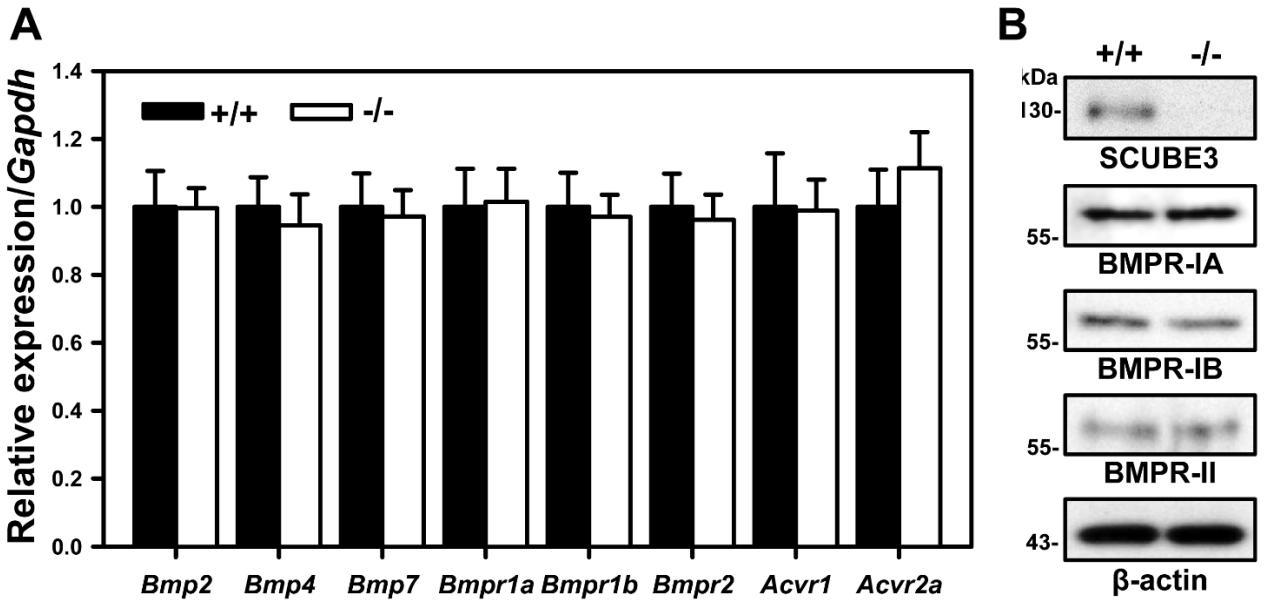

Figure S17. Expression of BMP signaling components and BMP receptor protein in primary cultured chondrocytes.

(A) Quantitative real-time RT-PCR of BMP signaling components in primary cultured chondrocytes from *Scube3*$^{+/+}$ or *Scube3*$^{-/-}$ animals (P2). Expression of BMP pathway genes, including bone morphogenetic protein 2 (*Bmp2*), bone morphogenetic protein 4 (*Bmp4*), bone morphogenetic protein 7 (*Bmp7*), bone morphogenetic protein receptor type 1a (*Bmpr1a*), bone morphogenetic protein receptor type 1b (*Bmpr1b*), bone morphogenetic protein receptor type 2 (*Bmpr2*), activin A receptor type 1 (*Acvr1*), and activin A receptor type 2a (*Acvr2a*), was normalized to *Gapdh* mRNA level. Data are mean ± SD (n=5 in each group). **, $P < 0.01$.

(B) *Scube3* knockout did not alter BMP receptor protein levels in primary cultured chondrocytes. Western blot analysis of the protein expression of BMP receptors in primary cultured chondrocytes. β-actin level was used as loading control. Representative blots from one experiment of three performed are shown.

Table S1. WES statistics and data output.

Subject F1S1 (Italy) (singleton)	
WES Enrichment Kit	Nextera Rapid Capture Kit
Sequencing Platform	NextSeq 550
Target regions coverage, 10x	94.9%
Target regions coverage, 20x	91.1%
Average sequencing depth on target	76x
Candidate disease genes (autosomal recessive inheritance)[1]	4[2]
Putative disease gene	1, *SCUBE3*
Subject F2S1 (India) (singleton)	
WES Enrichment Kit	Ion AmpliSeq Exome RDY Kit
Sequencing Platform	Ion Proton
Target regions coverage, 10x	98.5%
Target regions coverage, 20x	97.5%
Average sequencing depth on target	208x
Candidate disease genes (recessive inheritance)[1]	1[3]
Putative disease gene	1, *SCUBE3*
Subject F3S1 (Iran) (singleton)	
WES Enrichment Kit	Nextera Rapid Capture Kit
Sequencing Platform	NextSeq 500
Target regions coverage, 10x	94.4%
Target regions coverage, 20x	86.5%
Average sequencing depth on target	63x
Candidate disease genes (autosomal recessive inheritance)[1]	4[4]
Putative disease gene	1, *SCUBE3*
Subject F4S1 (UK) (trio)	
WGS library preparation	Illumina TruSeq DNA PCR-Free
Sequencing Platform	HiSeq X
Target regions coverage, 10x	99.7%
Target regions coverage, 20x	99.2%
Average sequencing depth on target	43x
Candidate disease genes (recessive inheritance)[5]	28
Candidate disease genes (autosomal dominant inheritance)	0
Putative disease gene	1[6], *SCUBE3*
Subject F5S1 (Turkey) (duo, affected sibs)	
WES Enrichment Kit	Agilent Sure Select XT V5
Sequencing Platform	HiSeq 4000
Target regions coverage, 10x	98.20%
Target regions coverage, 20x	93.59%
Average sequencing depth on target	79.0x
Candidate disease genes (autosomal recessive inheritance)[1]	1[7]
Putative disease gene	1, *SCUBE3*

Subject F6S1 (Saudi Arabia) (trio)	
WGS library preparation	Illumina TruSeq DNA PCR-Free
Sequencing Platform	HiSeq X
Target regions coverage, 10x	98.6
Target regions coverage, 20x	97.7
Average sequencing depth on target	38x
Candidate disease genes (autosomal recessive inheritance)[1]	1[8]
Putative disease genes	1, *SCUBE3*
Subject F7S1 (United Arab Emirates) (trio)	
WES Enrichment Kit	Agilent SureSelect Human All Exon V6
Sequencing Platform	HiSeq 4000
Target regions coverage, 10x	99.2
Target regions coverage, 20x	97.7
Average sequencing depth on target	153x
Candidate disease genes (recessive inheritance)[1]	NA[9]
Candidate disease genes (dominant inheritance)	0
Putative disease gene	1, *SCUBE3*
Subject F8S1 (Brazil) (singleton)	
WES Enrichment Kit	Agilent Sure Select All Exon V6
Sequencing Platform	HiSeq 2500
Target regions coverage, 10x	99.2%
Target regions coverage, 20x	97.5%
Average sequencing depth on target	132.9x
Candidate disease genes (recessive inheritance)[1]	3[10]
Putative genes (autosomal recessive inheritance)	1, *SCUBE3*
Subject F9S1 (Israel) (singleton)	
WES Enrichment Kit	Twist plus
Sequencing Platform	Illumina HiSeq 2500
Target regions coverage, 10x	96%
Target regions coverage, 20x	95%
Average sequencing depth on target	250
Novel/low frequency variants with predicted functional effect[1]	152
Putative disease genes (autosomal recessive inheritance)	4 (*SCUBE3, BTN2A2,ZNRD1,PPP1R10*)[11]

[1]Filtering retained genes with rare (MAF<0.1% gnomAD v.2.0, and <2% in house database [1,600 population-matched exomes]) variants, excluding those predicted as benign by CADD (scaled score <15) and M-CAP (score < 0.025) algorithms or considered as benign/likely benign by interVar (F1S1); filtering retained high-quality rare and clinically associated variants affecting coding exons and splice sites with MAF<0.1% in local and public databases and CADD score > 20 (F2S1); filtering retained genes with rare (MAF<0.1% each used for gnomAD v.2.0 and GME, and <2% in house database [130 exomes]) variants, excluding those predicted as benign by CADD (scaled score <15) and M-CAP (score < 0.025) algorithms or considered as benign/likely benign by interVar (F3S1); filtering retained high-quality rare and clinically associated variants affecting coding exons and splice sites with MAF<0.1% (or 2% for compound-heterozygotes) in all of the following reference databases: 100,000 Genomes Project reference samples, 1000 Genomes, ESP, TOPMed, UK10K, ExAC and gnomAD (excluding the Ashkenazi Jewish population), and prioritizing by a logistic regression model by using Exomiser tool (F4S1); high-quality nonsynonymous variants (excluding missense variants with a low PhyloP score) and variants within splice sites (+/-2) with frequency of <3% in gnomAD and GoNL databases and <2% in in-house database (F5S1); filtering retained genes with rare (MAF<0.1% in gnomAD v.2.0, and in house [approx. 70,000 exomes and genomes] databases) variants, excluding those predicted as benign by CADD (scaled score <15); filtering was not performed because of direct matching after considering *SCUBE3* as a novel clinically associated gene implicated in syndromic skeletal disorder (F7S1); filtering retained genes with rare

(MAF<0.1% in gnomAD v.2.0, ABraOM [approx. 600 exomes] and in house [approx. 750 population-matched exomes] databases) variants, excluding those predicted as benign by CADD (scaled score <15) and M-CAP (score < 0.025) algorithms or considered as benign/likely benign by interVar (F8S1); filtering retained genes with rare (MAF <0.1% in gnomAD V. 2.0 database and <2% in in-house database (population-matched 3500 exomes), and functionally relevant variants by excluding variants predicted as benign by CADD (scaled score <15) or benign/likely benign by Varsome (F9S1).

[2]*SCUBE3* (c.291C>G, p.Cys97Trp; CADD = 26.1), *TSC2* (c.649-7C>T; CADD = 4.5), *BFAR* (c.77A>G, p.Gln26Arg; CADD = 19.6), *CHRDL2* (c.432+8C>A, CADD = 8.8; c.195+3_195+10delAGGTTCCT; CADD = 14.9).

[3]*SCUBE3* (c.2444T>C, p.Ile815Thr; CADD=27.9).

[4]*SCUBE3* (c.1717C>T, p.Arg573*; CADD = 39), *ITPR1* (c.2183G>A, p.Arg728Gln; CADD 22.3), *HMCN2* (c.686C>A, p.Asp228Glu; CADD 24.9), *PCIF1* (c.1292G>A, p.Arg431Gln; CADD 24).

[5]According to TIERING table performed as described previously, see PMID: 29691228 and https://doi.org/10.6084/m9.figshare.4530893.v4.

[6]*SCUBE3* (c.2239+1G>A, p.Val747Aspfs*46; CADD = 34).

[7]*SCUBE3* (c.2599+2T>C; CADD = 27.2).

[8]*SCUBE3* (c.829+1_952del, p.Arg282_Cys322del; CADD, NA).

[9]*SCUBE3* (c.2444T>C, p.Ile815Thr; CADD = 27.9).

[10]*SCUBE3* (c.611G>A, p.Gly204Asp; CADD = 26.2); *TRAF3IP2* (c.440c>T, p.Ala147Val; CADD = 32); *SNTA1* (c.160G>C, p.Gly54Arg; CADD = 22.9)

[11]*SCUBE3* (c.2782C>T, p.R928*; CADD = 45); *BTN2A2* (c.583C>T, p.Q195*; CADD = 27.9); *ZNRD1 (*c.356+3G>A; near to splice site); *PPP1R10* (c.194+8G>C; near to splice site).

Table S2. Key resources

REAGENT or RESOURCE	SOURCE	IDENTIFIER
Antibodies		
Anti-ALP	GeneTex	GTX62596
Anti-BMPR-IA	abcam	ab59947
Anti-BMPR-IB	abcam	ab175385
Anti-BMPR-II	Santa Cruz Biotechnology	sc-20737
Anti-BrdU	GeneTex	GTX26326
Anti-Caveolin-1	Santa Cruz Biotechnology	sc-894
Anti-FLAG	Cell Signaling Technology	CST #14793
Anti-FLAG M2	SIGMA	F1804
Anti-HA	Cell Signaling Technology	CST #3724
Anti-Myc	Cell Signaling Technology	CST #2276
Anti-Osteocalcin	Santa Cruz Biotechnology	sc-30045
Anti-phospho-Smad1/5/8	Cell Signaling Technology	CST #9511
Anti-SCUBE3	Abnova	H00222663-A01
Anti-Smad1	Cell Signaling Technology	CST #9743
Anti-β-actin	Sigma-Aldrich	A5316
Alexa Fluor 488 Phalloidin	Cell Signaling Technology	8878
Goat anti-Mouse Alexa Fluor 594	Thermo Fisher Scientific	A-11020
Bacterial and Virus Strains		
DH5α	Yeastern Biotech Co., Ltd	#FYE607-8VL
Lentiviral	pSIN-MCS or pLKO.1 vector	
Chemicals, Peptides, and Recombinant Proteins		
Alcian blue	Sigma-Aldrich	A5268
Alizarin red S	Sigma-Aldrich	A5533
BMP2	R&D Systems	355-BM
BMP4	R&D Systems	314-BP
5-bromo-2'-deoxyuridine (BrdU)	Sigma-Aldrich	B9285
Calcein	Sigma-Aldrich	C0875
Collagenase D	Roche	11088858001
3,3'-diaminobenzidine (DAB) peroxidase	KPL	54-10-00
Eosin	Sigma-Aldrich	E4009
Entellan new	Merck	HX57317161
Hematoxylin	Sigma-Aldrich	H3136
Leukocyte (*TRAP*) *staining* kit	*Sigma*-Aldrich	*387A*
LumiFlash™ Femto Chemiluminescent substrate, HRP System	Visual Protein	LF24-100
Lipofectamine™ 3000	Life Technologies	L3000015
Noggin	R&D Systems	3344-NG
OptiPrep solution	Sigma-Aldrich	D1556
Orange G	Sigma-Aldrich	O3756
pGEM-T-Easy vector system	Promega	A1360
p-nitrophenol-phosphate	Sigma-Aldrich	N1890

Phloxin B	Sigma-Aldrich	P4030
Polybrene	Sigma-Aldrich	TR-1003
Protein A-agarose	GE	17-0780-01
Proteinase K	Roche	3115887001
Sirius red	Sigma-Aldrich	365548
T-Pro LumiLong plus chemiluminescence	T-Pro Biotechnology	JT96-K004M
TRIzol	Life Technologies	15596026
Experimental Models: Cell Lines		
C3H/10T1/2	American Type Culture Collection	CCL-226
HEK-293T	American Type Culture Collection	CCL-11268
Saos-2	American Type Culture Collection	HTB-85
Experimental Models: Organisms/Strains		
Scube3$^{-/-}$ mice	UCDavis	049572-UCD
Oligonucleotides		
Gapdh forward primer (5'-3') ATCATCCCTGCATCCACTGGTGCTG	Lin et al., 2015	RT-PCR
Gapdh reverse primer (5'-3') TGATGGCATTCAAGAGAGTAGGGAG	Lin et al., 2015	RT-PCR
Scube1 forward primer (5'-3') CGGCGGCGAACTTGGTGACTACA	Lin et al., 2015	RT-PCR
Scube1 reverse primer (5'-3') TTGATAAAGGACCGGGGGAACAT	Lin et al., 2015	RT-PCR
Scube2 forward primer (5'-3') TGACTACCTGGTGATGCGGAAAAC	Lin et al., 2015	RT-PCR
Scube2 reverse primer (5'-3') CAGTGGCGTGTGGGAAGAGTCA	Lin et al., 2015	RT-PCR
Scube3 forward primer (5'-3') TGCTCCCCGGGCCACTACTAT	Lin et al., 2015	RT-PCR
Scube3 reverse primer (5'-3') AGCGCTGTTGGCCTCACTGGTCTT	Lin et al., 2015	RT-PCR
Acvr1 forward primer (5'-3') CATCGCTTCAGACATGACCTC	Tsuji et al., 2006	Q-PCR
Acvr1 reverse primer (5'-3') CTAACCGTATCCAGAGTAGTG	Tsuji et al., 2006	Q-PCR
Acvr2a forward primer (5'-3') GTTGAACCTTGCTATGGTGATAA	Tsuji et al., 2006	Q-PCR
Acvr2a reverse primer (5'-3') AATCAGTCCTGTCATAGCAGTTG	Tsuji et al., 2006	Q-PCR
Alpl forward primer (5'-3') AACCCAGACACAAGCATTCC	Lin et al., 2015	Q-PCR
Alpl reverse primer (5'-3') GAGACATTTTCCCGTTCACC	Lin et al., 2015	Q-PCR
Bmp2 forward primer (5'-3') TGGAAGTGGCCCATTTAGAG	Tsuji et al., 2006	Q-PCR
Bmp2 reverse primer (5'-3') TGACGCTTTTCTCGTTTGTG	Tsuji et al., 2006	Q-PCR

Bmp4 forward primer (5’-3’) ACGTAGTCCCAAGCATCACC	Tsuji et al., 2006	Q-PCR
Bmp4 reverse primer (5’-3’) TCAGTTCAGTGGGGACACAA	Tsuji et al., 2006	Q-PCR
Bmp7 forward primer (5’-3’) TACGTCAGCTTCCGAGACCT	Tsuji et al., 2006	Q-PCR
Bmp7 reverse primer (5’-3’) GGTGGCGTTCATGTAGGAGT	Tsuji et al., 2006	Q-PCR
Bmpr1a forward primer (5’-3’) CCTGTTGTTATAGGTCCGTTCT	Tsuji et al., 2006	Q-PCR
Bmpr1a reverse primer (5’-3’) AGCTGGAGAAGATGATCATAGCA	Tsuji et al., 2006	Q-PCR
Bmpr1b forward primer (5’-3’) GGAAGACTCAGTCAATATCTGC	Tsuji et al., 2006	Q-PCR
Bmpr1b reverse primer (5’-3’) CTAGTCCTAGACATCCAGAGGTGAC	Tsuji et al., 2006	Q-PCR
Bmpr2 forward primer (5’-3’) AGCTGACAGAAGAAGACTTGGAG	Tsuji et al., 2006	Q-PCR
Bmpr2 reverse primer (5’-3’) CAAGCTAGAACTGGTACTGCTCA	Tsuji et al., 2006	Q-PCR
Col1a1 forward primer (5’-3’) ACGTCCTGGTGAAGTTGGTC	Lin et al., 2015	Q-PCR
Col1a1 reverse primer (5’-3’) CAGGGAAGCCTCTTTCTCCT	Lin et al., 2015	Q-PCR
Gapdh forward primer (5’-3’) CCAGAACATCATCCCTGCATC	Lin et al., 2015	Q-PCR
Gapdh reverse primer (5’-3’) CCTGCTTCACCACCTTCTTGA	Lin et al., 2015	Q-PCR
Ibsp forward primer (5’-3’) AAGCAGCACCGTTGAGTATGG	Lin et al., 2015	Q-PCR
Ibsp reverse primer (5’-3’) CCTTGTAGTAGCTGTATTCGTCCTC	Lin et al., 2015	Q-PCR
Ostcn forward primer (5’-3’) TGACAAAGCCTTCATGTCCA	Lin et al., 2015	Q-PCR
Ostcn reverse primer (5’-3’) TGCCAGAGTTTGGCTTTAGG	Lin et al., 2015	Q-PCR
Osterix forward primer (5’-3’) AGCGACCACTTGAGCAAACAT	This paper	Q-PCR
Osterix reverse primer (5’-3’) GCGGCTGATTGGCTTCTTCT	This paper	Q-PCR
Runx2 forward primer (5’-3’) GCAGTTCCCAAGCATTTCAT	Lin *et al*., 2015	Q-PCR
Runx2 reverse primer (5’-3’) GAAGGGTCCACTCTGGCTTT	Lin *et al*., 2015	Q-PCR
Sp7 forward primer (5’-3’) AGCGACCACTTGAGCAAACAT	This paper	Q-PCR

Sp7 reverse primer (5'-3') GCGGCTGATTGGCTTCTTCT	This paper	Q-PCR
Recombinant DNA		
pLKO.1	Addgene	#10878
pCMV-ΔR8.91	National RNAi Core Facility at	
pMD.G	National RNAi Core Facility at	
pFLAG-CMV1	Sigma-Aldrich	**E7273**
pSecTag2-HygroB	Thermo Fisher Scientific	V91020
pcDNA3.1	Thermo Fisher Scientific	V79020
pEGFP-C2	Addgene	#6083-1
Software and Algorithms		
ImageJ	https://imagej.nih.gov/ij/	
Prism 7	GraphPad Software	
SigmaPlot10.0	https://www.systat.com/	Serial #775066493

References

Kuczmarski, R.J., Ogden, C.L., Guo, S.S., et al. (2002) 2000 CDC growth charts for the United States: Methods and development. Data From the National Health Examination Surveys and the National Health and Nutrition Examination. Surveys Vital Health Stat 11(246). National Center for Health Statistics, Hyattsville, Maryland. DHHS Publication No. (PHS) 2002-1696.

Lin, Y.C., Roffler, S.R., Yan, Y.T., and Yang, R.B. (2015). Disruption of Scube2 Impairs Endochondral Bone Formation. J. Bone Miner. Res. *30*, 1255-1267.

Tsuji, K., Bandyopadhyay, A., Harfe, B.D., Cox, K., Kakar, S., Gerstenfeld, L., Einhorn, T., Tabin, C.J., and Rosen, V. (2006). BMP2 activity, although dispensable for bone formation, is required for the initiation of fracture healing. Nat. Genet. *38*, 1424-1429.

Appendix: The Genomics England Research Consortium

Ambrose J. C.[1], Arumugam P.[1], Baple E. L.[1], Bleda M.[1], Boardman-Pretty F.[1,2], Boissiere J. M.[1], Boustred C. R.[1], Brittain H.[1], Caulfield M. J.[1,2], Chan G. C.[1], Craig C. E. H.[1], Daugherty L.C.[1], de Burca A.[1], Devereau, A.[1], Elgar G.[1,2], Foulger R. E.[1], Fowler T.[1], Furió-Tarí P.[1], Hackett J. M.[1], Halai D.[1], Hamblin A.[1], Henderson S.[1,2], Holman J. E.[1], Hubbard T. J. P.[1], Ibáñez K.[1,2], Jackson R.[1], Jones L. J.[1,2], Kasperaviciute D.[1,2], Kayikci M.[1], Lahnstein L.[1], Lawson K.[1], Leigh S. E. A.[1], Leong I. U. S.[1], Lopez F. J.[1], Maleady-Crowe F.[1], Mason J.[1], McDonagh E.M.[1,2], Moutsianas L.[1,2], Mueller M.[1,2], Murugaesu N.[1], Need A. C.[1,2], Odhams C. A.[1], Patch C.[1,2], Perez-Gil D.[1], Polychronopoulos D.[1], Pullinger J.[1], Rahim T.[1], Rendon A.[1], Riesgo-Ferreiro P.[1], Rogers T.[1], Ryten M.[1], Savage K.[1], Sawant K.[1], Scott R. H.[1], Siddiq A.[1], Sieghart A.[1], Smedley D.[1,2], Smith K. R.[1,2], Sosinsky A.[1,2], Spooner W.[1], Stevens H. E.[1], Stuckey A.[1], Sultana R.[1], Thomas E. R. A.[1,2], Thompson S. R.[1], Tregidgo C.[1], Tucci A.[1,2], Walsh E.[1], Watters, S. A.[1], Welland M. J.[1], Williams E.[1], Witkowska K.[1,2], Wood S. M.[1,2], Zarowiecki M.[1]

1. Genomics England, London, UK
2. William Harvey Research Institute, Queen Mary University of London, London, EC1M 6BQ, UK.